This is to certify that the
dissertation entitled

BMI-1 COLLABORATES WITH H-RAS TO PROMOTE MAMMARY EPITHELIAL CELL TRANSFORMATION, TUMORIGENESIS, AND METASTASIS

presented by

Mark James Hoenerhoff

has been accepted towards fulfillment
of the requirements for the

Doctoral degree in Pathobiology and Diagnostic Investigation

Thomas McKearney
Major Professor's Signature

July 1, 2008
Date

BMI-1 COLLABORATES WITH H-RAS TO PROMOTE MAMMARY EPITHELIAL CELL TRANSFORMATION, TUMORIGENESIS, AND METASTASIS

By

Mark James Hoenerhoff

A DISSERTATION

Submitted to
Michigan State University
In partial fulfillment of the requirements
For the degree of

DOCTOR OF PHILOSOPHY

Department of Pathobiology and Diagnostic Investigation

2008

ABSTRACT

BMI-1 COLLABORATES WITH H-RAS TO PROMOTE MAMMARY EPITHELIAL CELL TRANSFORMATION, TUMORIGENESIS, AND METASTASIS

By

Mark James Hoenerhoff

The polycomb group protein Bmi-1 is a transcription repressor reported to regulate self-renewal of normal and cancer stem cells, and prevent cellular senescence through inhibition of cyclin-dependent kinase inhibitors p16Ink4a and p19Arf. Originally discovered as a cooperating oncogene with c-Myc in a murine model of leukemia, overexpression of Bmi-1 has since been reported in several forms of cancer, including breast cancer. A direct or collaborative role of Bmi-1 in the pathogenesis of breast cancer would be critical in the development of novel biomarkers for diagnosis and treatment of this disease. We demonstrate that overexpression of Bmi-1 alone and in combination with H-Ras in normal mammary epithelial cells (MCF10A) markedly changes cellular morphology, increases proliferative indices, and decreases the apoptotic response to apoptosis-inducing agents in vitro. Our data also suggests that overexpression of Bmi-1 confers stem cell-like properties, including the formation of spheroid structures resembling mammospheres in culture and overexpression of stem cell markers. Xenograft experiments in immunodeficient (SCID) mice demonstrate that 1) Bmi-1 overexpression alone in MCF10A cells cannot induce tumors; 2) H-ras overexpression induces development of tumors with vascular, smooth muscle, and mast cell components; whereas 3) the combination of Bmi-1 and H-Ras induces development of poorly-differentiated aggressive mammary neoplasms with greatly increased propensity for spontaneous distant metastasis to liver, spleen, and brain. Moreover, by using tail vein

injection experiments in SCID mice as a model of direct hematogenous spread to the lungs, combination of Bmi-1 and H-ras overexpression in mammary epithelial cells results in fulminant pulmonary metastasis leading to clinical signs of weight loss and dyspnea, whereas injection of cells overexpressing H-ras or Bmi-1 alone does not result in this aggressive metastatic phenotype. Additionally, our data suggests that Bmi-1 overexpression allows cells with H-ras overexpression to bypass senescence, avoid anoikis, and essentially overcome dormancy in order to form pulmonary metastases. These findings suggest augmented stem cell properties through overexpression of Bmi-1 in conjunction with H-ras overexpression that results in greater metastatic potential. Therefore, Bmi-1 may be an important marker for diagnosis and a target for the treatment of aggressive breast cancer.

ACKNOWLEDGEMENTS

I would like to thank everyone who had a part in the development of this dissertation research, including my Principal Investigator, Jeffery E. Green from the Transgenic Oncogenesis Group at the National Cancer Institute, my collaborators Dr. Goberdhan Dimri and Dr. Sonal Datta at the Feinberg School of Medicine and Robert H. Lurie Comprehensive Cancer Center at Northwestern University, my committee members Mark R. Simpson from the Comparative Molecular Pathology Unit at the National Cancer Institute, Thomas P. Mullaney, Kurt J. Williams, Michael Scott, Vilma Yuzbasiyan-Gurkan, and P.S. MohanKumar from the Department of Pathobiology and Diagnostic Investigation at Michigan State University. A special thanks to my fellow laboratory members at the National Cancer Institute who were instrumental in my introduction to benchwork and my education in molecular biology. I would like to thank my family and friends for their support, and most importantly I would like to thank my wife for her support of my scholarly endeavors, her patience during my research trials and tribulations, and her confidence in my success. I could not have achieved this goal without her.

TABLE OF CONTENTS

LIST OF FIGURES

Figures in this dissertation are presented in color.

INTRODUCTION

I. Epigenetic Regulation of Gene Expression

According to the American Cancer Society, breast cancer is the most common cancer in women in the United States, and is the second leading cause of cancer mortality. Traditionally breast cancer, and cancer in general, has been viewed as a genetic disease, in which the accumulation of genetic mutations over time results in the activation of oncogenes, or the inactivation of tumor suppressor genes, culminating in cellular transformation and a cancer phenotype [1]. However, it has become evident that non-genetic, or epigenetic, factors play a role in tumorigenesis. Epigenetic factors influence gene expression in a heritable way without altering the DNA sequence [1-3]. Examples include chromatin modification [4-7], epithelial-stromal interactions [8, 9], and RNA interference [10, 11], to name a few.

Regarding chromatin modification, it is well known that changes in the structure of chromatin can greatly influence gene expression. For example, when chromatin is associated with histones and condensed, the DNA is not accessible to transcription factors, and transcription does not occur, effectively "turning off" genes. When chromatin is in an open conformation on the other hand, promoters are accessible to transcription factors, and genes may be "turned on" as required [12, 13].

There are two major mechanisms of chromatin modification as a means of epigenetic regulation of gene expression; DNA methylation and modification of histones [3, 13, 14]. Methylation is the addition of methyl groups to areas of high cytosine and guanine concentration, or CpG islands, which prevents transcription binding to

promoters, resulting in gene silencing [15]. Histones are the basic protein units that associate with DNA to form chromatin. Four pairs of histones associate with 146 base pairs of DNA to form nucleosomes, the fundamental repeating units of eukaryotic chromatin [16]. When DNA is associated with histones, access to promoters by transcription factors is prevented. Through modification of histones, gene expression is suppressed by preventing disassociation of the DNA from the histone unit, preventing transcription factor binding, and effectively silencing gene expression [17].

One of the primary mediators of suppression of gene expression through histone modification is the polycomb proteins. These proteins bind to and modify chromatin to suppress transcription of Homeotic genes that are essential for basic body plan establishment and morphogenesis during development [18], and have been shown to be involved in epigenetic gene regulation, acting as heritable gene repressors to achieve a "memory" of cell identity by preserving transcriptional patterns in the face of dividing cells [19-21]. The polycomb proteins exist in two complexes, Polycomb-Repressive Complex 1 (PRC1), containing Bmi-1, BVX, PHC1-3, RNF1-2, and SCML1-2, [22, 23] and a second complex, Polycomb-Repressive Complex 2 (PRC2), containing the polycomb proteins ENX/EZH2, EED, and SUZ12 [20, 22, 24, 25]. The PRC2 is responsible for the initiation of transcriptional repression, and recruits the PRC1 to the site of gene suppression. The PRC1 is necessary for sustaining this repression by binding to chromatin and antagonizing the remodeling of nucleosomes [19, 20, 24, 26].

II. Bmi-1 in Stem Cell Regulation and Carcinogenesis

B lymphoma Moloney murine leukemia virus insertion region-1 (Bmi-1) is a member of the polycomb group of transcription repressors, first identified as a c-myc-cooperating oncogene in murine B and T-cell lymphoma [18, 27-30]. The bmi-1 gene has conserved homology across several species, and the gene structure in the human is very similar to that of the mouse; at the nucleotide level, it is 92.4% homologous with mouse bmi-1 in the open reading frame (ORF) [28]. Additionally, the ORF codes for a nuclear protein of 326 amino acids that shares 98% homology with the mouse bmi-1 protein at the amino acid level [28]. Bmi-1 has been shown to be a key regulator of the self renewal of both normal and malignant hematopoietic and neuronal stem cells [31, 32], including I-type neuroblastoma cells, thought to be derived from malignant neural crest stem cells [33, 34]. Importantly, bmi-1 has also been shown to regulate self-renewal of normal and malignant human mammary stem cells with the hedgehog signaling pathway [35]. In addition, several recent studies have suggested a link between Bmi-1 and mammary carcinogenesis [29, 31]. It has been shown that Bmi-1 is over-expressed in several human breast cancer cell lines, and that Bmi-1 regulates telomerase and can immortalize human mammary epithelial cells and fibroblasts [18, 29, 31, 36]. Additionally, overexpression of Bmi-1 has been reported in human cancers, including nasopharyngeal carcinoma [37], oral squamous cell carcinoma [38], neuroblastoma [39], medulloblastoma, [40], non-small cell lung cancer, [41], basal cell carcinoma [42], liver carcinoma [43], colorectal carcinoma [44] and other gastrointestinal tumors [45] and precancerous lesions of the gastrointestinal tract [46], in addition to human breast cancer [29], where it has been correlated with axillary lymph node metastasis in invasive ductal breast carcinoma [47].

In multiple types of human cancer, including prostate, breast, and lung cancer, overexpression of Bmi-1 is associated with a stem cell-like 11 gene expression microarray signature that has been determined to be a powerful predictor of short interval to distant metastasis in patients diagnosed with early-stage disease [48]. Bmi-1 and EZH2 have been shown to be tumor-associated antigens [49], and together their coexpression is associated with the degree of malignancy in B-cell non-Hodgkin lymphoma [25].

Bmi-1 has been shown to be critical in the maintenance of stem cell populations through a process known as self-renewal, as well as through prevention of senescence through suppression of the Inka-ARF tumor suppressor locus [18, 27, 32], which encodes the cyclin-dependent kinase (CDK) inhibitors p16 and 14 (p19 in mice). The Ink4a locus encodes p16, a CDK that prevents the association of cyclin D with its cyclin dependent kinases, CDK4 and 6, thus preventing phosphorylation of retinoblastoma protein (pRb), ultimately leading to cell cycle arrest, apoptosis, or senescence. The Arf tumor suppressor locus encodes p14, which promotes p53 activation by inactivating Mdm2, likewise leading to cell cycle arrest, apoptosis, or senescence [18, 27, 30, 32, 50]. In this way, Bmi-1 can act as an oncogene through binding of chromatin, resulting in inactivation of this tumor suppressor gene locus [51-53], and when overexpressed, can bypass senescence and extend the replicative lifespan of primary cells [18, 32]. Inactivation of these senescence pathways contributes significantly to carcinogenesis. Inactivation of Ink4a leads to several forms of human cancer including lymphoma, pulmonary adenoma, brain tumors, and melanoma [54-56], and deletion of the Arf locus is associated with increased incidence of sarcomas, lymphomas, and gliomas, as well as other types of cancer [57]. Given the important function in regulation of the stem cell pool in multiple

tissues as well as the implications in tumorigenesis, the role of Bmi-1 in regulation of the mammary epithelial stem cell compartment and further elucidation of the role this gene plays in mammary carcinogenesis of the mouse will be paramount in shedding light on the comparative pathology of the complex disease of human breast cancer, as well as provide powerful mouse models by which to further study the disease.

III. Collaborating Oncogenes in Carcinogenesis

Cooperation between oncogenes to produce neoplasia is a well-documented occurrence in many types of human cancers. Whether resulting from a combination of proliferative or of anti-apoptotic effects from overexpression of multiple oncogenes, or the abrogation of tumor suppressor genes, the process of oncogenesis commonly involves mutations of multiple genetic loci. In the multi-step process of carcinogenesis, it is generally thought that malignant phenotypes arise via a recurrent mechanism of clonal expansion triggered by epigenetic and genetic lesions that may frequently require multiple alterations affecting several levels of growth control [58-63]. Whether this includes a mutation inducing loss of function of one or more tumor suppressor genes that inhibit proliferation or detect and/or repair DNA damage, or activation of a protooncogene resulting from a number of possible mutagenic events depends on the cell type and inducing mutation. Collaborations between oncogenes indicate that regulatory mechanisms that preclude transformation by one oncogene can be circumvented by a second oncogene [62] Several reports have demonstrated this concept of collaborating oncogenes both in vitro in primary cell lines and through the use of gene transfer experiments and in vivo using transgenic mouse models [58, 60, 64-69].

In vitro, it has been shown that overexpression of a single oncogene is often insufficient to transform cells to a malignant state, and that this transformation often requires two or more oncogenes acting together [70-72]. Several cellular and viral oncogenes require the presence of additional oncogenes or loss of tumor suppressor genes to transform cells, although expression of these oncogenes alone may immortalize cells. For example, while polyomavirus large T-antigen is sufficient to immortalize primary cells, it is unable to cause transformation [71, 73]. Additionally, whereas transformation of established fibroblasts by polyomavirus only requires the middle T-antigen, transformation of non-established fibroblasts requires the small, middle, and large T-antigens collectively [71, 74]. Furthermore, transformation of rat embryonic fibroblasts by the *ras* oncogene requires concurrent expression of adenovirus-5 or SV40 large T-antigen [62][58]. Other viral and cellular oncogenes known to collaborate with ras to transform primary cells include PyMT, HPV16 E7, Adenovirus E1A, p53, c-fos, Notch, and myc [62, 71, 75] In fact, unless coexpressed with such collaborating oncogenes, nonestablished or early passage rodent cells are transformed by ras at very low frequencies [62, 71, 76, 77]. Additionally, transformation of primary Schwann cells by ras is a synergistic process that is dependent on coexpression of the simian virus 40 large T antigen [60, 78].

Constitutively active mutant forms of Notch appear to be involved in human T-cell leukemia and mammary carcinomas in mice, and transformation of these cells requires signals from the ERK-MAPK pathway downstream from Ras [75]. In addition, cell lines obtained from tumors from Notch4 transgenic mice require ras signaling for anchorage independent growth [75]. These data show that the effects of other oncogenes

on the transforming activity of ras are complementary, and that in combination, collaborating oncogenes allow release of cells from controls that prevent transformation by ras alone [71].

Overexpression of oncogenic Ras or c-myc in the mammary gland induces mammary tumors in rodent models, and when expressed together, the rate of tumor onset is significantly increased [79]. Additionally, by utilizing retroviral insertional mutagenesis, identification of oncogenes that collaborate with the transgene of interest in carcinogenesis has been achieved, and remains a powerful tool in the identification of such collaboration in the process of carcinogenesis [59].

Through the use of transgenic mouse models, much insight has been gained regarding the function of Bmi-1 and its role in collaboration with other oncogenes in oncogenesis. As a result of retroviral insertional mutagenesis using the Moloney Murine Leukemia Virus (MoMLV), Bmi-1 was shown to collaborate with c-myc in a Eμ-myc transgenic mouse model of B-cell lymphomagenesis [30, 52, 53, 80, 81]. As a result of Bmi-1 overexpression in this model, the incidence of B-cell lymphoma increased by 15% [28, 52, 82, 83]. Furthermore, breeding transgenic lines expressing Bmi-1 under the Eμ promoter (to target expression to the lymphoid compartment) with Eμ-myc transgenic mice caused a marked increase in early onset lymphoma compared with Eμ-myc or Eμ-Bmi-1 transgenic mice alone. Over 75% of double transgenic mice developed B-cell lymphoma by ten weeks of age, compared to zero in the single transgenic Eμ-myc or Eμ-Bmi-1 groups. Alternatively, heterozygosity for Bmi-1 results in inhibition of lymphoma development in Eu-myc as a result of enhanced c-myc-induced apoptosis [30]. These data

show that Bmi-1 collaborates with c-myc in lymphomagenesis, and that elevated expression of Bmi-1 is required to achieve the full oncogenic capability of c-myc.

Guney et al. (2006) found that there is a canonical c-myc binding site within the promoter of Bmi-1 and that direct binding of the c-myc protein to this site occurs; therefore, the bmi-1 gene is a direct transcriptional target of c-myc. Furthermore, direct downregulation of c-myc results in downregulation of Bmi-1, and inversely, upregulation of c-myc results in upregulation of Bmi-1, with resulting up- and downregulation of p16, respectively [19]. This provides further strong evidence that there is a direct relationship and synergistic collaborative effect between these two genes. In addition, through its effects on the Ink4a-Arf tumor suppressor locus, as a result of proviral insertion, Bmi-1 causes repression of p19 (p14) and p16, antagonizing the growth-inhibitory and proapoptotic effects of c-myc overexpression [19, 30]. In this way, Bmi-1 acts in concert and as a result of c-myc overexpression to contribute to dysregulation of cell cycle dysregulation and tumorigenesis.

Dysregulation of c-myc expression has been observed in several different human cancers [30, 84] and has been shown to induce tumorigenesis in transgenic mouse models [30, 85-87]. Given its collaborative role with c-myc in the induction of lymphomagenesis, we were interested in the potential collaborative role Bmi-1 may play with oncogenic pathways commonly dysregulated in human breast cancer, such as occurs through H-ras activation. While the incidence of ras mutation in breast cancer is less than 2% [88-90], overexpression of Ras protein and the downstream effectors is common due to activation of growth pathways or aberrant estrogen dependent effects [91-93] Overexpression of this oncogene has been shown to be present in up to 20% of human

breast cancer patients, and has been associated with concurrent overexpression of c-myc and her2neu, often arising late in the course of disease [94]. Additionally, Ras overexpression has been associated with a poor prognosis, [89, 94, 95], and overexpression of downstream mediators has been correlated with regional lymph node metastasis and more aggressive forms of breast cancer [89, 96, 97]. Interestingly, Bmi-1 is phosphorylated by 3pK, a MAPKAP kinase of the ERK and p38 pathways downstream of Ras that regulates association of Bmi-1 with chromatin [98], providing further evidence of an interaction between these two oncogenes.

IV. Experimental Design to Study the Collaboration of H-Ras and Bmi-1

In order to evaluate the effects of Bmi-1 overexpression alone and in combination with H-ras overexpression, we developed an overarching hypothesis stating that overexpression of Bmi-1 in the mammary epithelium will promote proliferation and invasion in vitro and primary and metastatic tumor formation in vivo through cooperation with other cellular oncogenes, in this case H-Ras. To answer this question, several specific aims were developed; specific aim 1 was to determine the effect of Bmi-1 overexpression alone and in combination with H-Ras overexpression on human mammary epithelial cells in vitro. Specific aim 2 was developed to investigate this effect in vivo, and specific aim 3 was developed to determine the effect of depression of Bmi-1 expression in established breast cancer cell lines that overexpress Bmi-1. To address specific aims 1 and 2, an overexpression model was developed using a retroviral expression vector to overexpress Bmi-1 or H-Ras alone and in combination in MCF10A cells. These cells are normal human mammary epithelial cells that have undergone

spontaneous immortalization in culture through loss of the Ink4a-ARF tumor suppressor locus by homologous recombination [99]. In this way, our model enables us to investigate Ink4a-ARF independent mechanisms of Bmi-1 function on oncogenesis. In vitro, this cell line forms plates of polygonal cells with well differentiated cell-cell junctions and has a relatively low rate of proliferation. In vivo, injection of these cells into the mammary fat pad results in a small residual population of well differentiated mammary ductal structures and epithelium, but does not result in tumorigenesis. These cells are used to represent the behavior of normal mammary epithelial cells, and are commonly used in the study of mammary gland biology [99]. Changes in cellular morphology, proliferation, apoptosis in response to DNA damage, and invasion were evaluated in vitro, and a severe combined immunodeficient (SCID) mouse xenograft model was used to evaluate the cells for oncogenic and metastatic properties.

Specific aim 3 was addressed by depressing, or "knocking down" expression of Bmi-1 in established human breast cancer cell lines that overexpress the oncogene. We hypothesized that depression of Bmi-1 expression in these cells would lead to decreased proliferation and invasion, and increased apoptosis in response to DNA damage in vitro, and decreased tumorigenesis and metastasis in vivo. Suppression of Bmi-1 expression was established by using shRNA technology, and knock down was confirmed by western blot. shRNA is commonly used as a means to determine functional effects of suppression of genes of interest by effectively targeting and destroying endogenous mRNA. In this way, expression of a gene of interest is suppressed by ablating or reducing its mRNA signal. The following data show that Bmi-1 collaborates with H-ras in determining an aggressive cell phenotype in vitro and in vivo, with an increased metastatic propensity to

distant sites. These data have relevance because they suggest that in breast cancers with H-Ras overexpression, Bmi-1 may play a pro-tumorigenic role, and breast cancers that overexpress both oncogenes may be more aggressive and metastatic. Furthermore, overexpression of Bmi-1 may be associated with more aggressive forms of breast cancer.

CHAPTER ONE

The transcription repressor polycomb Bmi-1: Differential expression in histologic subtypes of human breast cancer, wildtype mouse tissue, and genetically engineered mouse models of breast cancer

Abstract: Bmi-1 is a member of the polycomb group (PcG) of transcription repressors, which have been demonstrated to regulate stem cell self-renewal and prevention of senescence through inhibition of the cyclin-dependent kinase inhibitors $p16^{Ink4a}$ and $p19^{Arf}$. Stem cells are a critical subpopulation of cells in tissues that regulate the genesis of progenitors and mature resident cells through proliferation. Overexpression of Bmi-1 has been reported in several human cancers, and has been found to induce telomerase activity and immortalize human mammary epithelial cells. However, little is known about the endogenous expression of Bmi-1 in murine and human tissues, spontaneous and induced tumors, genetically engineered mouse (GEM) models of human breast cancer, and in histologic subtypes of breast cancer. Using human and mouse tissue microarrays, we determined the expression of Bmi-1 by immunohistochemistry in endogenous mouse tissues, tumors generated from GEM models, and histologic subtypes of breast cancer. In these studies, we show that there is differential expression of Bmi-1 that correlates with histologic phenotype in certain human breast cancers, which suggests that Bmi-1 may be involved in the pathogenesis of these tumors. Furthermore, we show that some aggressive genetically engineered mouse models of human breast cancer have upregulation of Bmi-1, suggesting that Bmi-1 may be involved in more aggressive and metastatic forms of

breast cancer. Lastly, we show that there is differential expression of endogenous Bmi-1 in mouse tissues, as well as among the different stages of estrus, pregnancy, lactation, and involution that implies a role of Bmi-1 in stem cell activation, proliferation, and inhibition of apoptosis at different stages of development of the mammary gland.

Introduction

Several lines of evidence exist that a variety of cancers including breast cancer may result from transformation of both stem and progenitor cells during carcinogenesis, and that cancer may be a stem cell disorder [27, 31, 100-107]. Transformed stem cells, or 'cancer stem cells' are defined as cancer cells that have the ability to self-renew to give rise to a malignant stem cell as well as undergo differentiation to give rise to phenotypically diverse cells within a tumor [27, 108]. The cancer stem cell hypothesis suggests that a small population of cells within a tumor have stem cell properties that maintain malignant populations [109]. In addition, tumors that are clonally derived yet display markers for multiple cellular lineages provide evidence for a multipotent cancer stem/progenitor cell of origin [103, 110]. Maintenance of normal stem cell and cancer stem cell populations has been shown to be regulated by the transcription repressor, B-cell Moloney murine leukemia virus insertion region-1 (Bmi-1) [31, 40, 111, 112].

Bmi-1 belongs to the polycomb group of transcription factors, critical for the regulation of gene expression during development [18]. By binding to cis-acting silencer regions called polycomb response elements (PRE), Bmi-1 acts to modify chromatin structure and regulate transcription of Homeobox (Hox) genes, which are necessary for the establishment of proper body morphogenesis [28, 113]. The Bmi-1 gene has conserved homology across several species, and the gene structure in the human is very

similar to that of the mouse: 92.4% homologous at the nucleotide level in the open reading frame (ORF) [28]. Additionally, the ORF codes for a nuclear protein of 326 amino acids that shares 98% homology with the mouse Bmi-1 protein at the amino acid level [28].

Bmi-1 has been shown to be a key regulator of the self renewal of hematopoietic stem cells [114, 115], central and peripheral nervous system neuronal stem cells, [31, 116], mesenchymal stem cells [117], and mammary stem cells [35, 103]. Several recent studies have suggested a link between Bmi-1 and mammary carcinogenesis [29, 118]. Given the important function of Bmi-1 in regulating the stem cell pool in multiple tissues as well its associations in tumorigenesis, defining the role of Bmi-1 in regulating the mammary epithelial stem cell compartment and understanding of the role this gene plays in mammary carcinogenesis will be paramount in shedding light on the pathophysiology of the complex disease of human breast cancer. Here we report the differential endogenous expression of Bmi-1 in various human breast cancer histologic subtypes, wildtype mouse tissues, and in genetically engineered mouse (GEM) models of mammary cancer that recapitulate genetic mutations found in the human disease.

Materials and Methods

Tissue microarrays. To characterize the immunohistochemical labeling of Bmi-1 in human breast cancer tissues, tissue microarray slides were obtained from two different commercial sources (US Biomax, Inc., Rockville MD and Super Bio Chips, San Diego, CA). Prognostic marker data including estrogen and progesterone receptor status and p53

status were provided for one of these (US Biomax, Inc., Rockville MD), as was survival information. To characterize Bmi-1 immunoreactivity in GEM model mammary tumors, two mouse-based tissue microarrays developed by the NCI Mouse Models of Mammary Cancer Collective were used that include tissue sections of mammary gland development, GEM model mammary tumors, and normal control tissues.

Human arrays: Routine pathological methods were employed to examine histopathology of carcinoma simplex (n=35), infiltrative ductal carcinoma (n=33), scirrhous mammary carcinoma (n=9), atypical medullary carcinoma (n=10), infiltrating lobular carcinoma (n=3), signet ring carcinoma (n=1), and solid papillary carcinoma (n=1).

Mouse arrays: Tissue sections including various stages of mammary gland development (proestrus [n=10], estrus [n=10)], diestrus [n=20], metestrus [n=10], pregnancy [n=15], lactation [n=15], involution [n=40]), spontaneous mammary tumors (n=10), GEM model mammary tumors, (MMTV-neu [n=24], MMTV-wnt [n=23], MMTV-myc [n=12], PyMT [n=38], C(1)3-SV40-Tag [n=8], BRCA1 [n=15], Notch 4 [n=9]) and normal mouse tissue (liver [n=2], brain [n=3], spleen [n=2], thymus [n=2], salivary gland [n=8], lung [n=2], heart [n=2], skeletal muscle [n=2], small intestine [n=2], and kidney [n=2]) were examined.

Histology and immunohistochemistry. All sections were examined using routine light microscopy, and upon confirmation of the diagnosis, samples were prepared for immunohistochemistry. Paraffin-embedded sections were routinely deparaffinized and rehydrated, followed by steaming in sodium citrate buffer pH 6.0 for antigen retrieval. Endogenous peroxidase activity was blocked with 3% hydrogen peroxidase in methanol,

and following 5% bovine serum albumin (BSA) block, a polyclonal rabbit anti-Bmi-1 antibody (Abgent, San Diego CA) at a dilution of 1:300 diluted in PBS containing 3% BSA was applied and tissues were incubated at 4 °C overnight. Following avidin-biotin blocking, sections were incubated in goat anti-rabbit secondary antibody (Vectashield, Burlingame CA) at a dilution of 1:10,000, and amplification of primary antibody binding was achieved using the labelled avidin-biotinylated enzyme complex (ABC) technique. Following washing, tissue sections were visualized using diaminobenzidine (DAB) chromogen substrate, and counterstained with Mayer's hematoxylin, washed in double distilled water, followed by immersion in bluing solution (Scott's tapwater) for 2 minutes followed by distilled water wash. The sections were then dehydrated through graded alcohols (70%, 95%, 100%) and mounted with coverslips following xylene immersion. Negative controls were obtained by substitution of the primary antibody with buffer solution. Selected areas were photographed using an Olympus DP70 (Olympus) digital camera, and labeling intensity measured as tinctorial change in the cytoplasm and nucleus was entered into a Microsoft™ Excel Spreadsheet. Labeling intensity was graded based on a 0-3 scale (0 = no labeling, 1 = mild labeling, 2 = moderate labeling, 3 = marked labeling). One way ANOVA was performed on all samples.

Quantitative real-time polymerase chain reaction (QRT-PCR).

RT-PCR was performed on brain, thymus, spleen, C(1)3-SV40-Tag tumor, PyMT tumor, MMTV-neu and MMTV-myc tumors. Brain, thymus, and spleen were chosen because they have previously been shown to express varying levels of Bmi-1 [30, 32]. Tissues

were suspended in liquid nitrogen and pulverized with a mortar and pestel, followed by mechanical grinding using a tissue macerator. For RNA samples for RT-PCR, 1 mL of Trizol reagent (Invitrogen, Carlsbad CA) was added to each sample, and RNA was extracted following the manufacturer's protocol.

Results

Endogenous Bmi-1 protein is differentially expressed in mouse tissues. Normal mouse tissues examined histologically and immunohistochemically were brain, liver, spleen, thymus, salivary gland, lung, heart, skeletal muscle, small intestine, kidney, testis, ovary, uterus, and mammary gland (Figure 1). Bmi-1 was expressed in splenic lymphocytes in the marginal zone of the lymphoid follicles and in megakaryocytes. Cells that did not stain in the spleen include endothelial and vascular smooth muscle, smooth mucle in the splenic cords, and lymphocytes around the periarteriolar lymphocyte sheath (PALS). In the thymus, Bmi-1 was expressed in lymphocytes within the medulla and outer cortex, but was absent in lymphocytes immediately surrounding cortical blood vessels. Similarly, by RT-PCR, Bmi-1 was expressed in the spleen and thymus (Figure 2). Immunohistochemically, Bmi-1 expression was present in the granule cell layer and Purkinje cell layer of the cerebellum and in occasional neurons of the cerebrum, but was absent from the white matter. Bmi-1 was expressed diffusely within hepatocytes, and in sections of kidney, Bmi-1 was expressed diffusely within renal tubular epithelium, whereas occasional glomerular mesangial cells had weak positive immunoreactivity. Sections of medulla were not included in the tissue microarray and were thus not examined. In sections of lung, there was scant Bmi-1 expression, limited to the

bronchiolar epithelium and occasional alveolar epithelial cells, but most alveolar epithelial cells did not have immunoreactivity to Bmi-1. Small intestinal sections showed Bmi-1 expression within the intestinal epithelium, with less immunoreactivity within the underlying lamina propria. Bmi-1 was expressed within ovarian follicular epithelium and corpora lutea, but was absent to scant within the surrounding theca cells and vascular endothelium. Within the testis, positive immunoreactivity was present within the cytoplasm and nucleus of the germ cell layers and Sertoli cells, but was weak or absent from interstitial Leydig cells. Expression of Bmi-1 in sections of uterus was limited to the endometrial epithelium, and was absent in the surrounding smooth muscle layers. In salivary gland, Bmi-1 was expressed diffusely within salivary epithelial cells but was absent from vascular endothelial cells.

Bmi-1 is differentially expressed within the mouse mammary gland depending on the stage of estrus, gestation, lactation, and involution. Within normal, non-pregnant, non-lactating mammary gland, expression was limited to the ductular epithelium. Expression was increased during proestrus, then decreased during estrus, and increased again reaching maximum expression during metestrus, and then decreased again during diestrus. There was a statistically significant difference in Bmi-1 expression between stages of proestrus, metestrus, and diestrus ($^*p < 0.05$) (Figure 3A). During early pregnancy, Bmi-1 was expressed at moderate to high levels through day 10, and then waned by day 18-21. During lactation, Bmi-1 expression was moderate early (day 1) and remained steady through day 5 to day 10 (Figure 3B). At the time of weaning (involution day 0), Bmi-1 expression remained high in the mammary epithelium, but by day 1 of

involution, Bmi-1 levels dropped dramatically to almost undetectable, and remained very low until about one week after the onset of involution. By two weeks involution, Bmi-1 levels were increasing back to proestrus levels. There was a statistically significant elevation in expression (*$p < 0.01$) during stages of lactation compared to pregnancy and involution (Figure 3C).

Bmi-1 overexpression is associated with aggressive GEM models of human breast cancer. In GEM mouse models of human cancer, Bmi-1 overexpression by real time quantitative polymerase chain reaction (QRT-PCR) was associated with the C(1)3Tag and polyoma middle T antigen models, two particularly aggressive GEM models that have a rapidly progressive and metastatic disease course. However, the c-myc and her2neu (cErbB2) models, two more slowly progressive GEM models, showed lower levels of Bmi-1 expression (Figure 2). Immunohistochemically, of the GEM mouse models examined (C3(1)SV40 T/t antigen, PyMT, c-myc, her2neu, BRCA1 knockout (KO), Notch, Wnt-1 and MMTV-induced), there was increased immunolabeling in each model examined, with little variation in the staining intensity (Figure 4). Of the GEM models examined, the BRCA1 KO model expressed the highest levels of Bmi-1 by immunohistochemistry ($p < 0.01$) using the grading scheme for labeling intensity.

Bmi-1 is differentially expressed in histologic subtypes of human breast cancer and high expression correlates with medullary breast carcinoma. In human breast tumor tissue, there was differential Bmi-1 expression (Figure 5), which was significantly correlated with histologic tumor subtype by immunohistochemistry based upon a grading

scale of 0-3 (0 = no labeling, 1 = mild labeling, 2 = moderate labeling, 3 = marked labeling). Of the histologic subtypes examined, atypical medullary carcinoma expressed the highest level of Bmi-1, followed by carcinoma simplex, infiltrating ductal carcinoma, and scirrhous carcinoma in descending order (Figure 6) (*$p < 0.05$, **$p < 0.01$). There was no evidence of a significant correlation between luminal and basal subtypes.

Discussion

This report demonstrates the level of endogenous Bmi-1 expression in wild type mouse tissues, expression in several genetically engineered mouse models of breast cancer, and expression in human breast cancer samples. From these data, we have shown that expression of Bmi-1 is associated with different stages of the estrus cycle, pregnancy, lactation, and involution in the mouse, aggressive subtypes of GEM models, and certain histologic subtypes in spontaneous human breast cancer based upon tumor morphology.

The differential endogenous expression of Bmi-1 in wild type mouse tissues is consistent with its role in the maintenance of stem cell populations through self-renewal [105]. Self-renewal is a process by which a stem cell pool maintains its numbers through symmetric and asymmetric division. In symmetric cell division, at least one of the progeny is identical to the initial stem cell; in asymmetric stem cell self-renewal, one of the two progeny is identical to the initial stem cell, whereas the other cell is a committed progenitor cell, which undergoes cellular differentiation [103, 105]. Through the tightly regulated process of self-renewal, stem cells are able to function over the lifespan of the host [27, 114].

We have shown that in many tissues, Bmi-1 expression is correlated with cell populations with more capacity for regeneration or proliferation, such as intestinal villous epithelium, hepatocytes, and renal tubular epithelium, whereas in tissues with lower regenerative capacity, such as skeletal muscle and brain, either few cells express this protein, or only those cells that function as a stable pool for adult tissue stem cell progenitors express it, as has been reported in the subventricular zone (SVZ) of the brain [28]. It has been shown that Bmi-$1^{-/-}$ have a reduced number of neurons in the external granular cell layer of the cerebellum [40]. In the normal developing post-natal mouse, signals from the Purkinje cell layer stimulate a proliferation of cerebellar granule neuron progenitors in this layer as a result of Sonic Hedgehog (Shh) signaling [119, 120]. As a result, granule neuron progenitors differentiate and migrate through the molecular layer into the internal granular layer where they remain for the life of the host [121]. Thus, the lack of Bmi-1 in the Purkinje cell layer leads to a loss of signaling to the cerebellar granular cell neurons, ultimately resulting in cerebellar aplasia.

We found that the spleen and thymus expressed high levels of Bmi-1. These findings are expected, as these are sites of centers of B and T lymphocyte genesis and propagation, and Bmi-1 has been reported to be highly expressed in these tissues and in certain types of leukemia in humans [31, 112, 122]. The germ cell layers of the seminiferous tubules and layers of the ovarian follicles have particularly prominent Bmi-1 expression, consistent with the germ/stem cell enrichment of these organs. Similarly, in the cycling, pregnant, lactating, and involuting mammary gland there is differential Bmi-1 expression supporting its function in the maintenance of stem cell pools and its proliferative and anti-apoptotic effects in development.

Within normal, non-pregnant, non-lactating mammary gland, expression is limited to the ductular epithelium. During the estrus stage, expression is minimal within the mammary ductular epithelium, and increases during proestrus, reaching maximum expression during metestrus, and then decreases during diestrus (Figure 3A). Interestingly, it has been reported that peak BrDU labeling, indicating the highest degree of proliferation, occurs during metestrus and early diestrus [123, 124]. Increased Bmi-1 expression may be important during these stages of the estrus cycle when proliferation of the ductular epithelium and lobuloalveolar formation is critical.

During early pregnancy, Bmi-1 is expressed at moderate to high levels through day 10, and then wanes by days 18-21. Increased expression during early to mid pregnancy supports the role of Bmi-1 in the mobilization of stem cells and progenitors to proliferate during states of physiologic hyperplasia. Bmi-1 is expressed at moderate to high levels throughout lactation, again supporting a role in proliferation and mobilization of stem cell pools in the mammary gland (Figure 4B).

Bmi-1 is highly expressed at the time of weaning, and drops dramatically during the first day of involution. Expression remains minimal through day 5 of involution, but eventually increases again to proestrus levels by two weeks following the start of involution (Figure 4C). Consistent with its role in preventing cell cycle arrest and apoptosis, these data suggest that during periods of time when the mammary gland is proliferating or mobilizing stem and progenitor cells to differentiate into luminal milk-producing cells, Bmi-1 is upregulated. Then, when the gland needs to involute following weaning, the massive apoptosis that characterizes this stage correlates with a drop in Bmi-1 expression to minimal levels. Taken together, these data show that Bmi-1

expression correlates with cell populations with a greater potential for regeneration and proliferation suggesting a function in mobilization of stem cell pools. Additionally, the loss of Bmi-1 expression during involution is consistent with the role of Bmi-1 as an anti-apoptotic mediator. These data are consistent with the function of Bmi-1 in mobilizing stem cell populations during growth and differentiation, and in preventing cell cycle arrest and apoptosis. Further correlation of Bmi-1 expression with markers of cellular proliferation (Ki67), apoptosis (Bcl-2, Bad), and mammary gland differentiation (estrogen receptor [ER], whey acidic protein [WAP], and beta-casein) will be important in characterizing the role of Bmi-1 in mammary gland proliferation, apoptosis, and differentiation.

By examining Bmi-1 expression by quantitative RT-PCR in GEM models of human breast cancer, we have determined that high levels of expression are correlated with two particularly aggressive models, the C3(1)SV40 T/tag model and the PyMT model. Each of these models is extremely useful in the study of the human disease because each possess molecular events that culminate in the transformation of mammary epithelial cells and subsequent metastatic disease in the host. The C3(1)SV40 T/t antigen model is characterized by progressive development of mammary lesions leading to invasive carcinoma formation through inactivation of the tumor suppressors p53 and Rb [125-127]. These mice develop lesions of atypical ductal hyperplasia by 8 weeks of age, progressing to mammary intraepithelial neoplasia (MIN) by 12 weeks, which is histologically similar to human ductal carcinoma in situ (DCIS). After 16 weeks of age, these animals develop invasive carcinomas, and approximately 15% of these animals develop metastases to the lungs in the FVB/N background, and 50% in the FVB/N X

Sv129 hybrid background [127-129]. This model is very useful in the study of the human disease because it progresses through multiple stages from precancerous to invasive carcinoma with pulmonary metastasis in a predictable manner, and represents a basal subtype of human breast cancer. The basal subtype of breast cancer is frequently very poorly differentiated, estrogen receptor (ER) and progesterone receptor (PR) negative, and associated with a poor prognosis [130, 131]. Interestingly, in our immunohistochemical evaluation of the various GEM models of mammary cancer, one such basal model, the BRCA1 KO model, consistently expressed high levels of Bmi-1. The BRCA-1 mutation is a well characterized mutation in humans that is responsible for 25-30% of familial cases of breast cancer [132]. Women harboring this mutation have a 56-84% estimated cumulative lifetime risk of developing breast cancer [132-134]. Histologically, BRCA-1 associated human breast carcinomas are poorly differentiated tumors that often have morphologic features of medullary or atypical medullary carcinoma [132, 134-136]. It has been proposed by Foulkes (2004) that BRCA1 functions as a mammary epithelial stem cell regulatory gene in the transition from the primitive basal to the glandular epithelial phenotype. This basal phenotype is also consistent with the genotype of medullary carcinoma by molecular profiling [137]. The correlation of Bmi-1 with these two basal type GEM models (C(1)3-Tag and BRCA1 KO) suggest that expression of Bmi-1 may promote a more aggressive and less differentiated phenotype, possibly related to a transformed stem cell phenotype. Correlation of basal markers such as cytokeratin 5/6 and 14, smooth muscle actin (SMA), and negative ER, PR, and Her2neu status in these GEM models will be important in further characterizing the role of Bmi-1 with the pathophysiology of the basal phenotype.

We also found elevated levels of Bmi-1 mRNA by real time QRT-PCR in MMTV-PyMT GEM model tumors. MMTV-PyMT transgenic mice express the mouse polyomavirus middle-T antigen (PyMT) under the control of the mouse mammary tumor virus (MMTV) promoter [138]. These animals develop multifocal mammary tumors that have a high incidence of metastasis to the lungs [139]. Similar to the C3(1)SV40 T/t-antigen model, these animals develop mammary lesions that develop progressively through distinct stages from in-situ proliferative precancerous lesions to invasive carcinoma with pulmonary metastasis. More importantly, this model shares morphologic similarities with the human disease, as well as several biomarkers that are indicative of a poor prognosis in humans such as the loss of estrogen and progesterone receptors, integrin-ß1 expression, and expression of ErbB2/Neu and cyclinD1 [140]. These characteristics make this model particularly useful when studying the biological progression of breast cancer in humans. The association of a high level of Bmi-1 expression with these particularly aggressive transgenic models of human breast cancer suggest that overexpression of Bmi-1 may play a role in the acquisition of an aggressive breast cancer phenotype. Study of the molecular mechanisms that occur between the stages of precancerous to invasive metastatic carcinoma may bear important light on the mechanism of Bmi-1 in the pathogenesis of these models as they relate to the human disease.

In general, human breast cancer can be divided into familial and sporadic causes [141]. Within sporadic and familial breast cancers, characterization is based on several factors, including histologic subtype. For invasive breast cancer, infiltrating ductal carcinoma is the most common histologic type of breast cancer, accounting for

approximately 70% of cases [132, 141]. Scirrhous carcinoma is a variant of infiltrative ductal carcinoma that is characterized by cords and packets of tumor cells embedded in an abundant desmoplastic matrix [142]. Carcinoma simplex is a subtype of infiltrative ductal carcinoma that is characterized by solid sheets of poorly differentiated epithelial cells with large vesicular nuclei and prominent nucleoli, often forming clusters with an indistinct cell border (syncitial growth pattern), and a broad pushing margin with a prominent lymphocytic infiltrate [132, 137, 143, 144]. The diagnosis of atypical medullary carcinoma is made when there is less lymphocytic infiltrate, or there is an invasive margin in part of the tumor [136]. Medullary or atypical medullary carcinomas are the predominant histologic types seen in patients with BRCA1 mutation, and they are typically higher grade tumors when associated with the BRCA1 mutation [134, 136]. Our immunohistochemical examination of Bmi-1 in this series of breast tumor specimens showed that Bmi-1 expression was statistically correlated with the histologic subtype of atypical medullary carcinoma (Figure 6). This supports our previous findings of increased Bmi-1 in the BRCA1 KO mouse model, and suggests that Bmi-1 overexpression is associated with a more aggressive basal tumor phenotype possibly related to transformation of a primitive precursor, such as a stem cell.

In summary, we showed that Bmi-1 expression is differentially expressed in wild type moues tissues, is associated with more aggressive GEM models of human breast cancer (PyMT, C3(1)SV40 T/t-antigen, and BRCA1 KO), and is associated with the BRCA1 tumor phenotype, medullary/atypical medullary carcinoma. These results suggest that 1) Bmi-1 functions in normal development to promote proliferation and prevent apoptosis in the mammary gland and 2) Bmi-1 plays a role in the promotion of more

aggressive types of breast cancer, possibly through the promotion of stem or progenitor cell pathways. It has recently been shown that BRCA1 is involved in human mammary stem/progenitor cell fate, and that loss of BRCA1 may result in the accumulation of genetically unstable breast stem cells that are targets for further transformation [145]. Furthermore, BRCA1 tumors contain mammary epithelial cells with a stem cell immunophenotype ($CD44^+$, $CD24^-$, $CD133^+$) with cancer stem cell characteristics [146]. Further evaluation of Bmi-1 with the basal subtype of breast cancer and in tumors associated with stem cell pathways associated with the basal phenotype (Wnt, Notch, BRCA1 KO), would be important in determining the role of Bmi-1 in the pathogenesis of mutations leading to transformation of mammary epithelial cells.

APPENDIX A

Figure 1: Endogenous expression of Bmi-1 in wildtype mouse (FVB) tissue. Anti-Bmi-1 polyclonal antibody, hematoxylin counterstain (Bar = 100 μm).

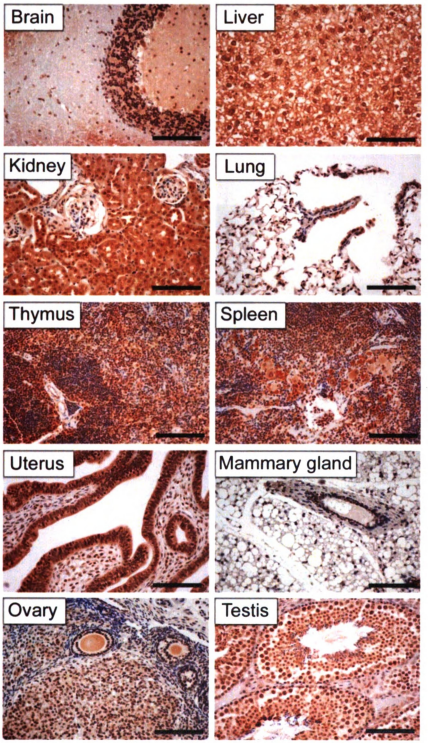

Figure 2: Endogenous Bmi-1 expression in wildtype mouse tissues and GEM tumors by QRT-PCR normalized to brain. There is a five-fold and an eight-fold increase in Bmi-1 mRNA expression in the thymus and spleen, respectively, compared to the brain. The C(1)3-SV40-T/t-antigen and MMTV-PyMT GEM models have 15 and four-fold increases in Bmi-1 mRNA expression, respectively, normalized to expression levels in brain.

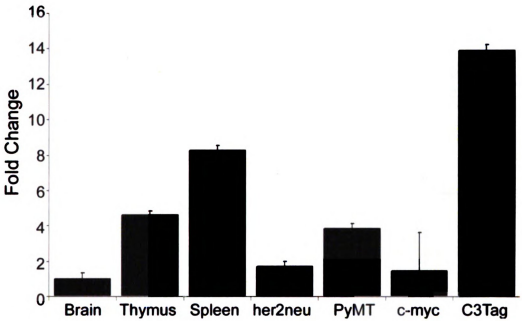

Figure 3: Bmi-1 expression during phases of the estrus cycle, pregnancy, and lactation. 3A: Bmi-1 expression during phases of the estrus cycle, immunohistochemical expression (above) and graphical representation (below) indicating a significant difference in Bmi-1 expression between stages of proestrus, metestrus, and diestrus (*a* vs. *c* and *b* vs. *c*, $p < 0.05$). 3B-C: Bmi-1 expression during stages of pregnancy, lactation, and involution. Above: immunohistochemical expression of Bmi-1 (Bar=100 μm). Below: graphic representation illustrating statistically significant elevation in expression (*a* vs. *b* and *b* vs. *c*, $p < 0.01$) during stages of involution (0 = no labeling; 1 = mild labeling; 2 = moderate labeling; 3 = marked labeling).

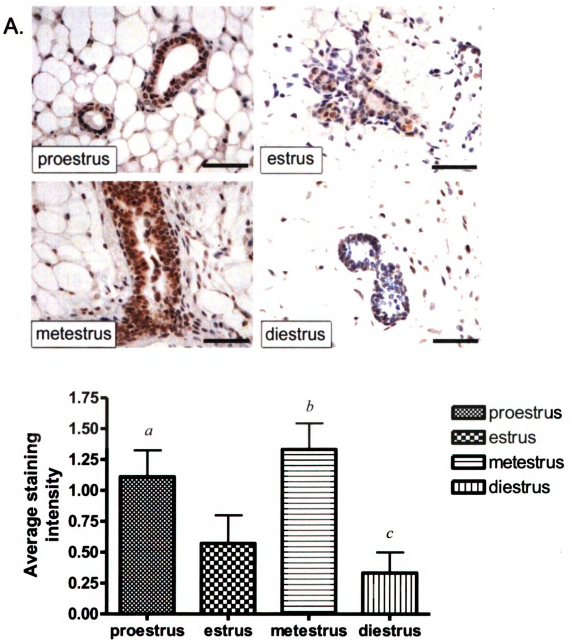

Figure 3 (continued)

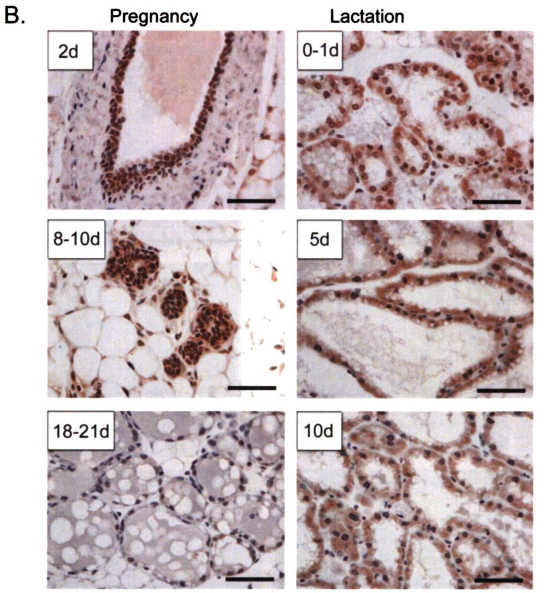

Figure 3 (continued)

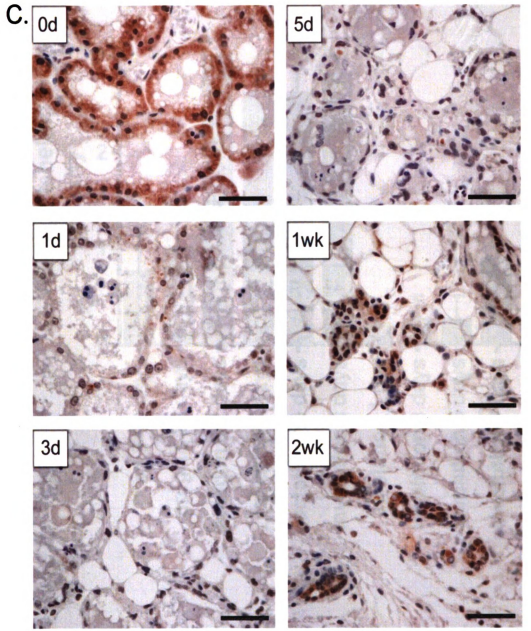

Figure 3 (continued)

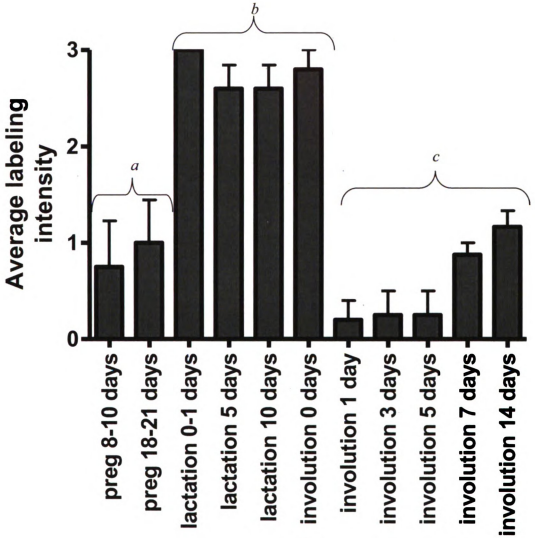

Figure 4: Bmi-1 expression in genetically engineered mouse models of human breast cancer. Top: anti-Bmi-1 polyclonal antibody, hematoxylin counterstain (Bar = 100 μm). Each GEM model expresses Bmi-1 diffusely within the nucleus and cytoplasm, with some minor variation in expression levels between tumors. Bottom: graphic representation of Bmi-1 expression in GEM tumors, indicating statistically significant difference in Bmi-1 expression in BRCA1 tumors compared to her2neu, p53 KO, Wnt, and Notch models, and between PyMT and her2neu models (*a* vs. *b*, $p < 0.05$; *d* vs. *b*, $p < 0.001$; *d* vs. *c* and *e*, $p < 0.01$, *d* vs. *f*, $p < 0.05$) (0 = no labeling; 1 = mild labeling; 2 = moderate labeling; 3 = marked labeling).

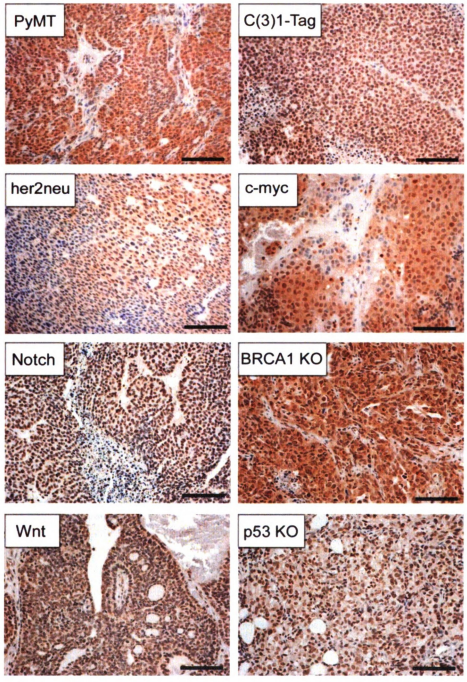

Figure 4 (continued)

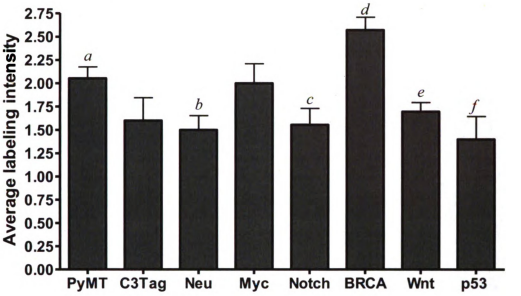

Figure 5: Bmi-1 expression in human breast cancer samples. A; Carcinoma simplex, B; atypical medullary carcinoma, C; infiltrative ductal carcinoma, D; scirrhous carcinoma. Anti-Bmi-1 polyclonal antibody, hematoxylin counterstain (Bar = 100 μm). Each tumor expresses Bmi-1 within the nucleus and cytoplasm, with some variation in staining intensity between tumors.

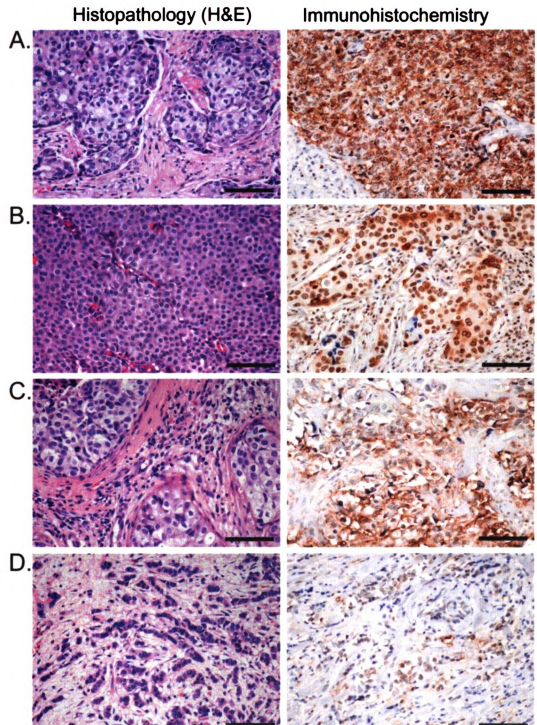

Figure 6: Bar graph illustrating the relative levels of Bmi-1 expression in histologic subtypes of human breast cancers by immunohistochemistry. There is a significant increase in Bmi-1 protein expression associated with the atypical medullary carcinoma phenotype (0 = no labeling; 1 = mild labeling; 2 = moderate labeling; 3 = marked labeling) (*a* vs. *c* or *d*, $p < 0.01$; *b* vs *d*, $p < 0.05$).

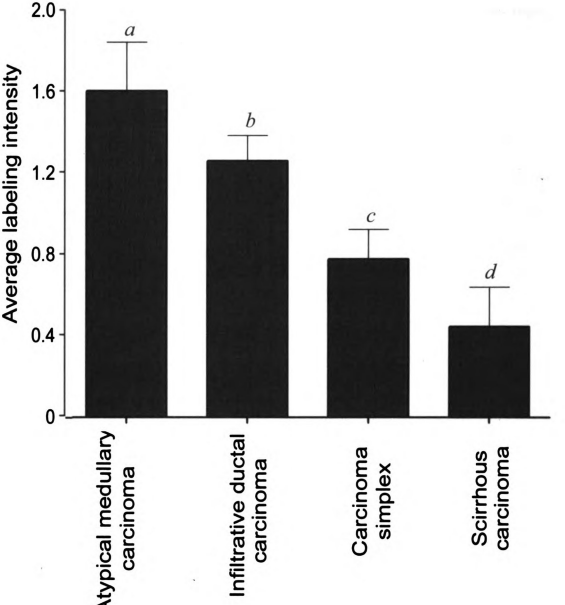

CHAPTER TWO

Hoenerhoff, M.J.*, Datta, S.*, Bommi, P., Sainger, R., Guo, W., Dimri, M., Band, H., Band, V., Green, J.E., Dimri, G.P. (2007) Bmi-1 cooperates with H-Ras to transform human mammary epithelial cells via dysregulation of multiple growth regulatory pathways. Cancer Research, 67:10286-10295.

*These authors contributed equally to this work.

CHAPTER TWO

Bmi-1 cooperates with H-Ras to transform human mammary epithelial cells via dysregulation of multiple growth regulatory pathways

Abstract: Elevated expression of Bmi-1 is associated with the malignant progression of many cancers including breast cancer. Here we examined the oncogenic potential of Bmi-1 oncoprotein in MCF10A, a normal but spontaneously immortalized strain of human mammary epithelial cells (HMECs). Bmi-1 overexpression alone in MCF10A cells did not result in oncogenic transformation. However, Bmi-1 co-overexpression with activated H-Ras (RasG12V) resulted in efficient transformation of MCF10A cells in vitro. When injected into nude mice, Bmi-1 and H-Ras overexpressing MCF10A cells formed poorly differentiated carcinomas with spindle cell features. Although, early passage H-Ras alone expressing MCF10A cells were not transformed, late passage H-Ras expressing cells exhibited features of transformation in vitro. Injection of these late passage H-Ras expressing MCF10A cells formed carcinomas with leiomatous, hemangiomatous, and mast cell components, which were quite distinct from Bmi-1 and H-Ras induced tumors. Bmi-1 and Ras co-overexpression in MCF10A cells also induced features of Epithelial-Mesenchymal Transition (EMT). Examination of various growth regulatory pathways suggested that Bmi-1 and H-Ras co-expression leads to activation of AKT, upregulation of CDK4 and cyclin D1, and downregulation of p53 expression in MCF10A cells. Furthermore, compared to control cells, late passage H-Ras expressing, and Bmi-1 and H-Ras co-expressing MCF10A cells showed an attenuated DNA damage response due to

substantially less p53 phosphorylation at ser-15 and ser-37 residues. Thus, our studies suggest that Bmi-1 overexpression together with H-Ras transforms HMECs, and promotes breast oncogenesis by deregulating multiple growth regulatory pathways.

Introduction

Polycomb group (PcG) proteins play an important role as epigenetic gene silencers during development [147]. In addition to their role in development, these proteins were recently reported to be overexpressed in various human cancers such as malignant lymphomas and various other solid tumors [148]. In particular Bmi-1 oncogene is overexpressed in a number of malignancies such as mantle cell lymphoma [149], B-cell non-Hodgkin lymphoma [25], myeloid leukemia [122], non-small cell lung cancer [41], colorectal cancer [44], breast and prostate cancers [44, 48]. In addition, we have recently reported that Bmi-1 is also overexpressed in nasopharyngeal carcinoma and oral cancer [37, 38]. Apart, from its role in oncogenesis, Bmi-1 has been shown to be required for self-renewal of hematopoietic stem cells and neural stem cells [31, 32, 115, 116]. In addition, recently it was shown that Bmi-1 regulates self-renewal of normal and cancer stem cells in breast, and that modulation of Bmi-1 expression in mammosphere-initiating cells alters mammary development in a humanized nonobese diabetic-severe combined immunodeficient mouse model [35, 103].

The polycomb proteins which are overexpressed in tumors, such as Bmi-1 and EZH2, appear to deregulate cell cycle progression [148]. Recent studies using in vivo mouse and in vitro cell culture models have shown that Bmi-1 regulates the expression of INK4A/ARF locus, which encode two important tumor suppressors $p16^{INK4A}$ and $p19^{ARF}$

($p14^{ARF}$ in human) [18, 150]. By downregulating $p16^{INK4A}$ and $p19^{ARF}$, Bmi-1 can potentially regulate p16-pRb and p53-p21 pathways of senescence [151]. Indeed, overexpression of Bmi-1 bypasses senescence in human and rodent fibroblasts, human mammary epithelial cells (HMEC), nasopharyngeal epithelial cells and normal oral keratinocytes [18, 29, 37, 150, 152]. Along these lines, we have recently reported that Bmi-1 downregulation by another PcG protein Mel-18, and Bmi-1 knockdown using an RNA interference (RNAi) approach, induce premature senescence via upregulation of $p16^{INK4A}$ [153]. Interestingly, in normal human oral keratinocytes (NHOK), the mechanism of extension of replicative life span by Bmi-1 does not appear to be via downregulation of $p16^{INK4A}$ suggesting the possible role of other unidentified targets of Bmi-1 that are involved in cellular proliferation [152].

Our recent data suggest that independent of its effect on p16Ink4a, Bmi-1 also regulates AKT activity [153], which may play a role in cell proliferation and survival of breast cancer cells. It is thought that the precursor cells for breast cancer are $p16^{INK4A}$ negative due to promoter methylation and silencing [154], suggesting that overexpression of Bmi-1 in $p16^{INK4A}$ negative tumors may contribute to oncogenesis via $p16^{INK4A}$-independent growth regulatory pathways. Here, we examined the oncogenic potential of Bmi-1 in an immortal but untransformed HMEC line MCF10A, which does not express $p16^{INK4A}$ due to deletion of the INK4A/ARF locus [155]. In addition to $p16^{INK4A}$ and $p14^{ARF}$ deletion, this cell line also does not express $p15^{INK4B}$ [155], which is another CDK4 inhibitor and a potential tumor suppressor. Using in vitro cell culture and in vivo mouse models, we show that overexpression of Bmi-1 alone is not sufficient for oncogenic transformation of immortal HMECs, which lack $p16^{INK4A}$, $p15^{INK4B}$ and

$p14^{ARF}$. However, the combined overexpression of the G12V mutant of H-Ras and Bmi-1 transformed HMECs in culture as determined by transformation assays. Furthermore, orthotopic injection of cells co-overexpressing Bmi-1 and activated H-Ras resulted in the formation of poorly differentiated and invasive tumors in severe combined immunodeficient (SCID) mice.

Materials and Methods

Cells, cell culture, expression vectors, retrovirus production and infection of HMECs. MCF10A and MCF10A-derived cell lines were cultured as described [29]. A retroviral vector overexpressing Bmi-1 has been described earlier [29, 153]. A retroviral vector pMSCV-Ras expressing H-Ras G12V mutant was constructed by subcloning cDNA of H-Ras from pcDNA3.1 obtained from UMR cDNA Resource Center (University of Missouri, MO). Stable cell lines expressing gene(s) of interest were generated by infection of the retroviral vector(s) expressing a particular gene and selecting cells in either puromycin, G418 or hygromycin as described [29, 153]. The retroviruses were produced by transient transfection of the retroviral vector together with pIK packaging plasmid into tsa 54 packaging cell line as described [29, 153].

Antibodies, western blot analysis, immunolabeling Matrigel, and soft-agar and wound healing assays. Bmi-1 was detected using either F6 mouse monoclonal antibody (mAb) from Upstate Cell Signaling Solutions (Charlottesville, Virginia), or 1H6B10G7 mAb from Zymed (S. San Francisco, CA). For the analysis of AKT pathway, antibodies to phospho-AKT 1/2/3 (Ser-473) (sc-7985-R), AKT-1 (B-1, sc-5298) and AKT-2 (F-7,

sc-5270) were obtained from Santa Cruz Biotech (Santa Cruz, CA). Among other antibodies, CDK4 (C-22, sc260), Cyclin D1 (A-12, sc-8396), H-Ras (F-235, sc-29), p21 (F-5, sc-6246), p53 (DO-1, sc-126), p53-Ser15 (sc-11764-R), PUMA (FL-193, sc-28226), Bax (6A7, sc-23959), ERK (C-16, sc-93), phospho-ERK (E-4, sc-7383), and PRAK (A-7, sc-46667) antibodies were obtained from Santa Cruz Biotech, Santa Cruz, CA. p53-Ser-37 mAb was obtained from Cell Signaling Technology (Beverly, MA). Vimentin, Fibronectin and E-Cadherin mAbs were obtained from BD Transduction Laboratories (Franklin Lake, NJ). β-Actin and β-Tubulin mAbs were obtained from Sigma-Aldrich (St. Louis, MO), and DSHB (University of Iowa, IA) respectively. To determine the AKT and ERK activity in synchronized cells, MCF10A cells were growth factor deprived using D3 medium [156] for 48 hrs and stimulated for 40 min by addition of D medium, which contains 12.5 ng/ml epidermal growth factor (EGF) [156]. Western blot analyses of total cell extracts using antibodies that detect various proteins were performed as described [29, 153]. Immunostaining for EMT markers such as E-Cadherin, fibronectin and vimentin, and soft-agar, matrigel and wound healing assays were performed as described [29, 153].

Mice and in vivo experiments. For mammary fat pad injection experiments, four cohorts of ten, six-week-old, female SCID mice each were used. Each cohort was injected in the right axillary mammary fat pad with 1×10^6 cells from each cell line. Tumor growth was measured weekly by caliper, and mice were euthanized by CO_2 asphyxiation once tumors reached 2 cm in diameter, or until mice became clinically ill. All animal work was performed following NIH guidelines under an approved animal protocol.

Necropsy, histopathology, histochemistry and immunohistochemistry. At necropsy examination, tumor tissue, brain, lung, heart, liver, spleen, and kidney were collected and fixed in 4% paraformaldehyde and routinely processed into paraffin blocks from which 4 μm sections were cut and stained with hematoxylin and eosin (H&E). Selected sections were stained using Masson's Trichrome and Giemsa histochemical methods. For immunohistochemical analysis, following deparaffinization, rehydration, antigen retrieval, and quenching of endogenous peroxidase activity, polyclonal and monoclonal primary antibodies were applied. Negative controls were obtained by substitution of the primary antibody with buffer solution. Sections for vimentin were pretreated by microwaving in sodium citrate buffer, sections for CD31 were pretreated by microwaving in EDTA, and sections for alpha smooth muscle actin (αSMA) were not subjected to antigen retrieval. Following washing, the labeled avidin-biotinylated enzyme complex technique was employed for amplification of primary antibody binding. For visualization, 3, 3-diaminobenzidine (DAB) was applied and counterstained with Mayer's hematoxylin. The sections were dehydrated through graded alcohols, immersed in xylene, and mounted with coverslips. Selected areas were photographed using an Olympus DP70 (Olympus) digital camera.

Results

Bmi-1 overexpression does not lead to transformation of HMECs. Although Bmi-1 is known to be overexpressed in many cancers including breast cancer, its exact role in oncogenesis, in particular breast cancer is unclear. To define the role of Bmi-1 in breast

cancer progression, we overexpressed Bmi-1 in MCF10A, a non-tumorigenic but immortal HMEC cell line (Figure 7A). Next, we examined the oncogenic potential of MCF10A cells overexpressing Bmi-1. Consistent with recent observation that 4 or more oncogenic events are required for the in vitro transformation of HMECs [157], Bmi-1 overexpressing MCF10A cells did not form colonies in soft-agar. This indicates that Bmi-1 is insufficient to cause transformation of immortal HMECs which also do not express $p16^{INK4A}$ and $p14^{ARF}$ tumor suppressors. Similar results were obtained using Bmi-1-overexpressing 76N HMECs, which do not express $p16^{INK4A}$ tumor suppressor and are immortal [29].

Overexpression of H-Ras together with Bmi-1 transforms MCF10A cells via deregulation of multiple growth regulatory pathways. Next, we overexpressed a constitutively active mutant G12V of H-Ras [158], in control MCF10A and Bmi-1 overexpressing MCF10A cells (Figure 7B). The pool populations of cells expressing H-Ras (MCF10A+H-Ras), Bmi-1 (MCF10A+Bmi-1) or both Bmi-1 and H-Ras (MCF10A+H-Ras+Bmi-1) were studied for transformed phenotype using soft agar and Matrigel assays (Figure 7C and 7D). The soft-agar assay indicated that cells expressing either Bmi-1 or H-Ras alone did not exhibit anchorage-independent growth, however, cells expressing both Bmi-1 and H-Ras readily formed colonies in soft-agar (Figure 7C), indicating that Bmi-1 and H-Ras co-overexpression leads to transformation of HMECs. To confirm, in vitro transformation potential of Bmi-1 and H-Ras expressing cells, Bmi-1, H-Ras and Bmi-1+H-Ras expressing cells were seeded in matrigel. After one week, cells were assessed for growth in matrigel. The results indicated that control MCF10A,

MCF10A+Bmi-1 and MCF10A+H-Ras cells formed normal spherical acini, while MCF10A- Bmi-1+H-Ras cells formed large irregular branched structures indicative of transformed phenotype of seeded cells (Figure 7D). According to the normal process of differentiation of MCF10A cells in Matrigel described by Grubbe et al [159], MCF10A cells grow in spherical colonies that ultimately undergo central apoptosis with lumen formation and polarization of epithelial cells around this central lumen. The formation of irregular branched structures indicates a block in this differentiation and a highly proliferative and transformed phenotype.

We have recently shown that Bmi-1 overexpression leads to activation of AKT/PKB [153], which is also a downstream target of H-Ras. The other known downstream effector targets of Ras include extracellular signal-regulated kinases ERK1 and ERK2. To assess the mechanism of Bmi-1 and H-Ras induced transformation of HMECS, we analyzed MCF10A and MCF10A derived cells for the expression of AKT and ERK kinases. The cells were starved for 48 hrs and then EGF containing D-medium was added for 40 min. The activities of ERK and AKT kinases were determined by western-blot analysis of phosphorylated and unphosphorylated forms.

The results indicate that control MCF10A and MCF10A-Ras cells have very little or no basal phospho-AKT (pAKT) expression, while MCF10A+Bmi-1 and MCF10A+H-Ras+Bmi-1 cells contained higher levels of activated AKT (pAKT) even under EGF starved conditions (Figure 8A). AKT activity was induced in all cells after EGF addition, and the induction of AKT activity was most noticeable in Bmi-1+H-Ras expressing cells. On the other hand, ERK activity was constitutively high in H-Ras and Bmi-1+H-Ras expressing cells regardless of EGF (Figure 8A). It was induced after addition of EGF in

MCF10A and MCF10A+Bmi-1 cells (Figure 8A). These results suggested that Bmi-1 and H-Ras could transform HMECs by activating AKT and ERK kinases.

Next, we determined the expression of cyclin D1 and CDK4, as the overexpression of these two cell cycle regulatory proteins has been linked to breast cancer progression [160, 161]. Our results indicate that, compared to control cells, Bmi-1 or H-Ras overexpression upregulated Cyclin D1, while Bmi-1 and H-Ras co-overexpression upregulated CDK4 as well as Cyclin D1 expression in MCF10A cells (Figure 8B). We also noticed a higher molecular weight form of CDK4 in Bmi-1 and H-Ras co-expressing cells, which may represent increased phosphorylation of CDK4 in these cells. We also determined the expression of pRb and p53 tumor suppressor in control and MCF10A-derived cells. Although, MCF10A cells are already $p16^{INK4A}$ negative and contain high amounts of hyper-phosphorylated pRb, MCF10A+Bmi-1 cells contained even higher amount of hyper-phosphorylated pRb (Figure 8B). On examining p53 expression, we found that MCF10A+H-Ras cells contained slightly higher p53 protein levels, while MCF10A+Bmi-1 and MCF10A+H-Ras+Bmi-1 cells showed downregulation of p53 (Figure 8B). Collectively, our data indicate that Bmi-1 together with H-Ras overexpression leads to activation of ERK and AKT, and upregulation of Cyclin D1 and CDK4 expression and downregulation of p53 protein.

H-Ras expressing late passage (LP) HMECs cells exhibit a transformed phenotype. It has been reported in the literature that in some instances, H-Ras overexpression alone can lead to transformation of MCF10A cells, while other reports suggest that overexpression of H-Ras alone cannot transform MCF10A cells [162-166]. In our case,

the early passage H-Ras expressing cells were not transformed. These early passage cultures of cells were also heterogeneous and exhibited mixed morphologies with some enlarged senescent cells and some small normal proliferating cells. The late passage (>5 passages) (LP) culture of H-Ras expressing cells, on the other hand, exhibited more uniform morphology with most cells proliferating. We considered whether these LP cells have undergone selection for rapidly proliferating cells and that during this selection may have acquired transformed properties.

To probe this hypothesis, late passage H-Ras and Bmi-1+H-Ras expressing MCF10A cells were plated on soft-agar and allowed to form colonies for 10-14 days. The results indicated that, similar to Bmi-1 and H-Ras expressing cells, MCF10A- H-Ras (LP) cells formed colonies in soft-agar indicating that H-Ras (LP) cells have also undergone transformation (Figure 9A). The late passage control and Bmi-1 overexpressing MCF10A cells still did not make any colonies in soft-agar, indicating that Bmi-1 expression alone is not sufficient to cause transformation of HMECs. Transformed phenotype of LP H-Ras cells was also confirmed by matrigel assays. These assays indicated that LP H-Ras and H-Ras+Bmi-1 MCF10A cells form very disorganized, highly branched structures, which ultimately connect through branches and appear like a big sieved structure (Figure 9B).

Bmi-1 expression together with H-Ras induces EMT phenotype in HMECs. When examining the morphology of MCF10A-derived cells, we noticed that cells expressing both H-Ras and Bmi-1 exhibited fibroblastic morphology, while control and Bmi-1 or H-Ras expressing cells exhibited more epithelial morphology. The fibroblastic morphology

of MCF10A+H-Ras+Bmi-1 cells suggested the induction of an EMT phenotype in these cells. To confirm the induction of an EMT phenotype, we examined control MCF10A and MCF10A derived cells for the presence of EMT markers by immunostaining and western-blot analysis (Figure 9D). The results indicated that control MCF10A and MCF10A+Bmi-1(LP) cells expressed E-Cadherin, a cell junction protein characteristic of epithelial cells, while MCF10A+H-Ras (LP) and MCF10A+H-Ras+Bmi-1 (LP) lost the expression of E-Cadherin expression. On the other hand, MCF10A+H-Ras (LP) and MCF10A+H-Ras+Bmi-1 (LP) cells expressed fibroblastic markers such as vimentin and fibronectin (Figure 9C). Similar results were obtained using western blot analysis using antibodies specific for E-Cadherin, fibronectin and vimentin (Figure 9D). These data indicate that Bmi-1 and H-Ras co-expression induces a strong EMT phenotype. Although, the early passage H-Ras cells did not show an EMT phenotype, late passage H-Ras cells also exhibit the EMT phenotype, although the late passage H-Ras cells still appear less fibroblastic compared to Bmi-1+H-Ras cells.

As H-Ras and Bmi-1+H-Ras expressing cells exhibited the EMT phenotype, which is closely linked to migration and invasion, we performed a wound healing assay (scratch test), which was repeated three times. The control MCF10A, and Bmi-1, H-Ras and Bmi-1+H-Ras overexpressing MCF10A cells were grown to 80% confluence, starved in D3 medium for 48 hrs. A wound was made in the middle of culture dish containing near-confluent cells and the cells were stimulated with EGF containing D medium for 15 hrs. Cells were photographed at 0 hr, before adding D medium and 15 hr after stimulating with D medium. The results indicated that Bmi-1+H-Ras cells have the highest migration potential and that these cells filled the wound quickly compared to other cells (Figure

9E). H-Ras expressing cells also showed migration, although much less compared to Bmi-1+H-Ras cells (Figure 9E). These cells tend to undergo cell death during migration. Control cells showed no migration, while Bmi-1 expressing cells exhibited minimal migration (Figure 9E). Thus, these data suggest that Bmi-1 and H-Ras co-overexpressing cells have acquired migration and invasion potential typical of highly transformed HMECs.

Expression level of H-Ras determines proliferation in H-Ras–expressing MCF10A cells. The differential ability of MCF10A–H-Ras (EP) and MCF10A–H-Ras (LP) cells to undergo transformation could be related to the different levels of Ras, which in turn may determine the proliferation in these cells. To examine this possibility, we determined expression of H-Ras by Western blot analysis in control MCF10A, and MCF10A-derived early- and late-passage cells, and did Ras and Ki-67 co-immunostaining in these cells (Figure 10). The Western blot analysis of control, early-, and late-passage cells indicated that H-Ras (EP) cells expressed a high level of Ras, whereas H-Ras (LP) cells expressed a low level of Ras (Figure 10A). On the other hand, Bmi-1+H-Ras (LP) cells expressed a high level of Ras (Figure 10A and B). Bmi-1+H-Ras (EP) cells and H-Ras (EP) cells expressed similar levels of Ras (Figure 10A and B). Because early-passage cultures are heterogeneous with cells expressing variable levels of Ras, it is possible that cells expressing Ras above a certain threshold level are not proliferating. At increasing number of population doublings, there may be selection for cells expressing a lower level of Ras, which permits continued proliferation. Accordingly, H-Ras (LP) cells will have low expression of Ras. Consistent with this hypothesis, on a single-cell basis, we observed that in H-Ras (EP) cultures, most cells with high Ras stained negative for Ki-67, a

proliferation marker, whereas cells with low Ras stained positive for Ki-67 (Figure 10C and D). On the other hand, H-Ras (LP) culture mostly contained cells with low Ras, which stained positive with Ki-67 (Figure 10C and D). The percentage of low Ras–expressing cells, which were Ki-67 positive, was also high in MCF10A–Bmi-1+H-Ras (EP) culture, although some cells in this culture also expressed high Ras, which were positive for Ki-67 (Figure 10C and D). Importantly, most Bmi-1+H-Ras (LP) cells expressed high Ras and stained positive for Ki-67, indicating that Bmi-1 permits proliferation of these cells despite high Ras (Figure 10C and D). In all cultures, variable percentages of low Ras–expressing cells were Ki-67 negative. Because of growth asynchrony in culture, such cells may not be proliferating at the time of staining.

MCF10A cells expressing H-Ras and MCF10A cells expressing Bmi-1 + H-Ras form histologically distinct tumors in vivo. As late passage MCF10A+H-Ras cells also exhibited features of transformation, we hypothesized that these cells will also give rise to tumors in vivo, as has been reported in some instances. However, such tumors may be different than the tumors that arise after injecting MCF10A+H-Ras+Bmi-1 cells. To examine the hypothesis that both late passage MCF10A+H-Ras and MCF10A+H-Ras+Bmi-1 cells will give rise to tumors in vivo, and that these tumors may differ in behavior due to the overexpression of Bmi-1, we injected MCF10A, MCF10A+Bmi-1 (LP), MCF10A+H-Ras (LP), MCF10A+H-Ras+Bmi-1 (LP) cells into the mammary fat pad. As expected, MCF10A control cells did not produce tumors in vivo. Injection of MCF10A+Bmi-1 cells also did not result in tumor formation even after 60 days, indicating that overexpression of Bmi-1 alone is not sufficient for neoplastic transformation of mammary epithelial cells in vivo.

In contrast, MCF10A+H-Ras and MCF10A+H-Ras+Bmi-1 cells produced progressively enlarging tumors in the mammary fat pad upon injection. Grossly, these tumors were strikingly different (Figure 11A); MCF10A+H-Ras+Bmi-1 cells formed tumors which were solid, firm, and irregular, and were whitish tan on the cut surface. In contrast, tumors formed by MCF10A+H-Ras cells were variably hemorrhagic and often cystic, composed predominantly of large thin cysts filled with clotted and/or unclotted blood (Figure 11A). Tumor growth rates when measured by tumor volume were not significantly different between these two groups; however, this was due to the general volume of tumors being similar, rather than the actual tumor mass.

Histologically, MCF10A+H-Ras and MCF10A+H-Ras+Bmi-1 tumors differed strikingly. MCF10A+H-Ras tumors consisted of variable populations of poorly to fairly well-differentiated smooth muscle, variably cystic irregular vascular spaces lined by poorly- to fairly well-differentiated endothelial cells, and multifocal clusters and nests of poorly- to well-differentiated mast cells (Figure 11B-C). In contrast, MCF10A+H-Ras+Bmi-1 tumors were composed of streams and bundles of poorly-differentiated spindle-shaped cells with scant, faintly eosinophilic fibrillar cytoplasm embedded in scant eosinophilic stroma, large round to oval hyperchromatic nuclei with multiple prominent nucleoli, and numerous mitotic figures (approximately 2-3/hpf) (Figure 11B-C). These cells often infiltrated into the surrounding fat pad, effacing normal ducts and adipose tissue, and, in one case, infiltrating and destroying the cortical bone of a subjacent rib and invading and effacing the bone marrow (Figure 11B).

Both tumor types were immunoreactive to antibodies against vimentin, whereas the MCF10A+H-Ras tumors were also immunoreactive to αSMA and CD31 (PECAM),

illustrating the smooth muscle and hemangiomatous components of these tumors (Figure 11C). Geimsa staining confirmed the multifocal mast cell clusters of varying differentiation in the MCF10A+H-Ras tumors, and Masson's Trichrome histochemical staining confirmed that the MCF10A+H-Ras+Bmi-1 tumors were composed of spindle cells with scant collagen production, more suggestive of a myogenic phenotype than a fibrosarcomatous one (Figure 11C). Animals with tumors formed by MCF10A+H-Ras cells were often very hemorrhagic, resulting in early morbidity possibly due to anemia as a result of bleeding from the tumors, rather than tumor burden in contrast to mice bearing tumors formed by MCF10A+H-Ras+Bmi-1 cells, which as a group lived longer with tumors than MCF10A+H-Ras tumor-bearing mice (Figure 11D).

MCF10A+H-Ras (LP) and MCF10A+H-Ras+Bmi-1 (LP) cells display defective p53 phosphorylation and attenuated DNA damage response. H-Ras is known to cause premature senescence or oncogene induced senescence (OIS) in primary cells, which is mediated by $p16^{INK4A}$ and p53-p21 pathways of senescence [167-169]. Using senescence-associated ß-galactosidase marker, we noticed senescence induction in a large proportion (40–50%) of MCF10A cells by H-Ras overexpression at early passages. Because MCF10A cells are $p16^{INK4A}$ negative, the partial OIS in these cells may depend on p53 and its target genes. Consistent with partial OIS, early-passage MCF10A-Ras cells also showed slower growth compared with vector control MCF10A and MCF10A cells co-overexpressing H-Ras and Bmi-1.

The senescent cells in MCF10A–H-Ras and MCF10A–Bmi-1+H-Ras cells were progressively lost, and rapidly proliferating cells were selected in later passages. We

hypothesized that the selection of rapidly proliferating cells in late-passage cultures of MCF10A–H-Ras and MCF10A–Bmi-1+H-Ras cells may depend on a defect in p53 pathway in these cells. To examine this hypothesis, we determined p53 expression in control MCF10A, MCF10A–Bmi-1 (LP), MCF10A–H-Ras (LP), and MCF10A–Bmi-1+H-Ras (LP) cells. The results indicated that unlike in MCF10A–H-Ras (EP) cells (Figure 8B), p53 was down-regulated in MCF10A–H-Ras (LP) cells (Figure 12A). To determine the mechanism of p53 down-regulation and its possible significance with respect to transformed phenotype of MCF10A–H-Ras (LP) and MCF10A–Bmi-1+H-Ras (LP) cells, we further studied p53 pathway in these cells.

MCF10A control and MCF10A-derived late-passage cells were treated with the DNA-damaging agent camptothecin (500 nmol/L) for the indicated amount of time, and expression of p53, phosphorylated p53, and p53 target genes was studied by Western blot analysis (Figure 12B). The results indicated that although MCF10A–H-Ras (LP) and MCF10A–Bmi-1+H-Ras (LP) cells had overall low p53 compared with control MCF10A and MCF10A–Bmi-1 cells, p53 remained inducible by camptothecin in all four set of cells, although the induced levels of p53 was still low in MCF10A–H-Ras (LP) and MCF10A–Bmi-1+H-Ras (LP) cells (Figure 12B). Further analysis of phosphorylated p53 indicated that MCF10A–H-Ras (LP) and MCF10A–Bmi-1+H-Ras (LP) cells were partially defective in phosphorylation of p53 at Ser-15 and Ser-37 residues (Figure 12B). Quantification of Western blot data showed reduced phosphorylation of p53 at Ser-15 in both MCF10A–H-Ras (LP) and MCF10A–Bmi-1+H-Ras (LP) cells at 4 and 8 h time points, whereas the basal levels of p53 Ser-15 were similar in all MCF10A-derived cells. Ser-37 phosphorylation was also compromised in MCF10A–H-Ras (LP) and MCF10A–

Bmi-1+H-Ras (LP) cells. Neither of these cell lines showed any induction of Ser-37 phosphorylation of p53 by camptothecin treatment.

Because it has been reported that PRAK mediates Ser-37 phosphorylation of p53 induced by H-Ras and that PRAK mediates Ras-induced OIS [168], we hypothesized that PRAK may be lost during selection of rapidly proliferating cells in H-Ras (LP) cells in culture. To examine this possibility, we determined PRAK expression in these cells by Western blot analysis. The results indicated that regardless of DNA damage, PRAK expression is not lost in control or H-Ras (LP) cells (Figure 12B). Interestingly, PRAK expression was up-regulated in H-Ras (LP) cells (Figure 12B). The up-regulation of PRAK is consistent with the notion that PRAK is an H-Ras target, which acts negatively to suppress H-Ras–induced proliferation [170]. Nonetheless, it seems that it is possible that this PRAK-mediated negative feedback regulation of H-Ras–mediated proliferation may be deficient in MCF10A–H-Ras (LP) cells, which may have allowed these cells to undergo transformation in culture.

Next, we studied the induction of p21 and PUMA (p53 up-regulated modulator of apoptosis), two well-known transcriptional targets of p53 [171, 172]. Our results indicated that both p21 and PUMA induction by camptothecin is partially compromised in MCF10A–H-Ras (LP) cells (Figure 12B), and p21 induction was more compromised in MCF10A–Bmi-1+H-Ras (LP) cells. Attenuated response of these targets of p53 is consistent with defective phosphorylation at Ser-15 and Ser-37 residues. We also examined expression of *Bax* and *PIG3* (p53-inducible gene 3), two other known targets of p53 [171]. Analysis of these two genes indicated that *Bax* is expressed at very low levels and is inducible in control MCF10A cells. However, MCF10A–H-Ras (LP) cells had

higher levels of Bax, which were not inducible by DNA damage (Figure 12B). Interestingly, among all four cell types, MCF10A–H-Ras (LP) cells expressed high BCL2, which may be related to transformed properties of these cells. *PIG3*, which usually has a delayed kinetics of induction by p53 [173], was not inducible in any of the cell types within the time frame used in our experiment (Figure 12B). Interestingly, compared with control MCF10A cells, MCF10A-derived (LP) cells showed significant down-regulation of *PIG3* (Figure 12B).

Discussion

Several recent studies have suggested that PcG proteins, in particular EZH2 and Bmi-1 are overexpressed in human cancers. Recent elegant studies have clearly shown that oncogenic transformation of human cells is a multi-step process [174]. It is very likely that overexpression of EZH2 or Bmi-1 alone is not sufficient to cause transformation of human cells. To gain an insight into breast cancer progression, we examined the transformation potential of Bmi-1 oncoprotein in immortalized HMECs. Although immortalized HMECs that we studied lack $p16^{INK4A}$ and $p14^{ARF}$, Bmi-1 expression still provides an oncogenic signal in these cells by the activation of PI3K-AKT pathway [153]. However, the oncogenic signal provided by Bmi-1 alone does not appear to be sufficient to cause transformation of HMECs, despite these cells being immortal, lacking three important tumor suppressors- $p15^{INK4B}$, $p16^{INK4A}$ and $p14^{ARF}$ [155], and overexpressing the Bmi-1 oncogene. This observation underscores the stringency of transformation in HMECs. Nonetheless, Bmi-1 overexpression is frequently

observed in invasive breast tumors [47, 48, 170], suggesting the involvement of additional oncogenic events during breast cancer progression in such tumors.

To understand the genetic basis of these presumptive additional oncogenic events, we overexpressed a constitutively active mutant, G12V of H-Ras [158], in Bmi-1 overexpressing MCF10A cells. G12V mutant of H-Ras promotes proliferation and oncogenesis via activation of mitogen-activated protein kinase (MAPK) kinase (MEK)/MAPK and the phosphoinositide 3-kinase (PI-3K)/AKT pathways. However, the activation of these pathways and their outcome is cell-type specific. For example, in primary cells, activation of these pathways led to induction of OIS, while in immortalized cells with compromised p53-p21 and/or $p16^{INK4A}$ pathways, H-Ras G12V may promote proliferation. Our reasoning behind using H-Ras G12V in these assays was based on its relevance to breast cancer, and its reported use in oncogenic assays involving HMECs [157]. Although, the direct mutational activation of H-Ras is rare in breast cancer, its hyperactivation by persistent growth factor signaling caused by EGFR and HER2/neu overexpression occurs in a large proportion (20-40%) of breast cancers [175, 176].

OIS caused by G12V mutant of H-Ras may require both functional $p16^{INK4A}$ and p53. In MCF10A cells, which have functional p53, we initially noticed the appearance of a heterogeneous culture with approximately 40-50% cells exhibiting senescent morphology upon H-Ras overexpression. Consistent with partial senescence induction, our western blot data also indicated upregulation of p53 protein in these cells. Senescence acts as a strong barrier to oncogenesis [151], hence the initial induction of senescence in a high proportion of MCF10A cells by H-Ras indicate an anti-oncogenic response. As expected, these early passage cells were not transformed by soft-agar and Matrigel

assays. However, late passage cultures, which were much more homogeneous and did not contain cells with senescent morphology, displayed transformed phenotype in Matrigel and soft-agar assays. Ras and Ki-67 costaining data also suggest that early passage culture of MCF10A-H-Ras are more heterogeneous in terms of Ras expression, whereas the late-passage culture of these cells are homogeneous in terms of Ras expression. Importantly, only low Ras–expressing cells tend to be Ki-67 positive, suggesting that low Ras permits proliferation, whereas high Ras blocks proliferation, possibly via OIS. This differential effect of Ras on proliferation explains the emergence of low Ras–expressing culture at late passages.

The H-Ras overexpression in Bmi-1 overexpressing MCF10A cells, on the other hand caused senescence in minority of cells when compared to H-Ras alone cells, and homogeneous culture with proliferating cells appeared much more rapidly from these cells. These data indicate that to some extent, Bmi-1 can overcome H-Ras induced OIS, even in $p16^{INK4A}$ negative cells, presumably via $p16^{INK4A}$- and $p14^{ARF}$-independent targets of Bmi-1. The homogeneous culture that rapidly emerged from Bmi-1+H-Ras–expressing cells continued to express high Ras. Most cells in this culture were Ki-67 positive despite expressing high Ras, suggesting that Bmi-1 permits proliferation of cells despite high Ras, and thus there is no selection for cells expressing low Ras. The biochemical basis for proliferation of MCF10A–Bmi-1+H-Ras (LP) cells despite high Ras remains to be elucidated.

On examination of Ser-37 and Ser-15 phosphorylation of p53 in response to DNA damage, we found that Ser-37 phosphorylation of p53 is significantly low and not inducible in both late-passage H-Ras and Bmi-1+H-Ras–expressing cells. In addition,

these cells also had much lower induction of Ser-15 phosphoryated p53, suggesting a possible defect in other p53-activating kinases such as ATM. A detailed analysis of various p53 phosphorylating kinases in late-passage MCF10A–H-Ras and MCF10A–Bmi-1+H-Ras remains to be done. Nevertheless, our data clearly indicate that these late-passage H-Ras– and Bmi-1+H-Ras–expressing cells have defects in p53 phosphorylating pathways, which results in attenuation of induction of p53 targets such as p21 and PUMA. This compromised induction of p53 targets may contribute to a transformed phenotype of MCF10A cells expressing Bmi-1 and H-Ras.

The differential behavior of early- and late-passage H-Ras–overexpressing MCF10A cells with respect to the transformed phenotype explains the different results that are reported in the literature[162-166]. Our data suggest that in cases where H-Ras–expressing MCF10A cells showed a transformed phenotype and gave rise to tumors in nude mice assays, late-passage H-Ras–expressing cells with defective p53 regulation may have been used. In other studies, where transformation of H-Ras–expressing MCF10A cells was not reported, early-passage H-Ras–expressing MCF10A cells may have been used. Alternatively, the transforming potential of H-Ras cells could be correlated with the level of expression of H-Ras. In studies where H-Ras alone was reported to be transforming, the expression of H-Ras may be low, which permits proliferation. On the other hand, in cases where Ras was reported to be insufficient for transformation, the expression of Ras may be very high, which causes proliferation arrest and OIS. Neither of these possibilities is mutually exclusive and both possibilities are likely to contribute to transformation of HMECs by H-Ras. Recently, it was shown that low levels of K-Ras induce proliferation and mammary epithelial cell hyperplasias, whereas high expression

of K-Ras induces proliferation arrest and OIS in doxycycline-inducible *K-Ras* transgenic mice [177]. In this report, it was also shown that inactivation of p53 permits transformation of mammary epithelial cells and tumor formation by high expression of Ras [177]. Our *in vitro* data are consistent with this report.

The results of histopathology, including special stains and immunohistochemistry, confirm that the MCF10A+H-Ras tumors are composed of multiple different populations of varying phenotypes (smooth muscle, hemangiomatous, and mast cells). The multiple populations present were differentiated along multiple mesenchymal lines, suggesting at least in part that portions of these tumors may be in part an in vivo response to the xenografted tumor population rather than original components of the neoplastic population that have undergone dedifferentiation and redifferentiation along multiple lines. For example, the large clusters well- to poorly-differentiated mast cells may have been recruited to the site of tumor formation by cytokines or other growth factors known to recruit mast cells, such as GM-CSF or IL-3 [178], produced by the xenografted tumor cells, rather than being of xenograft origin. This would explain the unusual phenotype of multiple differentiated populations. The MCF10A–Bmi-1+H-Ras tumors, on the other hand, represent a pure population of highly atypical, poorly differentiated, and infiltrative spindle cells. Although α-SMA immunohistochemistry was negative in these tumors, Masson's trichrome stain along with positive immunohistochemistry for vimentin would suggest that these cells may represent a myoepithelial phenotype consistent with EMT.

Although MCF10A–Bmi-1+H-Ras (LP) and MCF10A–H-Ras (LP) cells give rise to histologically distinct type of tumors, biochemically these cells show only minor differences in regulation of growth-regulatory pathways. The only significant difference

between these two cell lines is that H-Ras (LP) cells expressed higher levels of BCL2, which may contribute to the oncogenicity of these cells. In any case, we did not observe tumor formation by MCF10A–Bmi-1 cells, suggesting the involvement of additional oncogenic events such as down-regulation of p53, overexpression of CDK4 and cyclin D1, and up-regulation of AKT and ERK activities in the transformation of HMECs and breast cancer progression. Our data also indicate that Bmi-1 may cooperate with Ras in transformation by simply allowing high Ras–expressing cells to proliferate. The additional oncogenic events then may be largely contributed by H-Ras in the experiments described here. It remains to be determined which of these oncogenic lesions, together with Bmi-1, are sufficient to transform HMECs and form tumors *in vivo*.

APPENDIX B

Figure 7: Bmi-1 and H-Ras co-expression transforms HMECs. (A) Bmi-1 overexpressing MCF10A cells were generated by stable overexpression of Bmi-1, and cells (as indicated) were analyzed for Bmi-1 overexpression by western blot analysis. (B) H-Ras was introduced in control MCF10A and MCF10A+Bmi-1 cells, and cells were analyzed for H-Ras expression by western blot analysis. (C) MCF10A and MCF10A cells expressing H-Ras alone, Bmi-1 alone or Bmi-1 together with H-Ras (as indicated) were analyzed for anchorage-independent growth using soft-agar assays. MCF10A+Bmi-1+H-Ras cells form colonies in soft agar, indicating anchorage independent growth. (D) MCF10A and MCF10A-derived cells (as indicated) were analyzed for acini formation using Matrigel assays. While all other MCF10A-derived cell lines develop spherical colonies consistent with differentiated cells, MCF10A+Bmi-1+H-Ras cells develop highly branched proliferative structures indicative of a poorly differentiated population.

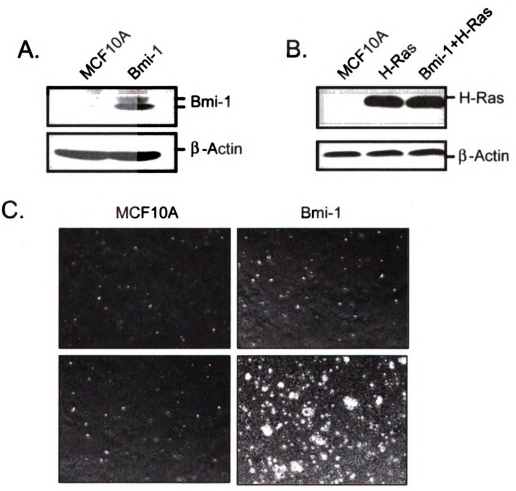

Figure 7 (continued)

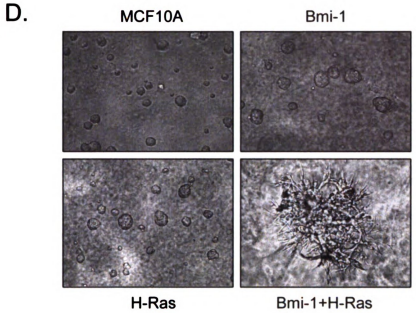

Figure 8: Various growth regulatory pathways are dysregulated in cells co-expressing Bmi-1 and H-Ras. (A) Western blot analysis of phospho-AKT, total AKT (AKT1 and AKT2), phospho-ERK and total ERK in control MCF10A and MCF10A-derived cells (as indicated) with and without EGF stimulation. Western blot analysis using α-actin served as a loading control. (B) Western blot analysis of CDK4, H-Ras, phosphorylated pRb (P-pRB), pRB, Cyclin D1, and p53 in asynchronously growing MCF10A and MCF10A-derived cells (as indicated). β-actin and QM are loading controls.

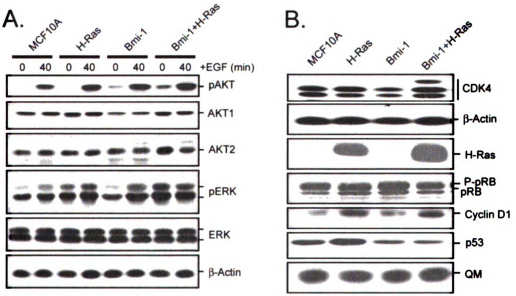

Figure 9: Late-passage H-Ras–expressing MCF10A cells exhibit transformed features. All MCF10A-derived cells were analyzed at passage 8. (A) Control MCF10A and MCF10A-derived late-passage cells (as indicated) were grown in soft agar to determine anchorage-independent growth potential of these cells. Cells were photographed (x4, final magnification) at day 14. (B) Three-dimensional growth of MCF10A–H-Ras (LP) and MCF10A–Bmi-1+H-Ras (LP) was analyzed using Matrigel assays as described in Materials and Methods. Cells in Matrigel were photographed (x10) at day 7. (C) EMT phenotype of MCF10A and MCF10A-derived late-passage cells was analyzed by immunostaining using antibodies specific for E-cadherin, vimentin, and fibronectin (as indicated). To visualize nuclei, cells were stained with 4',6-diamidino-2-phenylindole, and immunostained cells were visualized and photographed using Zeiss LSM510 UV META confocal microscope (x60). (D) EMT markers expressing in MCF10A and MCF10A-derived LP cells were analyzed by western blot analysis using antibodies specific for E-Cadherin, vimentin (lower bands), and fibronectin as described in materials and methods. α-tubulin is a loading control. (E) The migration potential of MCF10A and MCF10A-derived cells was determined by wound-healing assay. The control MCF10A, and Bmi-1–, H-Ras–, and Bmi-1+H-Ras–overexpressing MCF10A cells were grown to 80% confluence, starved in D3 medium for 48hr. A wound was made in the middle of culture dish containing near-confluent cells and the cells were stimulated with EGF-containing D medium for 15 h. Cells were photographed at 0 h, before adding D medium and at 15 h, after stimulating with D medium. Cells were photographed using a light microscope (x4).

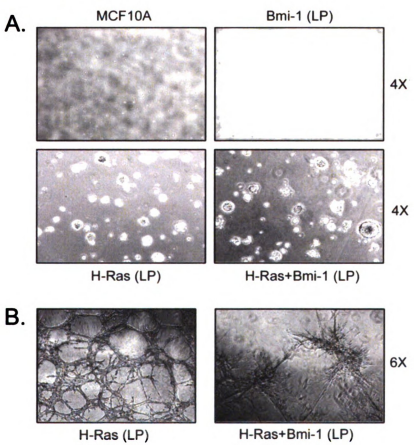

Figure 9 (continued)

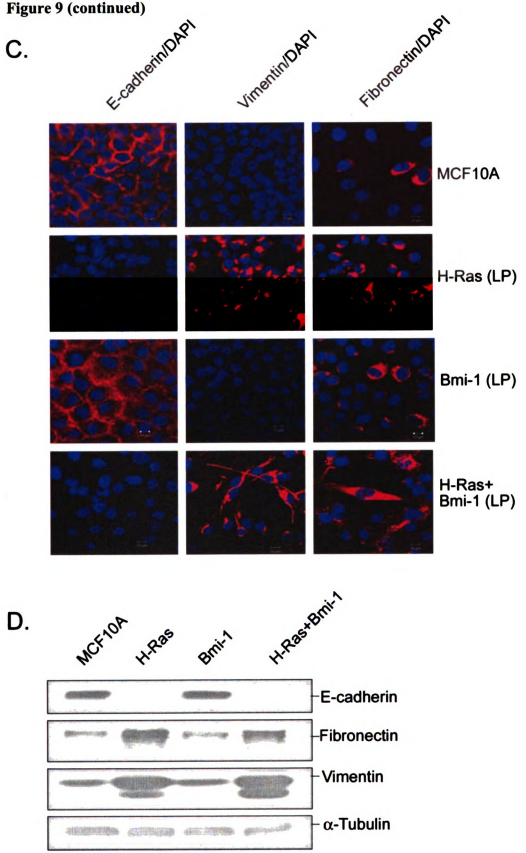

Figure 9 (continued)

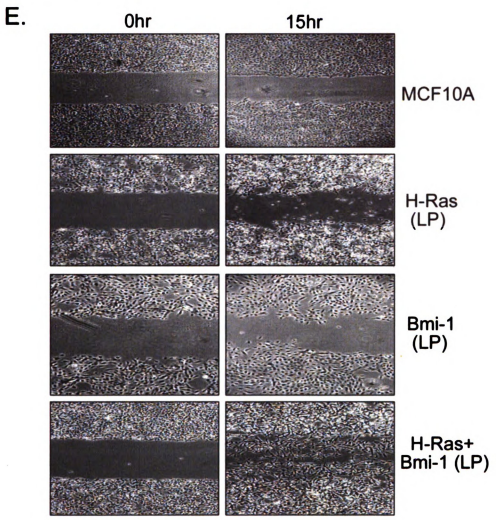

Figure 10: Expression level of H-Ras determines proliferation in MCF10A cells overexpressing H-Ras. (A) H-Ras expression in MCF10A control and MCF10A-derived early-passage (passage 2 after Ras selection) and late-passage cells (passage 8) was determined by Western blot and repeated four times. (B) To determine the relative expression of H-Ras in MCF10A and MCF10A-derived cells, its signal in each lane was quantified by densitometric analysis using ImageJ1.3 software (NIH) and normalized to α-tubulin signal. (C) H-Ras and Ki-67 co-immunostaining was done to determine proliferation in MCF10A-derived early-passage (passage 2) and late-passage (passage 8) cells. MCF10A cells were used as control because they do not express detectable Ras but are Ki-67 positive under our experimental conditions. Representative photos (60X magnification) of costaining in each cell line (as indicated). (D) Quantification of Ras- and Ki-67–expressing cells in MCF10A-derived early-passage (passage 2) and late-passage (passage 8) culture of H-Ras and Bmi-1+H-Ras cells. Co-staining was done in triplicates and a total of 100 to 200 stained cells were counted in multiple fields.

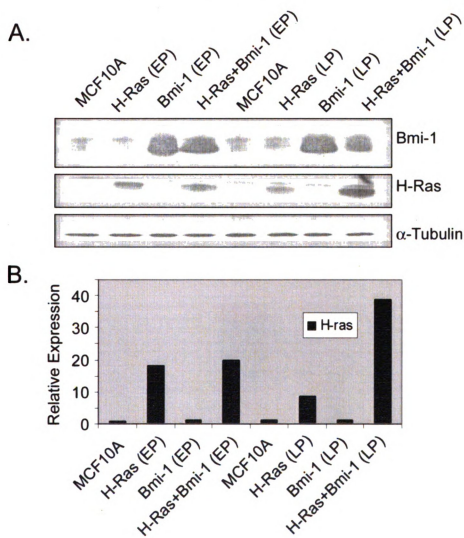

Figure 10 (continued)

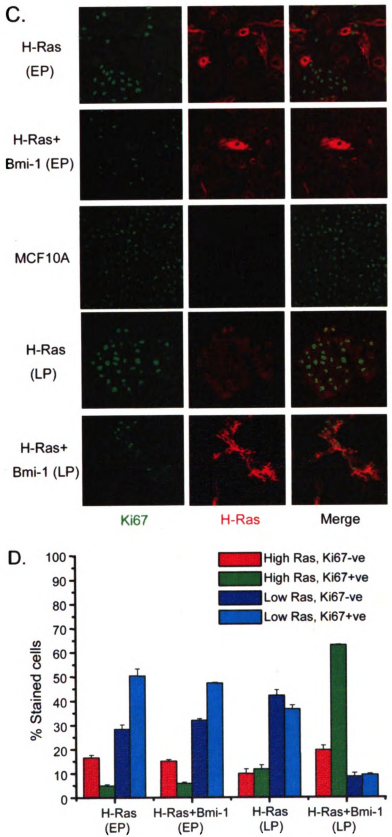

Figure 11: Gross morphology, histopathology, and immunohistochemistry of tumors originating from xenografts. (A) Gross morphology of tumors resulting from injection of MCF10A–H-Ras (LP) and MCF10A–Bmi-1+H-Ras cells (LP; as indicated). Left, tumors induced by MCF10A–H-Ras. Right, tumors induced by MCF10A–Bmi-1+H-ras cells. (B) Histopathology of tumors resulting from injection of MCF10A–H-Ras (left) and MCF10A–Bmi-1+H-Ras (right) cells. Left, tumors induced by MCF10A–H-Ras cells were composed of variable populations of poorly differentiated to well-differentiated endothelial cells forming haphazard vascular channels (top), spindle-shaped cells resembling smooth muscle (middle), and multiple variably-sized clusters of poorly-differentiated to well-differentiated mast cells (bottom) (Bar=100 μm). Right, tumors induced by MCF10A–Bmi-1+H-Ras cells were composed of a homogeneous population of sheets and intersecting bundles of poorly differentiated spindle cells (top) that infiltrated adjacent adipose tissue and bone (middle) (Bar=100 μm). Cells were poorly differentiated with large pleomorphic nuclei and frequent mitoses (bottom) (Bar=50 μm). (C) Histochemical and immunohistochemical staining of tumors induced by MCF10A–H-Ras (left) and MCF10A–Bmi-1+H-Ras (right) cells. Left, tumors induced by MCF10A–H-Ras were multifocally immunoreactive for antibodies against α-SMA and CD31; mast cell clusters were diffusely positive with Giemsa staining for mast cell granules, and tumors were diffusely negative for collagen by Masson's trichrome staining (Bar=100 μm). Right, tumors induced by MCF10A–H-Ras+Bmi-1 cells were diffusely negative for α-SMA and CD31 except for the presence of intratumoral capillaries (arrowheads), diffusely negative with Giemsa staining except for occasional resident mast cells (arrowhead), and showed very little collagen production with Masson's Trichrome (MT) stain (Bar=100 μm). (D) Kaplan-Meier survival curve. Whereas MCF10A and MCF10A–Bmi-1 xenografted mice did not develop tumors and survived throughout the course of the study, mice xenografted with MCF10A–H-Ras and MCF10A–Bmi-1+H-Ras had decreased survival after the development of palpable tumors. MCF10A–H-Ras xenografted mice had significantly decreased survival compared with MCF10A–Bmi-1+H-Ras mice ($P < 0.002$) (n=10 mice per group).

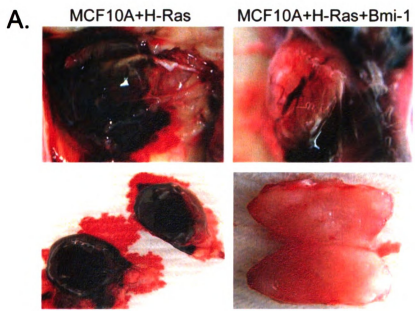

Figure 11 (continued)

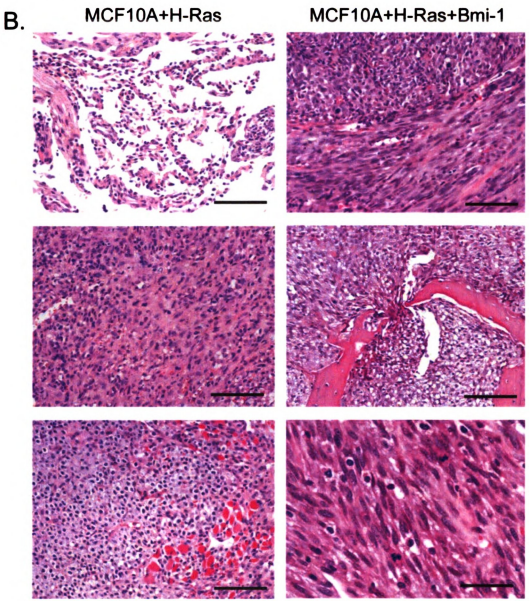

Figure 11 (continued)

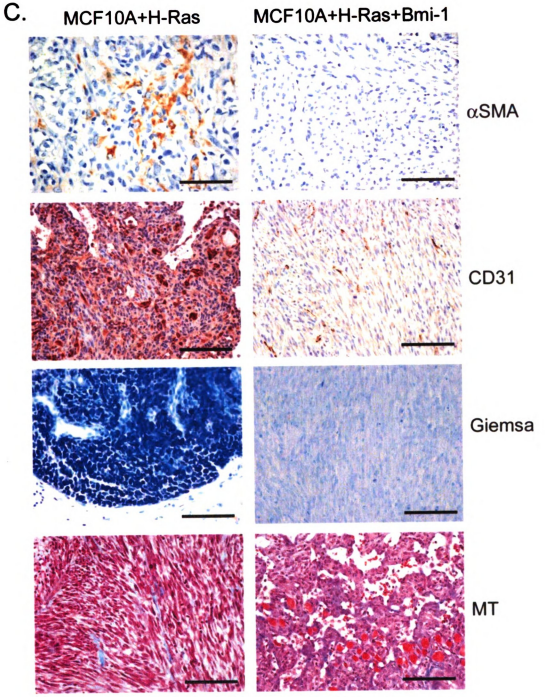

Figure 11 (continued)

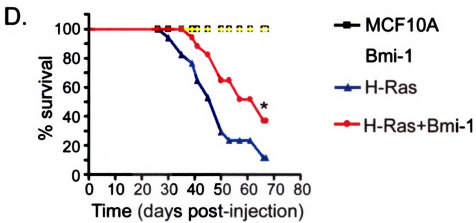

Figure 12: Analysis of p53 pathway in control MCF10A and MCF10A-derived late-passage cells. (A) Top, western blot analysis of Bmi-1, H-Ras, and p53 in control MCF10A and MCF10A-derived (LP) cells (as indicated) was done as described in Figure 2. Bottom, densitometric analysis of signals (of p53 and H-Ras) present in each lane was done, normalized to corresponding α-tubulin signal, and plotted to determine the expression levels of p53 and H-Ras as indicated. (B) Analysis of DNA damage response in MCF10A and MCF10A-derived late-passage cells. The cells were treated with camptothecin (CPT) for indicated amount of time, harvested, and analyzed by Western blot analysis for total p53, phosphorylated p53 (Ser-15 and Ser-37), p53 target genes (p21, PUMA, Bax, and PIG3), PRAK, and BCL2. ß-Actin was used as a loading control.

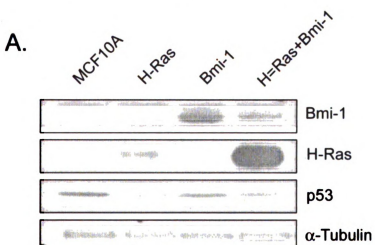

Figure 12 (continued)

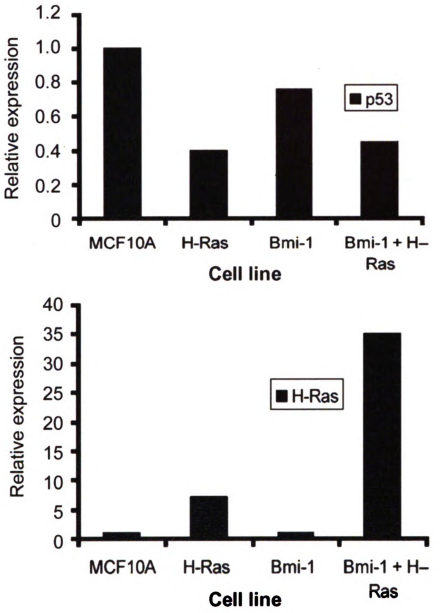

Figure 12 (continued)

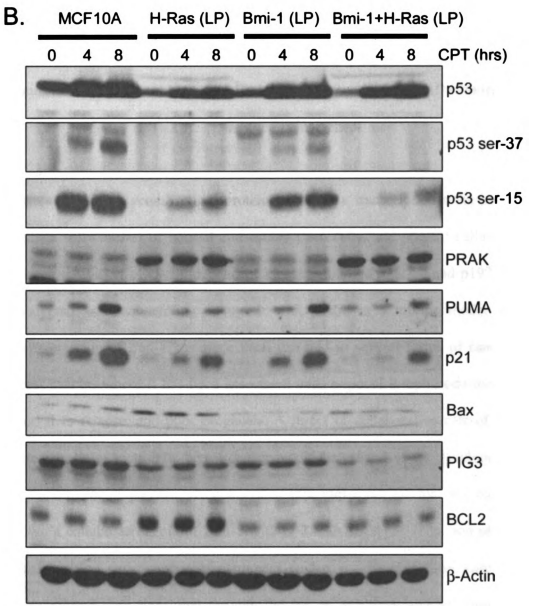

CHAPTER THREE

Bmi-1 and H-ras collaboration in mammary epithelial cells promotes an aggressive and metastatic phenotype, and Bmi-1 knockdown in xenograft tumors results in delayed tumor onset

Abstract: The polycomb group protein Bmi-1 is a transcription repressor reported to regulate self-renewal of normal and cancer stem cells, and prevent cellular senescence through inhibition of cyclin-dependent kinase inhibitors $p16^{Ink4a}$ and $p19^{ARF}$. Originally discovered as a cooperating oncogene with *c-Myc* in a murine model of leukemia, overexpression of *Bmi-1* has since been reported in several forms of cancer, including breast cancer, where it has been associated with regional lymph node metastasis, short interval to relapse, and poor prognosis. A direct or collaborative role of Bmi-1 in the pathogenesis of metastatic breast cancer would be critical in the development of novel biomarkers for diagnosis and treatment of this aggressive disease. We have previously shown a collaborative role of Bmi-1 with H-Ras exists in the induction of proliferation, transformation and invasion of mammary epithelial cells (MEC) in vitro and in vivo. These current data show that through the use of xenograft and tail vein experiments, simultaneous overexpression of Bmi-1 and H-Ras in MCF10A mammary epithelial cells promotes proliferation and invasion, and inhibits apoptosis due to detachment from the extracellular matrix, greatly potentiating a metastatic phenotype to the liver, spleen, and brain in vivo. These findings suggest that overexpression of Bmi-1 in conjunction with H-Ras overexpression results in greater metastatic potential. Additionally, we show that

knockdown of Bmi-1 in several breast cancer cell lines leads to decreased proliferation and invasion, and increased apoptosis in response to DNA damage induced by etoposide. Furthermore, knockdown of Bmi-1 expression delays tumor onset in two mammary fat pad xenograft models. These results suggest that Bmi-1 plays an important role in the behavior of several breast cancer cells lines, and may be an important marker for diagnosis and a target for the treatment of aggressive breast cancer.

Introduction

Cooperation between oncogenes to produce neoplasia is a well-documented occurrence in many types of human cancers [70-72]. Whether resulting from a combination of proliferative or of anti-apoptotic effects from overexpression of multiple oncogenes, or the abrogation of tumor suppressor genes, the process of oncogenesis commonly involves mutations of multiple genetic loci. Bmi-1 is a member of a group of transcription repressors called polycombs that inhibit transcription of various homeobox genes that are critical for body plan establishment and morphogenesis [20, 28, 113]. Through epigenetic mechanisms, it is possible that Bmi-1 may interact with various genetic loci and exert a suppressive effect on gene transcription throughout the genome. It has been shown that Bmi-1 is critical in the maintenance of stem cell populations by preventing senescence through suppression of the Ink4a-Arf tumor suppressor locus [18, 27, 150]. By suppressing this locus, the effects of the cyclin-dependent kinase inhibitors p16 and p19 are abrogated, resulting in prevention of p53 degradation and phosphorylation of retinoblastoma (Rb), respectively [18, 27, 150]. This results in prevention of cell cycle arrest and the resultant cellular senescence and apoptosis.

Therefore, if dysregulated or overexpressed, Bmi-1 may act as an oncogene through the suppression of gene transcription of tumor suppressor genes. In fact, Haupt et al. (1991) initially described Bmi-1 as a cooperating oncogene in a Eμ-myc murine model of B-cell lymphomagenesis, as a result of retroviral induced mutagenesis by the Moloney murine leukemia virus. It was found that Bmi-1 was a frequent target of retroviral insertional mutagenesis, and its resultant overexpression in this model increased lymphomagenesis by 75% [52, 83].

Since its discovery, Bmi-1 has also been implicated in the development of many different types of human cancers, including nasopharyngeal [37], liver [43], colorectal [44], brain [40], lung [41], and breast cancer [47]. One study has shown that Bmi-1 overexpression correlates with prognosis and regional lymph node metastasis in patients with infiltrative ductal carcinoma [47]. Given the collaborative role Bmi-1 plays with c-myc in lymphomagenesis, the following studies were undertaken to determine the relationship of Bmi-1 with protooncogenes commonly overexpressed in breast cancer (H-Ras) and its relationship in the pathogenesis of breast cancer metastasis.

The MCF10A (M1) cell line was derived as a non-transformed breast epithelial cell line derived from the spontaneous immortalization of normal breast epithelial cells obtained from a patient with fibrocystic disease [99]. In vitro, this cell line forms plates of polygonal cells with well differentiated cell-to-cell junctions and has a relatively low rate of proliferation. In vivo, injection of these cells into the mammary fat pad results in a small residual population of well differentiated mammary ductal structures and epithelium, but does not result in tumorigenesis [99, 179]. These cells are commonly used

to represent the behavior of normal mammary epithelial cells, and are commonly used in the study of mammary gland biology.

In this study, we used MCF10A cell lines engineered to overexpress Bmi-1 (MCF10A+Bmi-1), H-Ras (MCF10A+H-Ras), and Bmi-1 in combination with H-Ras (MCF10A+H-Ras+Bmi-1), to characterize the effects of overexpression of these oncogenes alone and in combination on the behavior of mammary epithelial cells in vitro and in vivo, including the ability to survive and establish metastasis in distant sites, either spontaneously or by introduction via tail vein injection. Our results demonstrate that Bmi-1 collaborates with H-Ras in the induction of an aggressive cell phenotype in vitro and in vivo, with a greatly increased metastatic propensity to distant sites. These data suggest that Bmi-1 may be an important target for diagnosis and treatment of aggressive breast cancer.

Materials and Methods

Cell lines, vectors, and plasmids. MCF10A+H-Ras and MCF10A+H-Ras+Bmi-1 cells were cultured in Dulbecco's modified eagle medium supplemented with 5% horse serum (Gibco, Carlsbad CA), penicillin/streptomycin (Gibco), human recombinant insulin (10 μg/ml, Gibco), epidermal growth factor (EGF) (20 ng/ml, Upstate), choleratoxin (100 ng/ml, Sigma), and hydrocortisone (500 ng/ml, Sigma, St. Louis MO). MDA-MB-231 and MCF7 cells were grown in DMEM high glucose 1X (Gibco) supplemented with 10% fetal bovine serum (FBS) (Gibco), and penicillin/streptomycin (Gibco). ZR75-1 cells were grown in RPMI 1640 with 2 mM L-glutamine (Gibco) supplemented with 10% FBS (Gibco), penicillin/streptomycin (Gibco), sodium bicarbonate (1.5 g/L, Gibco), glucose (4.5 g/L, Sigma), HEPES (10 mM, Gibco), and sodium pyruvate (1 mM, Gibco). Bmi-1

shRNA lentiviral vector (LV-pLL3.7+Bmi-1i) and empty shRNA lentiviral vector (LV-pLL3.7) were kindly provided by Max Wicha and have been described previously [35]. The shRNA lentiviral vectors LV-pLL3.7+Bmi-1i and LV-pLL3.7 were used to transfect 293T packaging cells, and viral supernatant was used to transduce each of four cell lines (MDA-MB-231, ZR75, MCF7 and MCF10A+H-Ras+Bmi-1). Significant knockdown of Bmi-1 was confirmed by western blot.

Western blot analysis. Bmi-1 was detected using F6 mouse monoclonal antibody (mAb) from Upstate Cell Signaling Solutions (Charlottesville, Virginia), and H-Ras was detected using the F-235 mouse monoclonal antibody from Santa Cruz Biotech, Santa Cruz, CA, as previously described [118].

Cell proliferation, apoptosis, and invasion assays. Cell proliferation assays were performed using the Cell Titer 96® Aqueous MTS-formazan proliferation assay (Promega, Madison WI). Cells were cultured in a 96-well plate at $1X10^3$ cells per well (with eight repeats), and growth curves were established by measuring the absorbance at 490 nm at 24 hr time intervals following the addition of 20µl of MTS reagent. The MTS reagent is converted by proliferating cells into a formazan dye that is read colorimetrically on a spectrophotometer at 490nm. The absorbance reading corresponds with the number of viable proliferating cells in the assay.

Apoptosis assays were performed using the Cell Death Detection ELISA^{PLUS} sandwich ELISA (Roche, Indianapolis IN). Cells were cultured in a 96 well plate at $1X10^3$ cells per well (with eight repeats) for 24 hours, then etoposide was added.

Apoptosis was measured following treatment of each cell line with 100 mM etoposide at 12 and 24 hr for MCF10A-derived cell lines and 48 hr for siRNA-induced cell lines. Cells were lysed with 200µl of lysis buffer, and following centrifugation, 20µl of supernatant was added to a strepavidin-coated 96-well plate containing 80ul immunoreagent (anti-histone biotin and anti-DNA-horseradish peroxidase) and incubated for two hours. During incubation, the anti-histone antibody binds to the histones contained in nucleosomes in each sample, and also binds the entire complex to the streptavidin-coated plate by biotinylation. The anti-histone antibody reacts with histones H1, H2A, H2B, H3, and H4 from several different species (man, mouse, rat, hamster, cow), and the anti-DNA-horseradish peroxidase binds to single- and double-stranded DNA. ABTS substrate is added to visualize the anti-DNA-horseradish peroxidase, and the amount of nucleosomes remaining in the sample (apoptosis) correlates with the absorbance measurement at 490nm of the horseradish peroxidase retained in the complex.

Invasion assays were performed using the BD Matrigel invasion chamber assay (BD Bioscences, Bedford MA) for the overexpression experiments, or the CytoSelect™ 24-well Cell Invasion Assay (Cell Biolabs Inc, San Diego CA) for the shRNA knockdown experiments. Cells were cultured in a 24-well Boyden chamber format. Boyden chambers are composed of an insert well containing a membrane with 4µm pores, overlain with Matrigel basement membrane extract. Cells were cultured at $1X10^3$ cells per chamber in serum-free media, and inserts were placed in a 24 well plate containing 10% fetal bovine serum to establish a chemoattractant serum gradient. Invasion was measured either manually and expressed as a percentage of invading cells (overexpression experiments) or measured colorimetrically using a spectrophotometer

(shRNA knockdown experiments). For manual measurement of invasion, cells were stained with 400ul of crystal violet and membranes were excised from the Boyden chambers and mounted on microscope slides. Invasion was measured as the number of cells present on the underside of the membrane (able to migrate through the Matrigel matrix and 4μm pores) of the Matrigel inserts compared to the number of cells present on the underside of control inserts (migrating through 4μm pores alone). For colorimetric measurements, cells were stained with crystal violent and then lysed from the membrane with 200ul lysis buffer. Then 100ul of lysate per sample was measured colorimentrically as absorbance on a spectrophotometer at 490nm. The absorbance measurement corresponds with the number of cells that migrated through the Matrigel and/or control inserts. Overexpression experiments were measured manually and shRNA knockdown experiments were measured colorimetrically. For statistical analysis of proliferation, apoptosis, and invasion assays, one-way ANOVA was performed on MCF10A derived cells (comparing four cell lines), and T-tests were performed on shRNA-induced cell lines (knockdown compared to empty vector control).

Animals, necropsy, and histopathology. We established six cohorts composed of 10 six-week-old female SCID mice (NCI Frederick, MD). Mice from each cohort were injected in the right axillary mammary fat pad with 1×10^6 cells from one of the previously described cell lines (MCF10A+H-Ras, MCF10A+H-Ras+Bmi-1, MCF10A+H-Ras+Bmi-1+Bmi-1i, MCF10A+H-Ras+Bmi-1+pLL3.7, MDA-MB-231+Bmi-1i, MDA-MB-231+pLL3.7). Tumor growth was measured weekly by caliper. Additionally, six cohorts of 10 six-week-old female mice each were injected with 1×10^6

cells via the tail vein. Mice were followed for six weeks for signs of clinical illness (weight loss, decreased body weight, roughened haircoat, difficulty breathing). Mice injected in the mammary fat pad were humanely euthanized by CO_2 asphyxiation once tumors reached 2 cm in diameter, or when mice became clinically ill. Tail vein injected mice were euthanized by CO_2 asphyxiation once clinical symptoms of weight loss, roughened hair coat, rapid respiration, or hunched posture were noted. All animal work was performed following NIH guidelines under an approved animal protocol. Following euthanasia, tumor (intramammary fat pad injected mice), brain, lung, heart, liver, spleen, and kidney from intramammary fat pad injected mice were collected, either frozen in OCT freezing medium or fixed in 4% paraformaldehyde (PFA), processed into paraffin blocks, sectioned at 4 μm, and stained with hematoxylin and eosin (H&E). Sections of tumors were snap frozen in liquid nitrogen for further protein and RNA analysis. Selected areas were photographed using an Olympus DP70 (Olympus) digital camera. Statistical analysis of tumor growth was analysed using a Two-Way ANOVA with a Bonferroni test for multiple comparisons.

Results

Bmi-1 and H-Ras collaborate to transform MCF10A human mammary epithelial cell phenotype in vitro. Overexpression of Bmi-1 or H-Ras alone and in combination markedly altered MCF10A morphology (Figure 13A-E). MCF10A cells were polygonal to polyhedral, with abundant cytoplasm and large round centralized nuclei, and grew in plates with clear cell-to-cell junctions (A). Overexpression of Bmi-1 resulted in a spindle-shaped morphology, without cell-to-cell contact (B). H-Ras overexpression resulted in rounded, triangular, and tear-drop shaped cells (C), whereas overexpression of H-Ras and

Bmi-1 together resulted in a more pronounced spindle-shaped phenotype, with thin cell processes often radiating from central clusters (D). After several passages in culture, MCF10A+H-Ras+Bmi-1 cells began to form spherical structures that detach and float freely in culture (E), similar to mammospheres that occur in suspension culture and have been shown to be enriched for stem cells. These structures remained viable in non-adherent culture, and when disassociated and re-cultured on adherent substrata, returned to an adherent phenotype; however, additional spheroid structures formed more readily on subsequent passages (Data not shown).

In three dimensional Matrigel culture, MCF10A cells formed round clusters with central cells undergoing apoptosis to form a central lumen, and well-polarized cells around this central lumen (Figure 14A). This phenotype is used to represent normal differentiation of human mammary epithelial cells into a luminal phenotype [159]. When Bmi-1 or H-Ras were overexpressed alone, clusters remained disorganized, without central lumen formation or polarization of cells (Figure 14B-C), indicating a block in the normal MCF10A differentiation. With Bmi-1 and H-Ras co-overexpression, cells grew in haphazard, highly disorganized and proliferative masses with a somewhat spindle-shaped morphology and frequent mitoses (D), indicating loss of differentiation as well as a highly proliferative phenotype. Phalloidin staining for f-actin with a DAPI overlay better illustrates the structure of these clusters by confocal microscopy in Figure 14A.

Bmi-1 cooperates with H-Ras to significantly increase cell proliferation and invasion, and inhibit apoptosis in MCF10A cells. Using the Cell Titer 96 Aqueous MTS-formazan proliferation assay, overexpression of H-Ras alone in MCF10A cells

resulted in a statistically significant increase ($p < 0.01$) in proliferation in comparison to parental MCF10A cells at 1 and 3 days (Figure 15A). At two days, overexpression of Bmi-1 or H-Ras alone led to a statisitically significant increase in proliferation over MCF10A alone ($p < 0.01$), and concurrent overexpression of both Bmi-1 and H-Ras resulted in statistically significant increase in proliferation over all cell lines at all time points ($p < 0.01$). Conversely, overexpression of Bmi-1 or H-Ras in MCF10A cells led to a statistically significant decrease in apoptosis in response to DNA damage due to etoposide treatment compared to MCF10A cells alone, and concurrent overexpression of Bmi-1 and H-Ras led to a further statistically significant decrease in apoptosis ($p < 0.01$) at 12hr. At 24hr, overexpression of Bmi-1 alone or in combination with H-Ras resulted in a statisitically significant decrease in apoptosis ($p < 0.05$), in comparison to MCF10A or MCF10+H-Ras cells (Figure 15B). The ability of the cell lines to degrade and migrate through extracellular matrix was measured using the CytoSelect™ 24-well Cell Invasion Assay (Cell Biolabs Inc, San Deigo CA). While MCF10A cells have negligible invasive capability in Matrigel (measured as the number of cells that migrated through the Matrigel barrier), MCF10A cells overexpressing Bmi-1 (+Bmi-1) or H-Ras (+H-Ras) had an 11% and 12% increase in invasion compared to MCF10A cells, and concurrent overexpression of Bmi-1 and H-Ras in MCF10A cells (+H-Ras+Bmi-1) caused a further three-fold increase in invasion ($p < 0.05$) (Figure 15C).

Reduction in Bmi-1 results in decreased proliferation and increased apoptosis in vitro. In order to confirm that overexpression of Bmi-1 in the MCF10A-derived cells was directly related to proliferation and apoptosis, short hairpin RNA (shRNA) for Bmi-1 was

used to reduce the expression of Bmi-1 in four cell lines that overexpress Bmi-1: MCF10A-Bmi-1+H-Ras, MCF7, MDA231, and ZR75-1. MCF10A-Bm-1+H-Ras cells were used as proof of principle as these cells show increased proliferation and decreased apoptotic response in vitro in comparison to MCF10A, MCF10A-Bmi-1 and MCF10A-H-Ras cells alone. Utilizing the Cell Titer 96® Aqueous MTS-formazan proliferation assay (Promega, Madison WI), proliferation of cells transduced with LV-pLL3.7+Bmi-1i was statistically significantly decreased in comparison to cells transduced with empty vector alone (LV-pLL3.7) (Figure 16A-D). Decreased proliferative indices in cells transduced with siRNA for Bmi-1 suggests that Bmi-1 is partially driving the proliferation of these human established breast cancer cell lines in vitro.

To assess the apoptotic response to DNA damaging agents, each cell line was treated with 100 μM etoposide for 24 hours, after which apoptosis was measured using the Cell Death Detection ELISA^{PLUS} (Roche, Indianapolis, IN). For the MDA231, ZR75-1, and MCF7 cell lines, there was a trend towards an increase in the apoptotic response to etoposide in cells transduced with siRNA for Bmi-1 (Figure 17A), suggesting that the expression of Bmi-1 in these established breast cancer cell lines confers a resistance to apoptosis induced by DNA damaging agents, consistent with our previous findings [118]. Finally, the CytoSelect™ 24-well Cell Invasion Assay (Cell Biolabs Inc, San Deigo CA) was used to assess the effect of Bmi-1 knockdown on invasion. In three of four cell lines tested, depression of Bmi-1 led to a decrease in invasion (Figure 17B). Together, these data show that Bmi-1 plays a role in proliferation, invasion, and resistance to apoptosis in breast cancer cell lines in vitro.

Bmi-1 increases metastatic propensity and incidence. We examined the ability of each of the four above cell lines to develop spontaneous metastases from a primary tumor. As in our previous data, whereas MCF10A and MCF10A+Bmi-1 cells did not form primary tumors, MCF10A+H-Ras and MCF10A+H-Ras+Bmi-1 cells produced primary tumors in 100% of xenografted animals [118]. In MCF10A+H-Ras xenografted animals, micro- and macro-metastases were only observed in the livers in 5/10 (50%) and in the spleens of 4/10 (40%) of the mice. In contrast, metastasis to both the spleens and livers were observed in 10/10 (100%) of MCF10A+H-Ras+Bmi-1 xenografted animals (Figure 18). Interestingly, spontaneous brain metastasis was found in 3/10 (30%) of MCF10A+H-Ras+Bmi-1 xenografts, whereas no spontaneous metastases to the brain were found in any of the MCF10A+H-Ras xenografted mice. The study of brain metastasis has been limited by the lack of cell lines and mouse models that reliably reproduce the metastatic disease seen in humans [180]. These data show a striking prevalence for brain metastasis as a result of the overexpression of Bmi-1 in collaboration with H-Ras overexpression, making it a very important target in the study of metastatic disease and aggressive breast cancer. These data support an increased propensity towards spontaneous metastasis to the spleen and liver, and novel metastasis to the brain, in cells overexpressing both H-Ras and Bmi-1, suggesting a role in increased metastasis due to Bmi-1 overexpression.

Tail vein injection of MCF10A+H-Ras+Bmi-1 resulted in fulminant pulmonary tumors, whereas injection of other cell lines did not. To further characterize the ability of these cell lines to escape anoikis, embolize, and develop metastatic foci at distant sites, we utilized the tail vein injection technique to introduce the cells directly into the venous

circulation. A significant decrease in weight was observed over a five week period following the tail vein injections in the MCF10A+H-Ras+Bmi-1 cohort. Collectively, these animals lost approximately 30% of their body weight during this period, whereas the body weight of all other cohorts remained stable (Figure 19A) and the mice remained clinically normal. The MCF10A+H-Ras+Bmi-1-injected mice developed a roughened haircoat, hunched posture, and elevated respiratory rate. At necropsy, fulminant gross metastases were evident involving large portions of all lung lobes of MCF10A+H-Ras+Bmi-1 injected mice at 4-5 weeks (Figure 19B). In contrast, lungs of MCF10A+H-Ras injected mice were grossly unremarkable at 4-5 weeks. Histologically, at 14-16 weeks, MCF10A+H-Ras injected mice had small (1-2mm), expansile, non-infiltrative, well-differentiated adenomatous lesions. In contrast, at 4 weeks, pulmonary metastases in the MCF10A+H-Ras+Bmi-1 injected mice were composed of sheets and bundles of poorly-differentiated spindle-shaped cells with large pleomorphic nuclei and a high mitotic rate (2-4/hpf), and effaced large portions of the normal pulmonary architecture (Figure 19C). These data support the above data that Bmi-1 as an important mediator in the development and progression of metastatic disease in H-Ras transformed cells.

Bmi-1 knockdown in MCF10A+H-Ras+Bmi-1 mammary fat pad xenografts slows tumor progression, but does not alter phenotype. To investigate whether Bmi-1 depression in MCF10A+H-Ras+Bmi-1 cells would slow progression of cell growth in vivo, we used the previously engineered MCF10A+H-Ras+Bmi-1 cells expressing empty vector (pLL3.7) or shRNA for Bmi-1 (Bmi-1i) for mammary fat pad xenograft experiments. While the histologic phenotype of neither mammary fat pad nor intravenous

MCF10A+H-Ras+Bmi-1 tumors was altered by knockdown of Bmi-1 (Figure 20A), at approximately 20-25 days post-injection, there was a statistically significant decrease in tumor volume in the xenograft group expressing shRNA for Bmi-1 (Figure 20B), that persisted until the end of the study ($p < 0.05$, Two-Way ANOVA with Bonferroni correction). Persistent knock-down of Bmi-1 in these tumors was confirmed by western blot (Figure 22). These data confirm the results of our previous xenograft experiments, and suggests that the collaboration of Bmi-1 and H-Ras may be important during the early development of some tumors.

Bmi-1 knockdown in MCF10A+H-Ras+Bmi-1 intravenous xenografts does not alter metastatic disease or phenotype. There was no significant difference in onset or progression of clinical signs (weight loss, roughened haircoat, hunched posture, rapid respiration) or in ultimate metastatic burden between tail vein xenografts expressing empty vector and those with Bmi-1 knockdown. Additionally, there was no significant difference in histologic phenotype between the groups (Figure 20A).

Bmi-1 knockdown in MDA231 xenografts does not alter metastatic incidence or tumor phenotype, but slows onset of primary tumor formation. The mammary fat pad and intravenous xenograft experiments were repeated with MDA231 cells expressing empty vector or shRNA for Bmi-1. In the mammary fat pad xenografts, there was no significant difference in primary tumor growth or spontaneous metastasis between xenografts expressing empty vector and those with knockdown of Bmi-1. Additionally, there was no significant difference between the histologic phenotype of mammary fat pad

xenografts expressing siRNA for Bmi-1 and those expressing empty vector (Figure 21A). However, there is a significant delay in the onset of primary tumor formation in tumors with Bmi-1 knockdown (Figure 21B). By days 49 and 56 post-injection, 60% ($p < 0.05$) and 70% ($p < 0.01$) of animals with MDA-MB-231 xenografts transfected with empty vector, respectively, developed palpable tumors, whereas only 10% of animals with xenografts transduced with shRNA for Bmi-1 had tumors at either time point (Two-way ANOVA). In the tail vein xenografts, there was no significant difference in metastatic disease between MDA231 tail vein xenografts expressing empty vector and those with knockdown of Bmi-1, and the histologic phenotype remained the same between groups (Figure 21A). Mammary fat pad tumors were harvested for protein analysis, and knockdown was confirmed by western blot (Figure 22).

Discussion

Our previous work has demonstrated that Bmi-1 cooperates with H-Ras to transform human mammary epithelial cells through the dysregulation of multiple growth regulatory pathways, including the AKT and MAPK/ERK pathways, and cell cycle mediators CDK4 and cyclin D [118]. This is consistent with our findings that overexpression of Bmi-1 and H-Ras leads to increased proliferative rates, and that co-overexpression of both oncogenes results in a further significant increase in proliferation. Furthermore, we have shown that overexpression of Bmi-1 or H-Ras in MCF10A cells confers a protective advantage against apoptosis in response to the DNA-damaging agent etoposide. We have previously shown that MCF10A+Bmi-1+H-Ras have the highest migratory potential in vitro when compared to MCF10A, MCF10A+Bmi-1, and

MCF10A+H-Ras using a wound-healing assay [118]. Given this increased migratory potential, and a spindle shaped morphology characteristic of an EMT phenotype which is closely linked to migration and invasion, we performed a Matrigel invasion assay to determine the invasive capacity of these cells. Compared to MCF10A cells, which have no invasive capability, our data show that H-Ras and Bmi-1 overexpression causes a significant increase in invasion of MCF10A cells, and that combined overexpression causes a further significant increase in this invasive capability. Therefore, our data suggest that overexpression of Bmi-1 and H-Ras causes MCF10A cells to acquire an increased invasion potential consistent with highly transformed HMECs.

Using intramammary fat pad injections in a SCID xenograft model, we showed that Bmi-1 overexpression alone in MCF10A cells was not sufficient to transform HMECs, whereas overexpression of H-Ras alone and in combination with Bmi-1 was [118]. Interestingly, the gross and histologic morphology of tumors from each group were strikingly different; tumors arising from MCF10A cells overexpressing H-Ras were grossly variably cystic and hemorrhagic, composed of vascular, smooth muscle, and mast cell elements, while tumors arising from MCF10A cells overexpressing both H-Ras and Bmi-1 were grossly solid and homogeneous on cut surface, and histologically were composed of locally infiltrative streams and bundles of poorly differentiated spindle-shaped cells with atypical features and a high mitotic rate. Thus, overexpression of Bmi-1 in the face of H-Ras overexpression leads to a more poorly differentiated, more aggressive phenotype.

The current data show that the overexpression of Bmi-1 concurrently with H-Ras overexpression leads to an increased incidence of spontaneous metastasis to the liver and

spleen, and novel metastases to the brain, in comparison to H-Ras overexpression alone in severe combined immunodeficient (SCID) mice. Overexpression of Bmi-1 has been associated with increased incidence of spontaneous regional lymph node metastasis in human gastric cancer [181], breast cancer [47, 182], and melanoma [183]. In addition, Bmi-1 has recently been associated with an 11-gene microarray signature indicative of short interval to disease recurrence, metastasis, and poor response to therapy in prostate, breast, lung, ovarian, and bladder tumors, as well as lymphoma, mesothelioma, medulloblastoma, glioma, and acute myeloid leukemia [184]. This is consistent with our xenograft data showing increased propensity of metastasis to liver, spleen, and brain. However, increased metastasis to regional lymph nodes was not seen in our model. This may be due to certain limitations with xenograft models, including impaired immune responses in immunocompromised mice, the lack of a humanized stromal component in the murine mammary gland, or because human cells are not fully adapted to growth in mice [185]. However, in our xenograft model, metastasis to the brain is of particular interest, because there are few reliable models of spontaneous brain metastasis, and this is a very important route of metastasis in human breast cancer. The incidence of clinical brain metastasis in human breast cancer is approximately 10% [186], and nearly 30% of patients with metastatic breast cancer have post-mortem evidence of metastasis to the brain [187, 188]. Furthermore, using tail vein injections as a model for direct hematogenous spread, we have shown that pulmonary tumors developed rapidly and early (4-5 weeks) in the MCF10A+H-Ras+Bmi-1 xenografts, but were still not grossly evident until 14-15 weeks in MCF10A+H-Ras xenograft mice. This shows that overexpression of Bmi-1 in conjunction with H-Ras overexpression leads to the rapid

development of fulminant pulmonary metastasis leading to clinical illness, whereas overexpression of H-Ras alone is not capable of inducing significant embolic pulmonary metastasis. This is consistent with behavior of the MCF10A derived lines of cells developed by Miller *et al.* Miller *et al.* (1993) derived the MCF10A immortalized normal (non-transformed) breast epithelial cell line from a patient with fibrocystic disease. Similar to the MCF10A+H-Ras cell line used in our experiments, MCF10At1k cells were subsequently created by stable transfection with the neomycin-resistance gene and the mutated T-24 *Ha-ras* gene [99, 189]. These cells form premalignant lesions that rarely progress to carcinomas when injected into the mammary fat pad, and do not populate the lung on tail vein injection [179]. Similar to Miller's MCF10At1k cell line, our MCF10A+H-Ras cell line does not result in significant pulmonary metastasis. This indicates that phenotype of severe pulmonary metastasis is related solely to the combination of overexpression of Bmi-1 and H-Ras, since cells overexpressing Bmi-1 alone do not form tumors on tail vein injection. These data demonstrate that the collaboration of Bmi-1 with H-Ras plays an essential role in the development of distant metastasis from a primary tumor, and that this collaboration is essential in the metastatic survival and growth of MCF10A HMECs in vivo. Additionally, these data suggest that breast cancers that overexpress both H-Ras and Bmi-1 may be more metastatic.

Lastly, we wanted to determine the importance of Bmi-1 in the behavior of established human breast cancer cell lines overexpressing Bmi-1. It has been shown that several breast cancer cell lines overexpress Bmi-1, and that overexpression of Bmi-1 induces telomerase activity and extends the replicative lifespan of mammary epithelial cells [29]. This would suggest that Bmi-1 overexpression may exert its effects on

telomerase in parental breast cancer cell lines that overexpress the protein. Thus, knockdown of Bmi-1 expression would potentially have a negative impact on the proliferative capacity of Bmi-1-overexpressing breast cancer cell lines. To address this question, we used small interfering RNA (siRNA) specific for Bmi-1, and achieved substantial knockdown of Bmi-1 expression at the protein level in the MCF10A-Bmi-1+H-Ras cells, as well as three established breast cancer cell lines (MCF7, ZR75-1, and MDA-MB-231) based upon their relatively high levels of protein expression. In vitro, through the use of MTS-formazan proliferation assays, we have shown that by decreasing the expression of Bmi-1 in these cell lines, rates of proliferation decreased significantly ($p < 0.05$) in comparison with empty vector controls. This is consistent with our previous findings that overexpression of Bmi-1 in collaboration with H-Ras overexpression dysregulates multiple growth pathways, including the ERK/MAPK and Akt pathways, and upregulates cell cycle mediators such as CDK4 and cyclin D [118].

Conversely, using an anti-histone sandwich ELISA to measure apoptosis in response to etoposide, we have shown that cell lines transduced with siRNA for Bmi-1 are more sensitive to apoptosis as a result of DNA damage, thus suggesting that Bmi-1 confers resistance to apoptosis, either as a result of cell cycle checkpoint regulation through p53 dependent pathways, or by influencing DNA repair. Indeed, it has been shown that Bmi-1 suppresses the Ink4a/Arf tumor suppressor locus, which encodes for p16 and p19, and that suppression of the locus leads to inhibition of retinoblastoma phosphorylation and p53 degradation, respectively, leading to inhibition of cell cycle arrest and resultant apoptosis or cellular senescence [18, 27, 30]. Additionally, we have

shown that Bmi-1 confers a protective effect against oncogene-induced senescence and apoptosis [118].

In human patients, overexpression of Bmi-1 has been correlated with metastatic disease in several types of cancer [184], and has been associated with regional lymph node metastasis in breast cancer [47]. Consistent with this, our data show that by depressing Bmi-1 expression in certain breast cancer cell lines, the ability of these cells to degrade and migrate through Matrigel is compromised in vitro. Taken together, our results suggest that by knocking down Bmi-1 expression, rates of proliferation, resistance to apoptosis, and invasive capability decrease in established breast cancer cell lines.

Next we sought to determine if decreasing the expression of Bmi-1 in established breast cancer cell lines would lead to altered biologic behavior. The MDA-MB-231 breast cancer cell line is an aggressive established cell line that forms tumors in vivo and has metastatic behavior in both intra-mammary fat pad and tail vein xenograft animal models [190]. Since we hypothesized that depressing Bmi-1 expression in xenografts would lead to a less aggressive phenotype, we used this cell line and the MCF10A+H-Ras+Bmi-1 cell line to evaluate for any decrease in tumor burden or metastatic disease in mammary fat pad and tail vein xenograft models.

In the MCF10A+H-Ras+Bmi-1 xenograft experiments, there was no difference in tumor incidence or phenotype in mammary fat pad or intravenous xenografts. The lack of difference in tumor incidence may be in part an effect of continual Bmi-1 expression in the face of H-Ras overexpression. The overexpression of Bmi-1 in these cells may be too great to overcome with the applied shRNA for Bmi-1. Likewise, the phenotype was unable to be reverted to the previously shown MCF10A+H-Ras phenotype [118], likely

due to the effects of continued Bmi-1 expression, although at lower levels, suggesting that Bmi-1 can act as a potent oncogene even when depressed to some degree. However, there was a significant effect on primary tumor progression in the mammary fat pad xenograft model, where animals with tumors expressing shRNA for Bmi-1 had a statistically significant decrease in tumor volume over time that persisted until the end of study. This is an important biological indication that, when overexpressed in vivo, one of the main functions of Bmi-1 is to exert a powerful proliferative effect on mammary epithelial cells. The fact that all animals ultimately still developed mammary tumors may be due to the possibility that the overexpression of Bmi-1 is still too great in the face of shRNA expression, or that the collaborative effect of H-Ras induced proliferation is affecting the tumor cell biological behavior.

In the MDA-MB-231 cell line, shRNA knockdown of Bmi-1 had no significant affect on tumor growth over time, incidence of spontaneous or tail vein-induced metastasis, or histologic phenotype. This may be due to several factors. First, it may be that that Bmi-1 alone does not have a prominent effect on MDA-MB-231 cell behavior in the tumor microenvironment. Despite the in vitro findings of decreased proliferation, increased apoptosis, and decreased invasion with shRNA knockdown of Bmi-1, it is not unusual that the in vivo cell behavior should differ substantially from the in vitro cell behavior. The MDA-MB-231 cell line has been shown to differ significantly in growth rates and behavior in vitro compared to in vivo in SCID mouse models [190]. It is also likely that several factors play a role in the overall aggressive and metastatic behavior of these cells in vivo. Interestingly however, is the finding that the time to onset of tumorigenesis in our mammary fat pad SCID xenograft model is significantly increased

in MDA-MB-231 cells that have shRNA induced knockdown of Bmi-1. Although this effect does not persist throughout the length of the experiment, it does show a significant outcome of Bmi-1 depression in these cells, suggesting that Bmi-1 may be involved in the early stages of tumorigenesis. However, we cannot rule out the possibility that expression of the shRNA for Bmi-1 was lost during a selection event in vivo that selected for more proliferative cells not expressing the shRNA. This would lead to an outgrowth of more highly proliferative cells that eventually would lead to increased tumor growth.

In conclusion, we show that the collaboration of Bmi-1 and H-Ras overexpression in human mammary epithelial cells leads to a more aggressive phenotype in vitro and in vivo, and induces a more highly metastatic phenotype. We also show that depression of Bmi-1 in several breast cancer cell lines leads to a less aggressive phenotype in vitro, including decreased proliferation and invasion, and increased apoptosis as a result of DNA damage. In vivo, we have shown that depression of Bmi-1 in certain breast cancer cell lines leads to a change in biologic behavior related to tumor progression or time to tumor onset in xenograft models. These data support our hypothesis that Bmi-1 plays a significant role in the biologic behavior of certain established breast cancer cell lines in vitro and in vivo. Should Bmi-1 play an important role in the early growth of tumors or in the sustainability of tumor progression over time, this would serve as an important target of study in breast cancer disease, especially related to tumor recurrence and dormancy.

APPENDIX C

Figure 13: Morphology of MCF10A-derived cell lines in two dimensional culture. MCF10A cells (A) grow in typical epithelioid fashion, with a polygonal shape, clear cell-to-cell junctions, abundant cytoplasm, and round centralized nuclei; MCF10A+Bmi-1 cells (B) acquire a mesenchymal appearing spindle cell morphology; MCF10A+H-Ras cells (C) are rounded, tear-drop shaped to triangular; MCF10A+H-Ras+Bmi-1 cells (D) have an exaggerated spindle shaped morphology, often radiating outward from central clusters; spheroid structures (E) arising from MCF10A+H-Ras+Bmi-1 cells after several passages in culture.

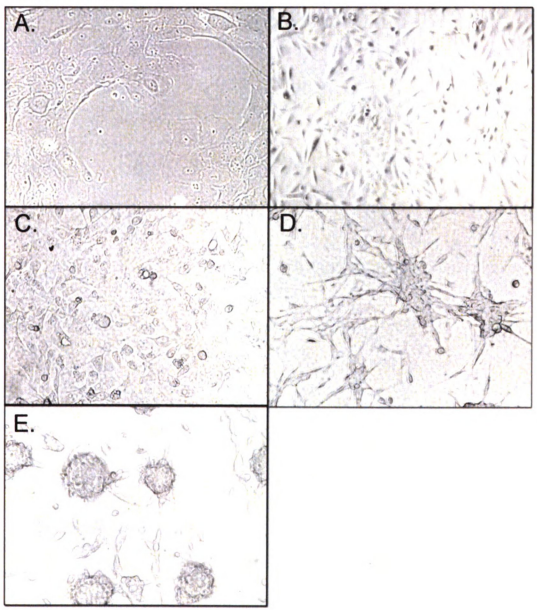

Figure 14: Morphology of MCF10A-derived cell lines in three-dimensional Matrigel culture. Hematoxylin and eosin staining (left column) and phalloidin immunohistochemistry under confocal microscopy (right column): MCF10A cells show a typical differentiation pattern with central lumen formation and polarization of cells around this central lumen; MCF10A+Bmi-1 (B) and MCF10A+H-Ras cells (C) remain small disorganized clusters without lumen formation or polarization; MCF10A+H-Ras+Bmi-1 cells (D) form disorganized highly proliferative clusters of cells with somewhat spindle-shaped morphology and high mitotic rate.

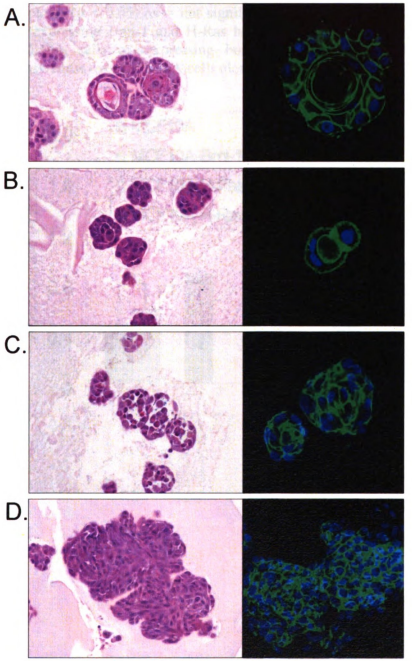

Figure 15: Proliferative indices, apoptotic response to DNA damage, and invasive properties of MCF10A-derived cell lines in vitro. (A) MTS-formazan proliferation assay. MCF10A cells overexpressing H-Ras have significantly increased proliferation over MCF10A cells, and overexpression of both Bmi-1 and H-Ras causes further increase in proliferation at days 1, 2, and 3 ($p < 0.01$) ns = not significant. (B) Anti-histone cell death detection ELISA. MCF10A cells overexpressing Bmi-1 or H-Ras have a decreased apoptotic response to DNA damage, and overexpression of both induces a further significant decrease in the apoptotic response at 12 hr ($p < 0.01$). At 24 hr, Bmi-1 overexpression or Bmi-1+H-Ras overexpression exerts a protective effect against apoptosis ($p < 0.05$) ns = not significant. (C) Matrigel Invasion Assay. MCF10A cells overexpressing Bmi-1 and H-Ras have a 12% and 11% increase in invasiveness, and MCF10A cells overexpressing both Bmi-1 and H-Ras have a 31% increase in invasiveness over MCF10A cells alone.

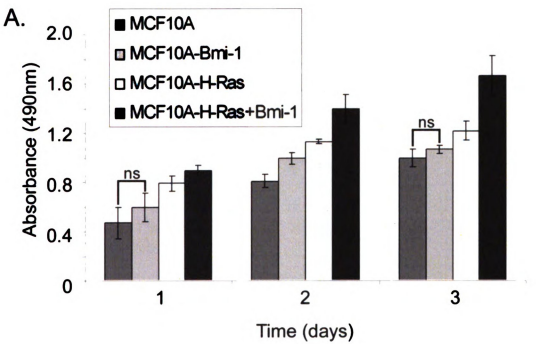

Figure 15 (continued)

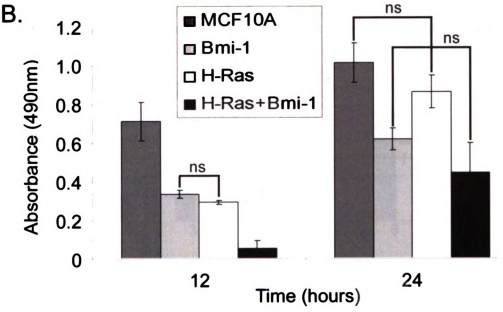

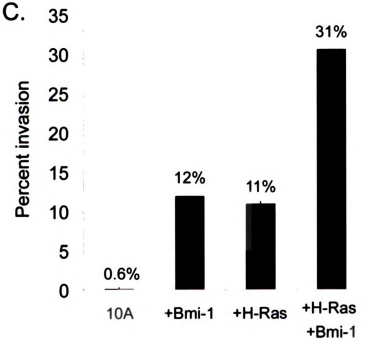

Figure 16: MTS-formazan proliferation assay in siRNA-Bmi-1i induced established breast cancer cell lines. In MCF10A+H-Ras+Bmi-1 (A), MCF7 (B), MDA231 (C), and ZR75-1 (D) cell lines, induction of siRNA for Bmi-1 induces a decrease in proliferation over time (*$p < 0.05$, **$p < 0.01$) in comparison to cell lines transduced with empty vector alone.

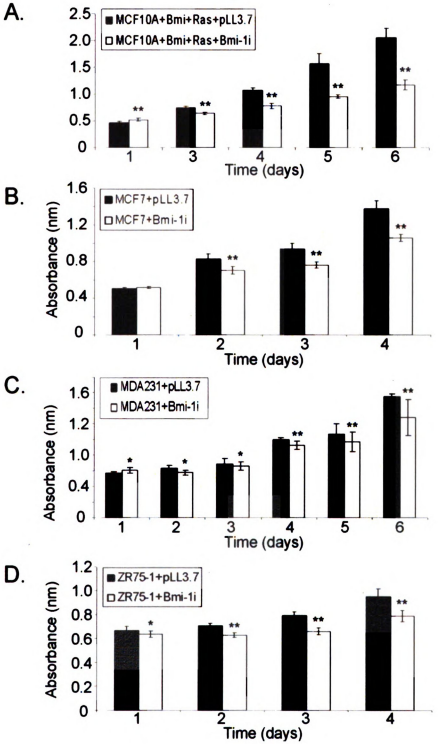

Figure 17: Anti-histone cell death detection ELISA and Matrigel Invasion Assay in siRNA-Bmi-1i induced established breast cancer cell lines. (A) In each cell line transduced with siRNA for Bmi-1, there is a significant increase in apoptosis in response to DNA damage compared to cells transduced with empty vector alone. (B) Matrigel Invasion Assay. There is a significant decrease in invasiveness in the MCF7, MCF10A+H-Ras+Bmi-1, and MDA231 cell lines transduced with siRNA for Bmi-1 in comparison to cells transduced with empty vector alone ($p < 0.05$).

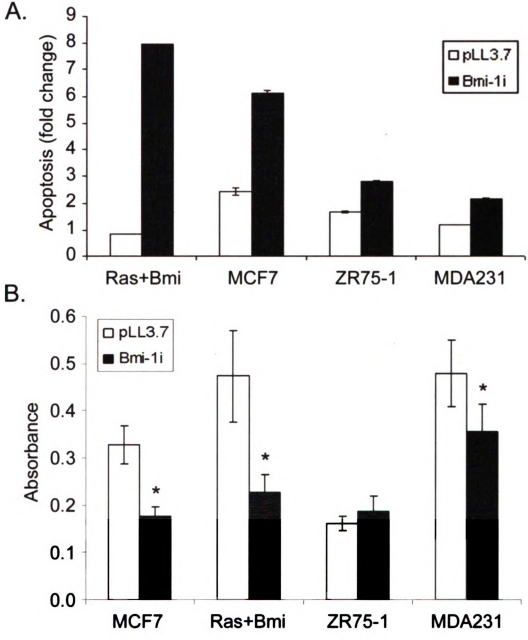

Figure 18: Spontaneous metastasis from intra-mammary fat pad MCF10A+H-Ras and MCF10A+H-Ras+Bmi-1 xenografts. In the MCF10A+H-Ras+Bmi-1 xenograft model, spontaneous metastasis occurred to the liver and spleen in 100% of animals, and brain metastasis occurred in 30%. In contrast, in the MCF10A+H-Ras xenograft model, metastasis to the liver occurred in 50%, and to the spleen in 40% of animals, while no brain metastases were observed (Bar = 100 μm).

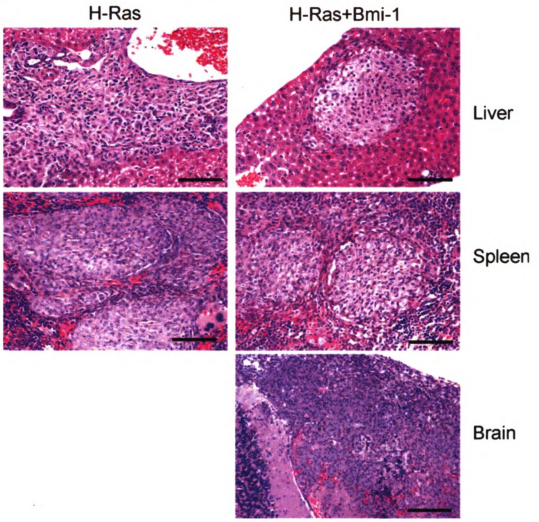

Figure 19: MCF10A+H-Ras and MCF10A+H-Ras+Bmi-1 tail vein xenograft model. (A) Graph of body weight over time. By 4-5 weeks post-injection, mice injected with MCF10A+H-Ras+Bmi-1 cells lost ~30% of their body weight (*) in comparison with other xenografts. (B) Grossly, mice with MCF10A+H-Ras+Bmi-1 tail vein xenografts had fulminant pulmonary metastases involving all lung lobes, while MCF10A, MCF10A+Bmi-1, and MCF10A+H-Ras tail vein xenografts had grossly unremarkable lung fields. (C) Histologically, mice with MCF10A+H-Ras tail vein xenografts had small, random, expansile lesions resembling adenomas or hyperplastic foci, while MCF10A+H-Ras+Bmi-1 xenografts had aggressive lesions that effaced large portions of the lung (Bar = 100 μm).

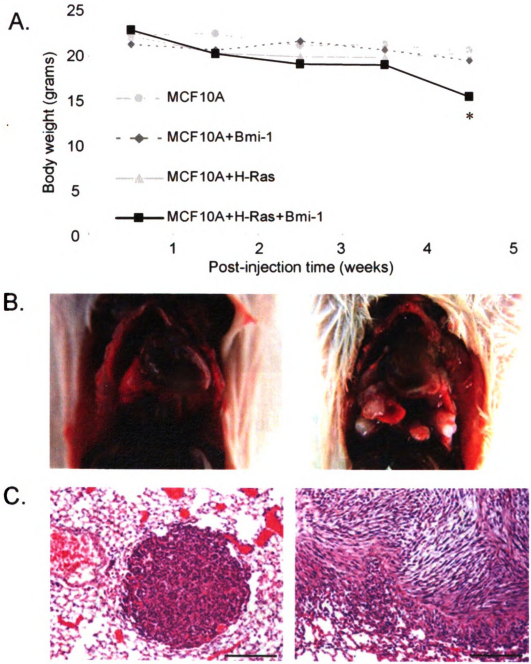

Figure 20: Mammary fat pad and tail vein model using MCF10A+H-Ras+Bmi-1+pLL3.7 and MCF10A+H-Ras+Bmi-1+Bmi-1i cells. Histologically, there is no difference in morphology between xenografts transduced with empty vector and those transduced with siRNA for Bmi-1 in mammary fat pad (SQ) (Bar = 100 μm, inset 40X objective) or intravenous (IV) models (A) (Bar = 200 μm, inset 40X). Mammary fat pad xenografts with shRNA knockdown of Bmi-1 show a statistically significant decrease in tumor volume over time (B) (Two-way ANOVA with Bonferroni correction*$p < 0.05$, **$p < 0.01$, ***$p < 0.001$).

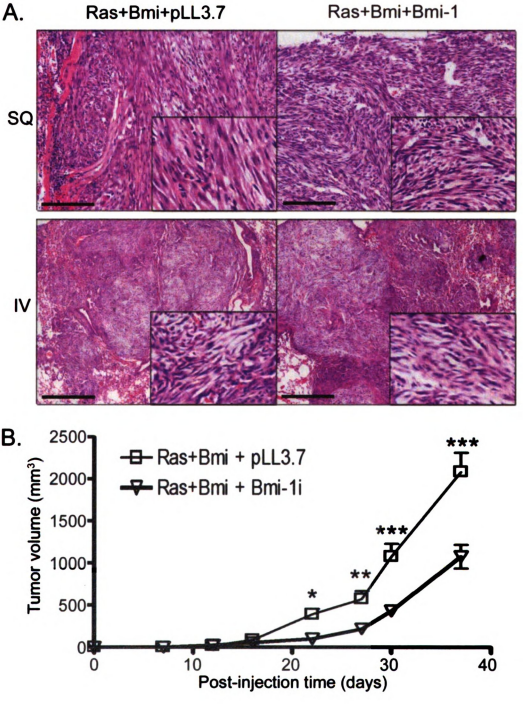

Figure 21: Mammary fat pad and tail vein model using MDA231+pLL3.7 and MDA231+Bmi-1i cells. Histologically, there is no difference in morphology between xenografts transduced with empty vector and those transduced with siRNA for Bmi-1 in mammary fat pad (SQ) (Bar = 100 μm, inset 20X) or intravenous (IV) models (A) (Bar = 200 μm). Mammary fat pad xenografts with shRNA knockdown of Bmi-1 show a statistically significant lag in tumor formation at 60-65 days post-injection (B) (Two-way ANOVA with Bonferroni correction, $*p < 0.05$, $**p < 0.01$).

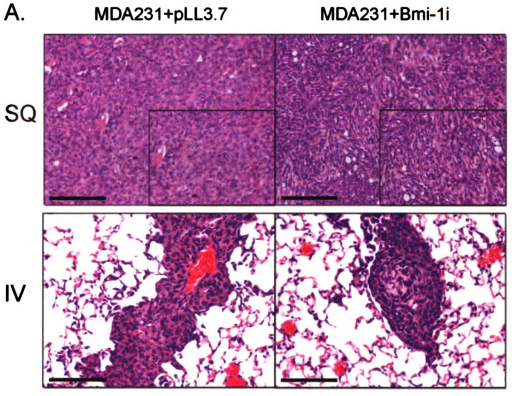

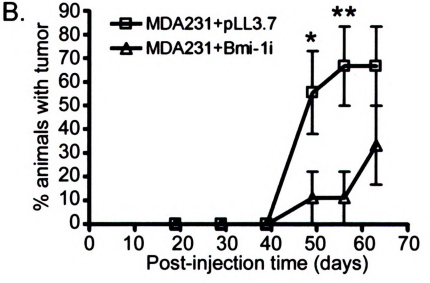

Figure 22: Western blot illustrating stable siRNA knock down of Bmi-1 expression in MCF10A+H-Ras+Bmi-1 and MDA231 xenografts.

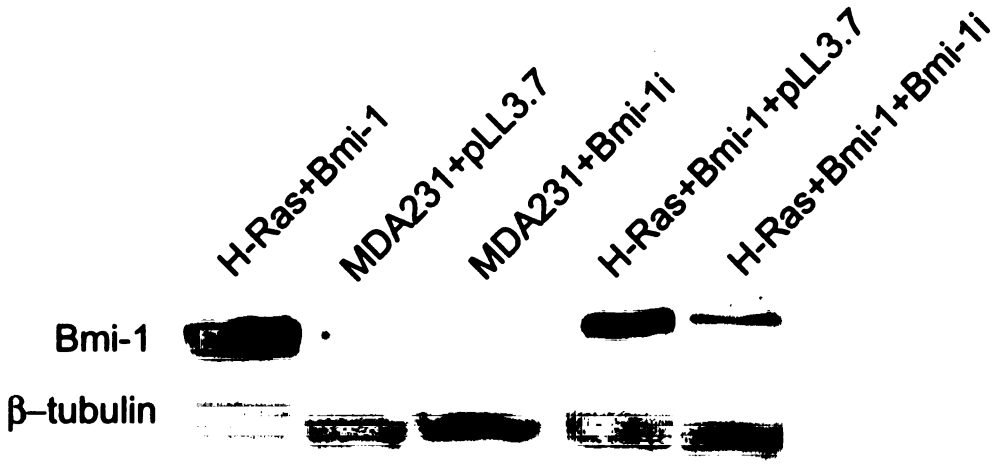

CHAPTER FOUR

Bmi-1 contributes to the outgrowth of embolic human breast cancer cells in the lungs of SCID mice through increased proliferation and prevention of apoptosis

Abstract: Evasion of anoikis (apoptosis in response to lack of adhesion or inappropriate adhesion) is an important mechanism by which tumor cells persist in the vasculature and at distant metastatic sites. Bmi-1 has been reported to be associated with anoikis resistance, and we have previously shown that MCF10A cells overexpressing H-Ras and Bmi-1 (MCF10A+H-Ras+Bmi-1) are able to survive and form aggressive distant metastases in the lungs of tail vein-injected SCID mice in a xenograft model of direct hematogenous spread, in contrast to MCF10A cells overexpressing Bmi-1 (MCF10A+Bmi-1) or H-Ras (MCF10A+H-Ras) alone. In this study, by using an ex-vivo imaging system, we show that increased proliferation and resistance to apoptosis, or anoikis, are two primary mechanisms enabling MCF10A+H-Ras+Bmi-1 cells to survive and proliferate in the pulmonary vasculature to form fulminant metastases leading to clinical morbidity.

Introduction

Metastasis and dormancy are particularly important areas of study in breast cancer research, because metastasis remains the major cause of mortality in patients with breast cancer [191]. In addition, although clinicians have seen an overall improvement in long-term survival over the years due to improved treatments [192], many patients with minimal disease (small primary tumor, no evidence of regional lymph node involvement,

no detectable metastatic disease) can have recurrence rates up to 30% after being followed for 10-15 years [193-195]. The major cause of mortality in patients with breast cancer is metastasis [191] Although the molecular mechanisms leading to metastasis of breast cancer are poorly understood, the cellular mechanism of metastasis generally follows several steps in its pathogenesis: invasion of surrounding tissue, intravasation into the circulation, avoidance of adherence-independent apoptosis (anoikis), arrest in the circulation at distant sites, extravasation, and growth within a new microenvironment [191].

We have previously shown (Chapter 3) that human mammary epithelial cells engineered to overexpress H-Ras concurrently with Bmi-1 (MCF10A+H-Ras+Bmi-1) exhibit aggressive tumorigenesis and metastatic disease when injected into SCID mice when compared with MCF10A cells that overexpress H-Ras alone (MCF10A+H-Ras). We have also shown that there is a significant increase in tumorigenesis, aggressiveness, and metastasis of xenograft tumors produced by MCF10A+H-Ras+Bmi-1 cells in both mammary fat pad and tail vein-induced models. MCF10+H-Ras+Bmi-1 tumors are poorly differentiated and locally infiltrative, and in the tail vein model cause severe and rapid pulmonary metastasis that effaces and destroys large portions of all lung lobes in contrast to MCF10A+H-Ras cells, which develop small adenomatous or hyperplastic lesions only after extended periods of time. Consistent with these data, overexpression of Bmi-1 has been associated with regional lymph node metastasis in patients with infiltrative ductal carcinoma [47], and has also been associated with an 11 gene microarray signature that is a powerful predictor of a short interval to disease recurrence, marked propensity towards metastatic dissemination and death following therapy in

patients with multiple different types of cancer [48]. Additionally, it has been shown that Bmi-1 overexpression is associated with anoikis-resistance of circulating human prostate carcinoma precursor cells, and that human prostatic carcinoma cells with siRNA knockdown of Bmi-1 are less resistant to anoikis, possibly due to a reduction in Survivin [196]. These data suggest that Bmi-1 is an important regulator of metastatic spread, survival, and growth in distant sites.

To determine the mechanisms leading to the striking differences in pulmonary phenotypes between MCF10A+H-Ras and MCF10A+H-Ras+Bmi-1 cells, we used a SCID mouse tail vein xenograft model to determine the ability of disseminated cells to intravasate and grow in the lungs. Each cell line was transduced with a lentivirus expressing green fluorescent protein (GFP), and injected into the tail vein of SCID mice. Using an ex-vivo imaging system, cells were followed in the lungs over several weeks, and sections of lung were examined for changes in proliferation and apoptosis by Ki67 immunolabeling and TUNEL staining, respectively. We report here mechanisms leading to the genesis of an aggressive metastatic phenotype due to Bmi-1 expression in collaboration with H-Ras.

Materials and Methods

Cells, constructs, and animals: MCF10A-H-Ras and MCF10A-Bmi-1+H-Ras cells were labeled with a GFP-tagged lentivirus and sorted by Fluorescence Activated Cell Sorting (FACS), gating for high GFP expression. Two cohorts of 10 six-week-old female mice each were used, and each cohort received 1×10^6 MCF10A-H-Ras+GFP or MCF10A-Bmi-1+H-Ras+GFP cells via tail-vein injection. Mice were euthanized at two

days, one week, and four weeks after injection. Lungs were harvested at the time of necropsy, infused with 1 ml 1× PBS, and visualized under a fluorescent microscope to detect GFP-labeled cells (Zeiss, Thornwood NY). GFP signal was measured at 4X magnification and quantified using ImagePro image analysis software (Media Cybernetics, Bethesda MD) and expressed as average pixels per field. Statisitical analysis was performed using GraphPad Prism 4.02, and Student's T-test was performed on all samples.

Immunohistochemistry and TUNEL assay: Paraffin-embedded and frozen sections of primary tumors and lungs with metastatic lesions were stained with a rabbit polyclonal antibody for Ki67 (Vector Laboratories) and stained with a TUNEL ApopTag in situ kit (Chemicon, Temecula CA). Formalin-fixed, paraffin-embedded sections were deparaffinized in xylene and rehydrated in graded alcohol. Frozen sections were thawed and fixed in 4% paraformaldehyde for 10 min. Antigen retrieval was performed by microwaving in a pressure cooker for 4 min in citrate buffer (pH 6.0), followed by cooling for 25 min. Endogenous peroxidases were blocked with 1.5% H_2O_2 in methanol and protein block was performed with 10% goat serum for 30 min. Sections were incubated in primary antibody (1:10,000) at RT overnight in 10% blocking serum, and biotinylated goat anti-rabbit secondary antibody (1:1000) in 10% blocking serum for 30 min. Following washing, the labeled avidin-biotinylated enzyme complex (ABC) technique was employed for amplification of primary antibody binding. For visualization, 3,3-diaminobenzidine (DAB) was applied and counterstained with Gill's hematoxylin. For Apoptag (TUNEL) staining, proteolytic digestion was done with proteinase K (20

μg/ml) for 15 min at RT, and quenched in 2% H_2O_2 in PBS for 5 min at RT. 1× Equilibration Buffer was applied and sections were incubated for 15 min at RT. Sections were then incubated with TdT enzyme for 30 min at 37 °C, washed in stop buffer for 30 min, and incubated with anti-digoxigenin-peroxidase for 30 min at RT. 3,3-diaminobenzidine (DAB) was applied and counterstained with lithium carbonate. The sections were dehydrated through graded alcohols, immersed in xylene, and mounted with coverslips. Ki67 and Apoptag staining was assessed at 10X magnification and signal was quantified either as labeled cells per field, or by using ImagePro image analysis software (Media Cybernetics, Bethesda MD) as labeled pixels per field. Statisitical analysis was performed using GraphPad Prism 4.02 (La Jolla CA), and Student's T-test was performed on all samples.

Results

Bmi-1 contributes to the outgrowth of embolic breast cancer cells in the lungs. To determine whether the mechanism leading to the fulminant metastatic phenotype in MCF10A+Bmi-1+H-Ras is due to the effect of Bmi-1 on proliferation and prevention of apoptosis, MCF10A-Bmi-1+H-Ras and MCF10A+H-Ras cells were lentivirally tagged with GFP and flow sorted for GFP expression. 1×10^6 cells were administered via tail vein injection to two cohorts of ten female SCID mice each. Mice were sacrificed two hours, two days, one week, and four weeks following tail vein injection, and lungs were examined by ex-vivo imaging to detect the presence of GFP-expressing metastatic foci using a Zeiss Axiovert 200 inverted microscope, Hamamatsu imaging camera, and ImagePro software to quantify the GFP signal (Figure 24A-B). By day two post injection,

there was a significant decrease in the number of cells in the lungs of MCF10A+H-Ras injected mice, indicating massive die-off ($p < 6X10^{-6}$) compared to MCF10A+H-Ras+Bmi-1 injected mice. At one and four weeks following injection, MCF10A+H-Ras+Bmi-1 cells continued to proliferate, ultimately culminating in large tumor masses, in contrast to MCF10A+H-Ras injected mice, in which few cells were detectable. These data suggest that the mechanism of action of Bmi-1 overexpression on MCF10A cells overexpressing H-Ras is a combination of decreased cell death and increased proliferation, leading to the ability to escape anoikis, implant in the pulmonary vasculature, and result in severe metastatic pulmonary disease.

MCF10A+H-Ras+Bmi-1 xenografts have increased proliferation and decreased apoptosis compared to MCF10A+H-Ras xenografts at end-stage disease. To answer the question of whether the difference in phenotype in the mammary fat pad xenografts and tail vein model of metastasis (Chapter 3) is due to Bmi-1 overexpression leading to an increase in proliferation, increased resistance to apoptosis, or both, we examined Ki67 immunohistochemistry and TUNEL staining in pulmonary tumors at disease endpoint (5 weeks post-injection for IV xenografts and approximately 60 days after injection for mammary fat pad xenografts). There was significantly greater staining for Ki67 in MCF10A+H-Ras+Bmi-1 fat pad ($p < 1.3X10^{-7}$) and intravenous ($p < 0.0002$) xenografts compared to MCF10A+H-Ras xenografts (Figure 25A-B), indicating that one mechanism of collaboration between H-Ras and Bmi-1 in vivo is through induction of proliferation. In contrast, TUNEL staining was significantly increased ($p < 0.0002$) in mammary fat pad MCF10A+H-Ras xenografts in comparison to MCF10A+H-Ras+Bmi-1 xenografts.

The increased cellularity of tumors and decreased TUNEL staining suggests that prevention of apoptosis is a major mechanism of tumor promotion in MCF10A+H-Ras+Bmi-1 mammary fat pad xenografts. There was a lack of significant TUNEL staining in either intravenous model (Figure 26A-B), suggesting that these cells may have been selected over time in vivo for the ability to escape anoikis within the pulmonary vasculature. Taken together, growth of a primary tumor within the mammary fat pad as well as within the pulmonary vasculature is significantly impacted by Bmi-1 overexpression, suggesting that this collaboration between H-Ras and Bmi-1i is essential for the survival and growth of metastatic cells in vivo.

MCF10A+H-Ras+Bmi-1 xenografts have increased proliferation and decreased apoptosis compared to MCF10A+H-Ras xenografts early in the process of hematogenous spread. To determine the difference in kinetics of intravascular growth over time leading to the phenotype observed at disease endpoint, frozen OCT-embedded lungs collected from tail vein-injected mice at two days and one week after injection were stained for Ki67 and TUNEL. There was a statistically significant increase in Ki67 labeling at two days ($p < 0.01$) and one week ($p < 8X10^{-12}$) in intravascular tumor cells in the MCF10A+H-Ras+Bmi-1 group as compared to the MCF10A+H-Ras group, indicating that Bmi-1 overexpression imparts a proliferative advantage early in the course of hematogenous spread (Figure 27A). TUNEL staining demonstrated that there was a statistically significant decrease in apoptosis in intravascular tumor cells ($p < 0.05$) in the MCF10A+H-Ras+Bmi-1 group as compared to the MCF10A+H-Ras group (Figure 27B), suggesting that Bmi-1 overexpression imparts a protective effect against apoptosis

resulting from anchorage dependence, or anoikis, an important mechanism in metastatic spread. Taken together, these results show that Bmi-1 overexpression exerts a proliferative and anti-apoptotic effect which, in the presence of H-Ras overexpression, leads to an aggressive and fatal pulmonary phenotype. This indicates that the collaboration of Bmi-1 and H-Ras in mammary epithelial cells is essential for metastatic survival and growth.

Discussion

We have shown that, in this tail vein xenograft model, Bmi-1 collaborates with H-Ras to produce an aggressive metastatic phenotype. While MCF10A cells overexpressing H-Ras at most form micrometastases resembling adenomas and hyperplastic foci, cells overexpressing both H-Ras and Bmi-1 rapidly produce poorly differentiated pulmonary metastases. Animals receiving cells overexpressing H-Ras alone survive for long periods of time and do not develop clinical illness, whereas animals receiving cells overexpressing H-Ras and Bmi-1 concurrently develop clinical morbidity early in the course of disease, characterized by rapid weight loss, hunched posture, and rapid respiration.

One mechanism leading to the difference in this pulmonary phenotype is the marked increase in proliferative ability of MCF10A+H-Ras+Bmi-1 cells. The results of ex-vivo imaging show that these cells continue to proliferate in an exponential manner over the course of the disease. We have previously shown that these cells have an increased proliferative capacity in vitro in comparison to MCF10A cells overexpressing Bmi-1 or H-Ras alone [118], and the results of Ki67 immunohistochemistry support this

biologic behavior in vivo. It is known that Ras activation leads to activation of multiple growth and differentiation pathways as a result of signaling through multiple effectors such as the Raf kinase and MAPK/ERK signaling cascade [197]. In our study, we document Ki67 immunolabeling in the tail vein injected MCF10A cells overexpressing H-Ras both early in the disease and at disease endpoint. However, there is a marked increase in Ki67 immunolabeling in MCF10A+H-Ras+Bmi-1 cells within the pulmonary vasculature both early in the disease and at end-stage in comparison with MCF10A+H-Ras cells. It is known that Bmi-1 can act as an oncogene when overexpressed or dysregulated, through its suppression of the Ink4a-Arf tumor suppressor locus [29, 118]. This locus encodes for p14/p19ARF and p16INK4A, which downregulate MDM2 and CDK4-6/cyclin D binding, respectively (Figure 28). MDM2 is a major suppressor of p53 by binding directly to it and preventing its transcription [198]. Inhibition of CDK4-6/cyclin D binding results in prevention of Rb phosphorylation, and together with inhibition of p53, causes cell cycle arrest. Thus, by inhibiting this locus constitutively, Bmi-1 overexpression results in a highly proliferative state with the cell remaining in the cell cycle. We have previously shown that Bmi-1 overexpression in vitro increases proliferation of MCF10A cells and that Bmi-1 collaborates with H-Ras through dysregulation of multiple growth pathways such as PI3K, Akt, and MAPK/ERK, and cell cycle regulators such as cyclin D and p16 [118]. Ries et al. (2002) have shown that MDM2 is also driven by the Raf/MAPK/ERK pathway downstream from Ras signaling. They show that activated Raf induces MDM2 to degrade p53 in the absence of p14/19ARF. This results in inhibition of cell cycle arrest through a p53-dependent mechanism. Taken together, the collaboration of H-Ras and Bmi-1 on both p53 function

as well as through dysregulation of several growth pathways results in fulminant and destructive metastases in the tail vein model of direct hematogenous spread.

Another mechanism leading to the aggressive metastatic phenotype is the ability of MCF10A+H-Ras+Bmi-1 cells to evade anoikis. Anoikis is apoptosis in response to lack of adhesion or inappropriate adhesion [199]. Other than providing a physical scaffold on which cells reside, signaling between components of the extracellular matrix (ECM) and epithelial cells is important in the prevention of apoptosis in normal biological processes such as proliferation and differentiation, as well as in metastasis. Important mediators in cell-matrix signaling in prevention of apoptosis are the focal adhesion kinases (FAKs), which mediate the function of several downstream pathways associated with growth and prevention of apoptosis, such as MAPK/ERK, PI3K, and Src [199, 200]. Ras also exerts its proliferative effects through a shared downstream pathway, the MAPK/ERK cascade. However, in our study, we have demonstrated that MCF10A cells overexpressing H-Ras undergo massive cell death following tail vein injection. This may result from the conflicting proapoptotic and antiapoptotic functions of Ras when overexpressed. The proliferative effects of Ras signaling through the MAPK/ERK and PI3K pathways are well known [197], and p53-independent anti-apoptotic effects have been shown through Raf induced upregulation of MDM2, leading to p53 degradation [198]. However, multiple pathways exist for Ras induction of apoptosis. For example, Raf also activates the MDM2 inhibitor, p14/19ARF, leading to MDM2 inhibition and accumulation of p53, resulting in cell cycle arrest [198]. In addition, overexpression of constitutively active Ras in established cell lines results in cyclin-dependent kinase inhibitor induction of cell cycle arrest, or in apoptosis [167, 201, 202]. Overexpression of

Ras may lead to apoptosis through p53 dependent pathways via $p14^{ARF}$ activation and subsequent MDM2 inhibition, or through p53 independent pathways [203, 204]. Nevertheless, our data support that in the balance of pro-apoptotic and anti-apoptotic signaling through Ras, in the in vivo environment of the pulmonary vasculature, H-Ras overexpressing cells are unable to escape anoikis and undergo massive apoptosis early in the course of the disease. In contrast, by the endpoint of study, H-Ras overexpressing cells are able to establish a few micrometastases within the pulmonary parenchyma. However, at endpoint of disease, there was no detectable TUNEL staining within these micrometastases, suggesting that there was eventually proliferation of non-apoptotic H-Ras overexpressing outgrowths within the lung.

In contrast, MCF10A cells overexpressing H-Ras and Bmi-1 have a strikingly different behavior during the course of disease. We have previously shown that Bmi-1 exerts a protective effect against apoptosis due to DNA damage in vitro. However, these experiments were performed in two-dimensional adherent culture, and therefore may not be translatable to the in vivo environment. It is known that Bmi-1 acts to prevent cell cycle arrest through inhibition of the Ink4A-ARF tumor suppressor locus, which encodes the cyclin-dependent kinase inhibitors $p16^{INK4A}$ and $p14^{ARF}$ [29, 118]. Therefore, it is not surprising that overexpression of Bmi-1 should be protective against apoptosis due to DNA damage and cell cycle arrest through p53-dependent mechanisms. However, little is known about the effect of Bmi-1 on the prevention of apoptosis due to anchorage independence. The results of TUNEL staining in the current tail vein model suggest that Bmi-1 exerts a protective effect against anoikis in the pulmonary vasculature. While there is some apoptosis occurring early in the disease, the amount of apoptosis is significantly

reduced in comparison with MCF10A cells overexpressing H-Ras alone. Similar to H-Ras overexpressing cells, there was no detectable TUNEL staining at disease endpoint, suggesting outgrowth of non-apoptotic cell populations.

In conclusion, we show that overexpression of H-Ras and Bmi-1 together in MCF10A mammary epithelial cells in the tail vein xenograft model results in fulminant and aggressive pulmonary metastasis through massive induction of cell proliferation and inhibition of apoptosis. Whether this phenomenon is primarily due to the collaboration between Bmi-1 and H-Ras, due to stem cell properties induced by Bmi-1 overexpression in the face of H-Ras overexpression, or both, needs further investigation. The results of this work are in agreement with previous studies by Glinsky et al. that show the Bmi-1 pathway is associated with an 11 gene microarray signature that predicts a marked propensity towards metastatic dissemination in patients with multiple different types of cancer [48], as well as resistance to anoikis [196]. Should Bmi-1 play a major role in the pathophysiology of anoikis resistance and metastasis, it would be a critical molecular target in patients with cancer and metastatic disease. If Bmi-1 expression could be detected early in the course of disease, it may be valuable both diagnostically and prognostically as a predictor of metastatic propensity. Furthermore, if it does indeed function in this capacity, the Bmi-1 pathway would be a promising target for molecular therapy.

APPENDIX D

Figure 23: MCF10A+H-Ras and MCF10A+H-Ras+Bmi-1 GFP expressing cells in the lungs of mice at 2 hours, 2 days, one week, and four weeks after injection. (A) At two hours, there are similar numbers of cells present in the lungs of mice injected with MCF10A+H-Ras (H-Ras) and MCF10A+H-Ras+Bmi-1(H-Ras+Bmi-1) (4X magnification). There is progressive and rapid loss of GFP expressing cells in the MCF10A+H-Ras group, while GFP expressing cells persist in the MCF10A+H-Ras+Bmi-1 group. By one and four weeks, there are scant GFP expressing MCF10A+H-Ras cells; by four weeks there are fulminant GFP expressing metastatic lesions (4X magnification). (B) Graphic representation of data from 24A. There is significant loss of GFP-expressing MCF10A+H-Ras cells, and a steady increase of GFP expressing MCF10A+H-Ras+Bmi-1 cells in the lungs over time ($*p < 6X10^{-6}$, Student's T-test).

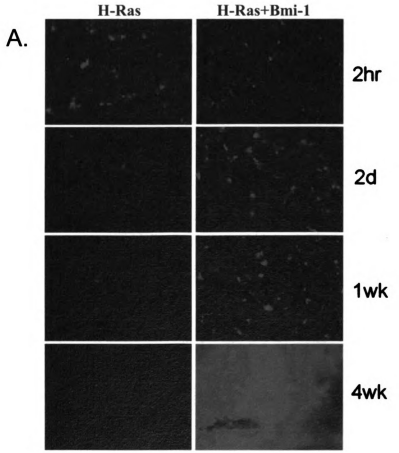

Figure 23 (continued)

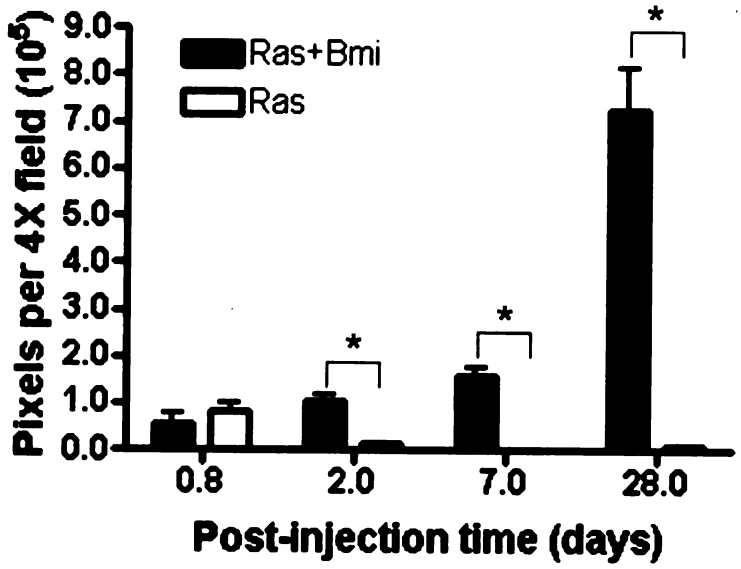

Figure 24: Ki67 immunohistochemistry in MCF10A+H-Ras (Ras) and MCF10A+H-Ras+Bmi-1 (Ras+Bmi) mammary fat pad (SQ) and intravenous xenograft models at end-stage disease. (A) There is a significant increase in Ki67 immunolabeling in the MCF10A+H-Ras+Bmi-1 mammary fat pad and intravenous xenografts (right) compared to MCF10A+H-Ras xenografts (left). (B) Graphic representation of data from 25A (pixels per 10X field). There is a significant increase in proliferation in MCF10A+H-Ras+Bmi-1 compared to MCF10A+H-Ras xenografts (*$p < 1.3X10^{-7}$, **$p < 0.0002$, Student's T-test).

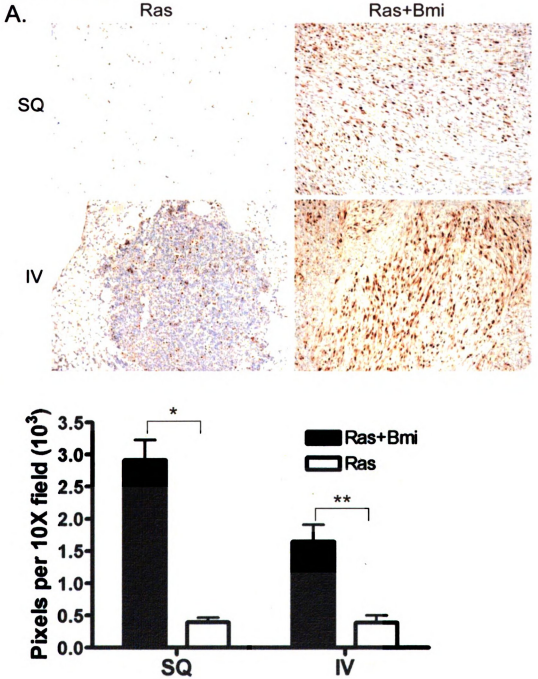

Figure 25: TUNEL staining in MCF10A+H-Ras (Ras) and MCF10A+H-Ras+Bmi-1 (Ras+Bmi) mammary fat pad and intravenous xenograft models at end-stage disease. (A) There is a significant increase in TUNEL staining in MCF10A+H-Ras mammary fat pad, but not intravenous xenografts, compared to MCF10A+H-Ras+Bmi-1 xenografts. (B) Graphic representation of data from 26A (pixels per 10X field). There is a significant increase in apoptosis in MCF10A+H-Ras mammary fat pad xenografts compared to MCF10A+H-Ras+Bmi-1 xenografts (*$p < 0.0002$, Student's T-test). There is no statistically significant difference in apoptosis in intravenous xenograft models at end-stage disease.

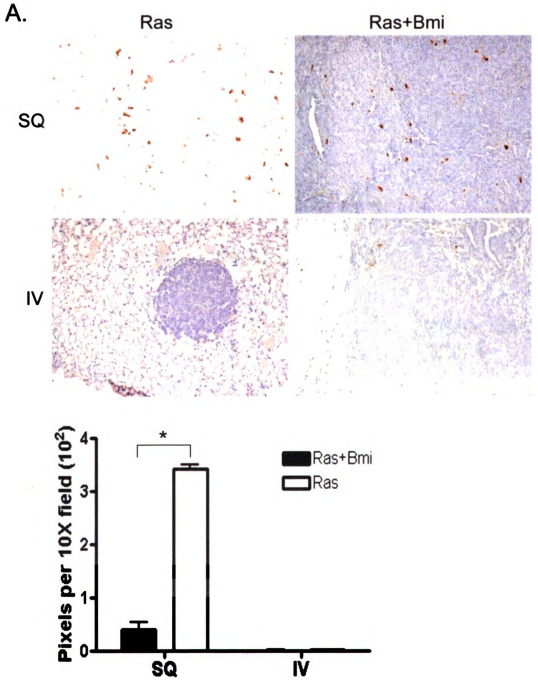

Figure 26: Ki67 immunolabeling and TUNEL staining in MCF10A+H-Ras (Ras) and MCF10A+H-Ras+Bmi-1 (Ras+Bmi) intravenous xenografts during early progression of disease. (A) At 2 days and 8 days, there is a significant increase in Ki67 immunolabeling in MCF10A+H-Ras+Bmi-1 xenografts compared to MCF10A+H-Ras xenografts (*$p < 0.01$, **$p < 8X10^{-12}$, average cell number per field at 20X magnification, Student's T-test). (B) At 2 days and 8 days, there is a significant decrease in TUNEL staining in MCF10A+H-Ras+Bmi-1 xenografts compared to MCF10A+H-Ras xenografts (*$p < 0.05$, average cell number per field at 20X magnification, Student's T-test).

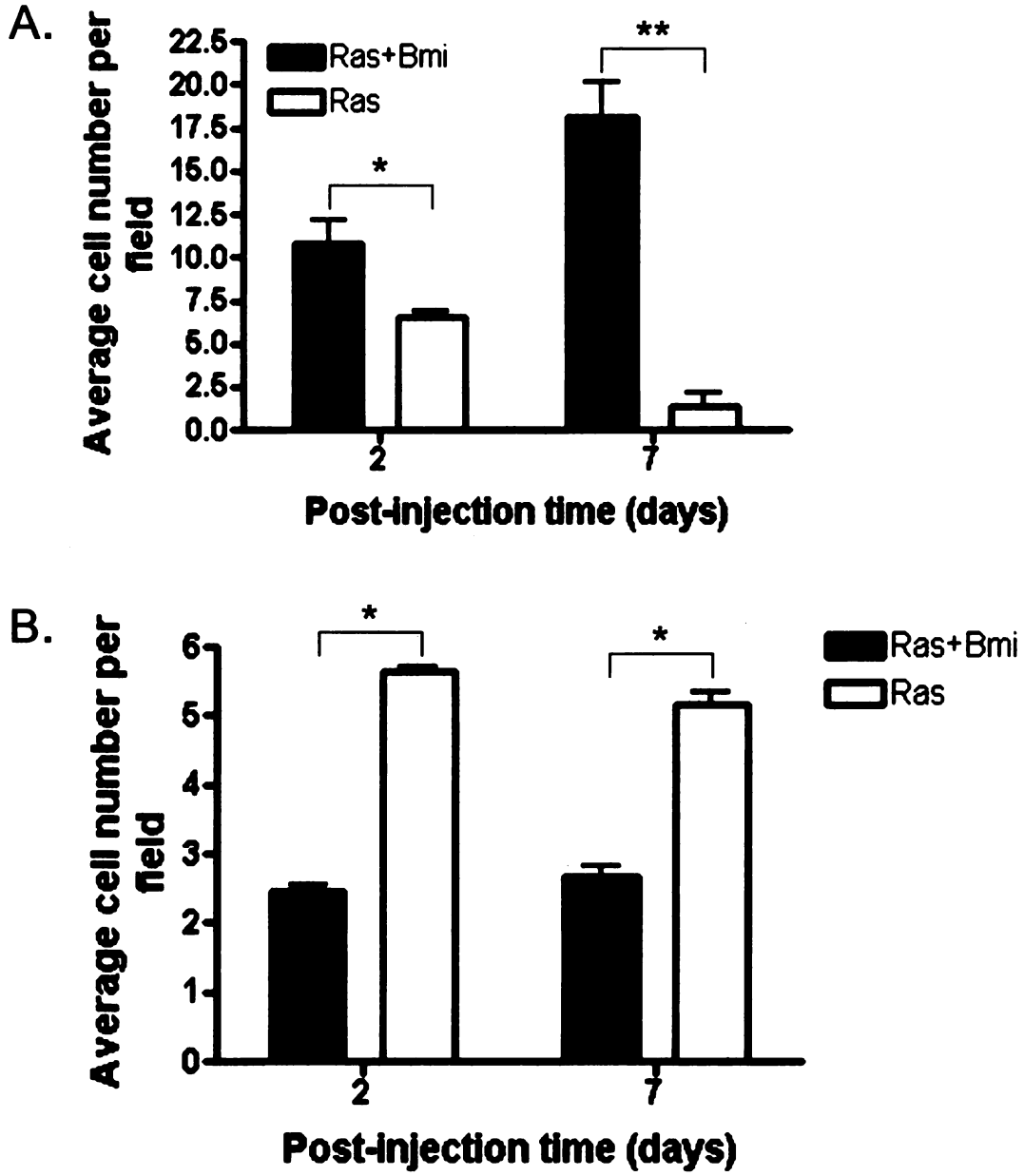

Figure 27: Bmi-1 prevents cellular senescence, cell cycle arrest and apoptosis by inhibiting the Ink4a-Arf tumor suppressor locus. Normally, p19 suppresses RB phosphorylation and p16 prevents degradation of p53, leading to cell cycle arrest, with resultant apoptosis or senescence. Bmi-1 suppresses the actions of p16 and p19 through inhibition of the Ink4A-Arf tumor suppressor locus, leading to degradation of p53 and suppression of RB phosphorylation, thus preventing cell cycle arrest, senescence, and apoptosis.

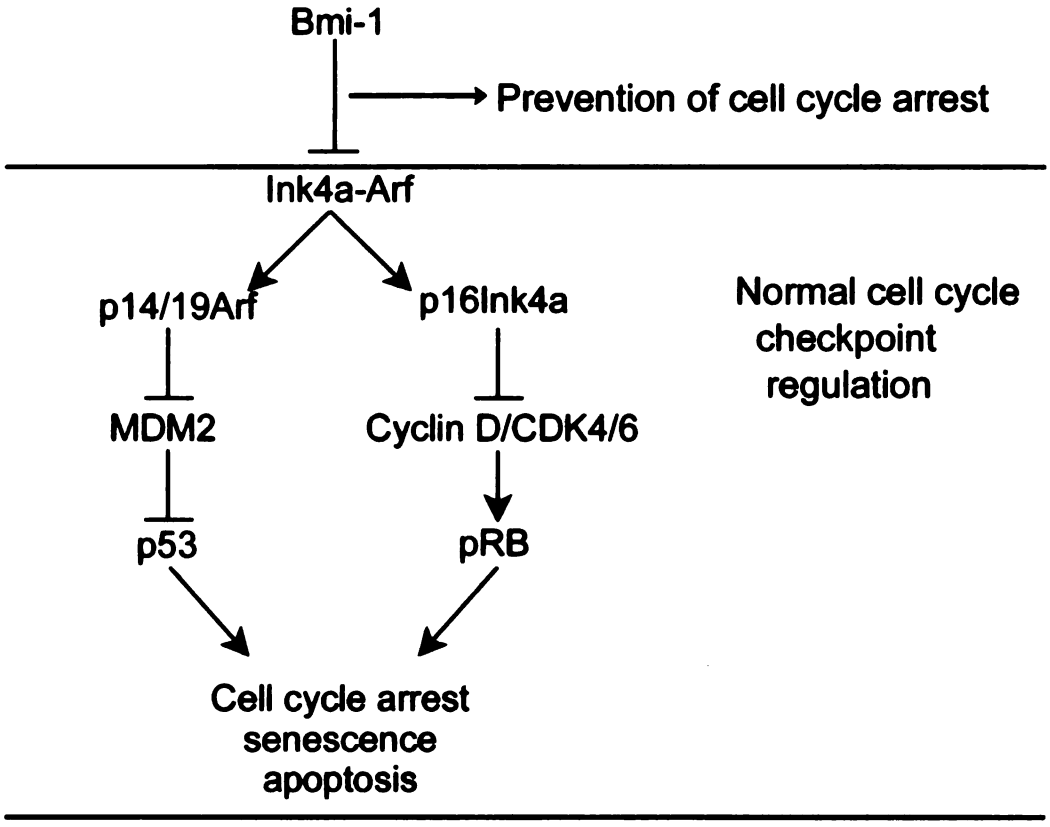

CHAPTER FIVE

Significance and Future Directions

I. Conclusions and Significance

We have shown that Bmi-1 plays a major role in promoting many cellular functions related to transformation and metastasis. I have addressed the effects of Bmi-1 overexpression in normal immortalized human mammary epithelial cells (MCF10A) alone and in collaboration with H-Ras overexpression in vitro and in vivo. To elucidate the effects of Bmi-1 overexpression on MCF10A cells alone and in combination with H-Ras overexpression in vitro, I examined 1) changes in cellular morphology in two- and three-dimensional culture, 2) proliferation, 3) invasion, and 4) apoptosis due to DNA damage in MCF10A cells overexpressing Bmi-1, H-Ras, and Bmi-1 concurrently with H-Ras. Conversely, to determine what effect depressing Bmi-1 has in established breast cancer cell lines that overexpress it in vitro, shRNA was employed to knock down the expression of Bmi-1 in several breast cancer cell lines, and changes in proliferation, invasion, and apoptosis were similarly examined.

First, we found that the cellular phenotype in vitro changes dramatically based upon the oncogene or combination of oncogenes overexpressed. While MCF10A cells grow in a typical epithelioid fashion in two dimensional culture, with clear cell-to-cell junctions, abundant cytoplasm and centralized nuclei, with Bmi-1 overexpression MCF10A cells take on a spindle shaped, mesenchymal phenotype. With H-Ras overexpression, cells become more rounded to triangular to stellate, and with the

combination of Bmi-1 and H-Ras overexpression, cells become markedly spindloid, often radiating out from central clusters. Interestingly, after several passages in culture, these cells form spheroid structures that are similar to mammospheres grown in three dimensional suspension culture, which have been shown to be enriched for stem cell markers. Further analysis of these spheroids for stem cell markers and evidence of stem cell properties is an important future direction, and is forthcoming.

In three-dimensional culture in Matrigel basement membrane extract, we found that there is a block in differentiation with either Bmi-1 or H-Ras overexpression. While normal MCF10A cells differentiate normally towards generation of luminal structures through central apoptosis of cell clusters and well-organized cellular polarity around this central lumen, with Bmi-1 or H-Ras overexpression, no such luminal formation occurred and cells remained in disorganized clusters, indicating a block in differentiation. Furthermore, with Bmi-1 and H-Ras overexpression together, cells became more spindloid and highly proliferative, forming large disorganized clumps of cells with a high mitotic rate, illustrating a very proliferative and poorly differentiated phenotype as a result of overexpression of both oncogenes. This provides evidence of the transforming ability of these oncogenes in concert in a three dimensional in vitro context that is designed to mimic the in vivo environment, giving significance and purpose to the subsequent in vivo experiments to demonstrate tumorigenesis.

Given the effects on differentiation and proliferation that were observed in culture, we sought to quantify these changes in vitro. We found that with Bmi-1 or H-Ras overexpression, proliferation of mammary epithelial cells increased significantly in an

MTS-formazan proliferation assay. With overexpression of both oncogenes, proliferation then increased significantly farther. Conversely, we have shown that H-Ras and Bmi-1 overexpression alone have a protective effect against apoptosis due to DNA damage using an anti-histone sandwich ELISA assay, and when overexpressed together, a significant further inhibition of the apoptotic response is seen. Lastly, to evaluate effects on invasive capability of cells in a three-dimensional in vitro context, cellular invasion was measured using a Matrigel invasion assay. Bmi-1 or H-Ras overexpression led to a significant increase in cellular invasion in this assay, and overexpression of both oncogenes led to a statistically significant increase in proliferation over MCF10A cells with overexpression of either oncogene alone. It was further determined through western blotting that overexpression of H-Ras in combination with Bmi-1 led to dysregulation of multiple growth pathways, including the MAPK/ERK and AKT pathways, as well as cell cycle regulators such as p53, pRB, and Cyclin D. This gives further confirmation of the induction of an aggressive phenotype with Bmi-1 and H-Ras overexpression in vitro.

Next we sought to determine the effects of Bmi-1 and H-Ras overexpression, alone and in combination, on MCF10A cells in the in vivo context to ascertain the true biologic effects within the host microenvironment. Importantly, MCF10A cells overexpressing Bmi-1 did not form tumors in the intramammary fat pad xenograft model, suggesting that overexpression of Bmi-1 alone is insufficient to transform human mammary epithelial cells. H-Ras overexpression induced hemorrhagic and cystic lesions composed of smooth muscle, hemangiomatous, and mast cell components that progressed more slowly over time than those overexpressing both Bmi-1 and H-Ras. Importantly, the xenografts overexpressing both Bmi-1 and H-Ras developed poorly differentiated tumors

resembling and epithelial to mesenchymal transition phenotype (EMT) that were locally infiltrative and more highly metastatic than those tumors resulting from H-Ras overexpression alone. Xenografts overexpressing both oncogenes consistently metastasized to the spleen and liver at a greater rate than those overexpressing H-Ras alone, and only those xenografts overexpressing both oncogenes metastasized to the brain. This is particularly significant because it confirms the collaborative role of Bmi-1 and H-Ras in transformation of the MCF10A cell line in vivo, and recapitulates an important route of metastasis in the human disease, the brain, that is particularly difficult to consistently repeat in animal models of the human disease. Additionally, the marked phenotypic difference between the tumors suggests significant differences in biologic pathways in the development of each tumor phenotype. Further work to characterize the mechanisms of the differences in phenotype is necessary, and is forthcoming.

The tail vein xenograft model of direct hematogenous spread to the lungs was used to determine the metastatic capability of MCF10A cells overexpressing Bmi-1 or H-Ras or both oncogenes together. This experiment showed the marked capacity of MCF10A cells overexpressing both oncogenes to escape anoikis, implant in the pulmonary vasculature, and rapidly proliferate in comparison to those cells overexpressing either oncogene alone. This further corroborates our hypothesis that Bmi-1 collaborates with H-Ras to induce a highly aggressive phenotype, consistent with its known role in lymphomagenesis with c-myc. This phenotype was determined to be a result of marked proliferation and a substantial resistance to apoptosis of MCF10A cells overexpressing both Bmi-1 and H-Ras in comparison to H-Ras alone. Again, this

illustrates important differences in biologic pathways leading to the ability of these cells to cause significant metastatic disease and clinical morbidity.

Given the results we obtained in the first set of experiments, we sought to determine whether reduction of Bmi-1 had a direct effect on the biology of established human mammary breast cancer cell lines that overexpress Bmi-1. Using shRNA technology and lentiviral delivery, we established several cell lines with Bmi-1 knockdown. These tumor cell lines exhibited decreased proliferation by MTS-formazan proliferation assay, decreased invasion in Matrigel, and increased apoptosis in response to DNA damage. This work is significant because it confirms our previous findings in the MCF10A cell line overexpressing both Bmi-1 and H-Ras and illustrates the direct biologic effects of Bmi-1 non-engineered, established breast cancer cell lines derived from human tumor samples. Thus, this reflects a true biologic role in the development of some forms of breast cancer.

Next we evaluated two of the most aggressive cell lines for changes in tumorigenesis and metastasis in vivo by using the xenograft mouse models illustrated above. While the overall incidence of tumorigenesis and metastasis did not change, there was a significant delay in tumor onset in one cell line, and overall tumor progression in the other. This may suggest that Bmi-1 is important in the early stages of the progression, or in the continued growth and survival, including apoptosis resistance, of some forms of breast cancer.

Because of these new findings, it is important to better define the mechanism leading to the differences in the observed phenotype and biologic behavior of cells

overexpressing H-Ras, Bmi-1, or both oncogenes in vitro, and tumors induced by H-Ras alone or in combination with Bmi-1 in vivo. In order to better define the mechanisms related to the differences in behavior and phenotype, microarray functional analysis is underway and validation of important pathways is forthcoming. In addition, it is important to study the effects of Bmi-1 within a model of true genetic expression to effectively determine the biologic effects of Bmi-1 in the host in vivo environment. Therefore, we have developed a novel in vivo system to study the effects of Bmi-1 overexpression within the mammary gland on development and within the context of expression of other oncogenes: an inducible, mammary gland specific transgenic mouse model of Bmi-1 overexpression.

II. Microarray analysis of MCF10A-derived cell lines

Microarray analysis is an efficient means to evaluate differences in gene expression between biological samples in a high-throughput manner. Several thousand genes can be assayed in a short period of time in a number of patient or research samples to determine up- and down-regulated genes in each set [205]. This technology provides a wealth of information on disease pathways and mechanisms that can be related to cancer phenotype, biologic behavior, prognosis, and response to treatment [206-208]. Assaying gene expression of thousands of genes in different types of cancer has led to the identification of several reproducible portraits of several cancer types [208, 209], and has been used to group breast cancer subtypes based upon hormone receptor status, basal/luminal phenotype, and prognosis [208]. Further, microarray technology has been used to determine gene signatures associated with tumor progression [210], treatment

failure, and death-from-cancer phenotypes[48]. Bmi-1 has been shown to be associated with gene signatures predictive for poor prognosis and metastasis associated with a stem cell phenotype in multiple types of cancer [48]. To further determine the mechanisms associated with the Bmi-1 – H-Ras collaboration in our system, we used microarray technology to identify differentially expressed genes between each of the cell lines engineered, including the spontaneously arising spheroids generated from the MCF10A+H-Ras+Bmi-1 cells.

Preparation of samples for microarray analysis: Each of the five cell lines (MCF10A, MCF10A+Bmi-1, MCF10A+H-Ras, MCF10A+H-Ras+Bmi-1, and MCF10A+H-Ras-Bmi-1 spheroids) were grown in T75 flasks under previously described culture conditions [118]. Cells were lysed and RNA was extracted using 1 ml Trizol reagent. RNA was isolated using phenol-chloroform extraction, and cleaned with the RNeasy mini kit (Qiagen, Valencia, CA). Approximately 15 μg RNA was used for each cell line for microarray analysis.

Data normalization and analysis. RNA samples were sent to the microarray core facility (Frederick, MD) for analysis. All mRNA chips were normalized using the G-C Robust Multi-Array (GCRMA), Robust Multi-Array (RMA), or Microarray Suite 5 (MAS5) procedure (www.bioconductor.org) or using GCRMA in Partek Genomic Suite (www.partek.com). For each contrast of classes, probesets were filtered based on the detection calls derived from MAS5 procedure according to majority rule. Then the data either from RMA or MAS normalization for those filtered probes were subjected to Significance Analysis of Microarrays (SAM) procedure to determine the significant gene

lists based on intended false discovery rate (FDR), and then t-test p-values for those genes were used for further filtering for final significant gene lists. Alternatively, one way ANOVA model was used to derive the differentiated genes from different contrasts of different treatment and phenotypes in Partek Genomic Suite (www.partek.com).

The analysis of pathway/network and enrichment analysis was performed using in-house software WPS [211]. Briefly, Fisher's exact test was performed based on 2 x 2 contingency tables, to determine whether a gene is in a given list or not versus whether this gene is associated with a pathway (gene set, term) or not. A one-sided Fisher's exact test was used to measure whether a particular Biocarta pathway (www.biocarta.com), GSEA gene set term (www.broad.mit.edu/gsea/), or GO term (www.geneontology.org/) was enriched in a given gene list. The terms were ranked based on their Fisher's exact test P-values with the most enriched term listed at the top. To compare biological themes at the pathway, gene set, and GO term level across multiple gene lists of different contrasts, these gene lists were also subjected to a pathway-level pattern extraction pipeline (Yi and Stephens, unpublished work). Briefly, after batch computation of Fisher's exact test for the gene lists, the log-transformed p-values were retrieved and combined into an enrichment score matrix for clustering analysis or pathway pattern extraction. The terms (pathways, or GO terms) of selected clusters with interests were further used to retrieve the associated genes from the original gene list. Interested pathways were displayed along with the data in WPS program.

Results

Comparison of MCF10A cell lines overexpressing Bmi-1 yields a distinct Bmi-1 signature. By hybridizing the labeled cDNA from each cell line to the Affymetrix Human Genome US133 Array, the expression of 13,000 genes could be analyzed. We set cut-offs for the gene analysis at $p < 0.05$ and 1.5 fold change. Comparing the gene expression signatures of MCF10A with MCF10A+Bmi-1 and MCF10A+H-Ras with MCF10A+H-Ras+Bmi-1 resulted in a unique set of differentially expressed genes. Figure 29 shows the differentially expressed gene expression pathways associated with enriched BioCarta pathways unique to this Bmi-1 signature in a dendrogram heatmap. Several genes associated with the ATM growth pathway, and G2/M cell cycle checkpoint, including p53 and Rb pathways, were most differentially expressed within this analysis. Some important target genes that were found to be downregulated in this analysis included p53, p21 (CDKN1A), and Rad51, while c-Abl was upregulated (Figure 30), consistent with the role of Bmi-1 in suppression of the p53 cell cycle checkpoint. p21 is a universal inhibitor of cyclin-dependent kinases [212], suggesting that inhibition of p21 would result in increased proliferation and possibly transformation. Rad51 complexes with BRCA2 to repair DNA double strand breaks, and dysfunction of this complex leads to increased chromosomal instability and susceptibility to breast cancer [213]. Interestingly, c-Abl is a protein tyrosine kinase that is activated by DNA damage and in turn induces cell cycle arrest and apoptosis, which requires MAPK6 activation [214], consistent with our findings of a collaborative role of H-Ras activation and Bmi-1 function. Gene-Ontology Biological Processes associated with this Bmi-1 signature included cell cycle control, cell proliferation, and mitosis (Figure 31). These data are

consistent with our in vitro experiments that show Bmi-1 overexpression is associated with increased proliferation of MCF10A cells.

Future Directions

The preliminary microarray analysis that has been performed has confirmed our previous in vitro data and has shed some new light on other interesting pathways that may influence the phenotype of MCF10A cells transformed by Bmi-1 and H-Ras. It will be critical to analyze the array data further for differential gene expression specific to each cell line to identify pathways that would explain the differences in the in vivo tumor phenotype as well as the dramatic difference in metastatic phenotype. In addition, we plan to determine the critical differences between the MCF10A+H-Ras+Bmi-1 adherent cells and the spontaneously derived spheroid structures originating from the same cell line. It would be important to determine if there are stem cell pathways upregulated such as the Notch, Wnt, and Shh pathways that would provide evidence of enrichment for stem cells and even support for Bmi-1 in the tumor stem cell hypothesis in this model. Overall, several promising pathways for study have been discovered through the use of microarray technology that may further aid in the determination of the mechanisms of Bmi-1 overexpression in tumorigenesis and metastasis. Validation of targets identified by gene microarray will be performed, and interesting genes will undergo functional analysis to ascertain their biologic relevance to oncogenesis and metastasis. These data sets hold great potential in identifying important targets in the pathogenesis of breast cancer, and may yield insight into targets for translational research of clinical relevance.

III. Development of a tissue-specific conditional transgenic mouse model of Bmi-1 overexpression in the mammary gland

To determine the role of Bmi-1 in mammary gland development and tumorigenesis, a tissue-specific conditional mouse model of Bmi-1 overexpression restricted to the mammary gland was developed. Using the tetracycline responsive element to drive the expression of Bmi-1 under the control of the CMV promoter, transgenic mice overexpressing the Bmi-1 gene in the presence of doxycycline were developed. These mice were bred to the MMTV-rtTA mouse model to obtain double positive transgenic mice expressing both the pTRE-CMV-Bmi-1 and MMTV-rtTA construct. The MMTV-rtTA construct employs the MMTV promoter, a mammary gland-specific promoter, to drive the expression of the reverse tetracycline transactivator (rtTA) protein specifically in the mammary gland. The rtTA protein associates with the tetracycline responsive element (pTRE) in the presence of doxycycline, and activates the CMV promoter to drive Bmi-1 expression. Thus, animals harboring both transgenes overexpress Bmi-1 within the mammary gland upon the addition of doxycycline in the diet. This model provides a powerful tool in the study of Bmi-1 in mammary gland development and tumorigenesis because of its tissue specific and inducible nature, allowing study of the biologic effects of Bmi-1 overexpression at specific stages of development. Additionally, overexpression can be terminated by removal of doxycycline from the diet, to evaluate for regression of any phenotypic changes that may occur once Bmi-1 expression is turned off. Given the collaborative role Bmi-1 plays with other oncogenes, this model will be useful in experiments where oncogenes are co-expressed in

other mouse models to evaluate in vivo collaborative effects of Bmi-1 on oncogene function.

Construction of pTRE-CMV-hBmi-1 Plasmid: Wild type human Bmi-1 (hBmi-1) cDNA is 3.2kb in size, located on chromosome 10p13, and contains ten exons. The ORF encodes 326 amino acids and the protein product is 44-46 kD. The human gene shares 92% nucleotide sequence and 98% amino acid sequence identity with the gene in the mouse (mBmi-1).

The pTRE-CMV-hBmi-1 construct was created by subcloning the human Bmi-1 cDNA into the pTRE-tight expression vector. The pBabepuro-hBmi-1 plasmid was obtained from Dr. Goberhan Dimri from the Feinberg School of Medicine at Northwestern University (Figure 32A). The pBabepuro vector is 5169 bp and the internal human Bmi-1 (hBmi-1) fragment is 981 bp in size. The plasmid contains an ampicillin resistance gene (*Amp*) for propagation in bacteria and a puromycin resistance gene (*Puro*) for selection in mammalian cells. The human Bmi-1 cDNA fragment was excised from the pBabe-puro expression vector with *BamHI* and *SalI*. The 981 bp hBmi-1 cDNA was inserted into the *BamHI* and *SalI* sites of the pTRE-tight expression vector (Figure 32B). The pTRE-tight expression vector contains a modified Tet response element (pTRE), which consists of seven repeats of a 36-bp sequence that contains the 19-bp tet operator sequence (tetO). The pTRE is upstream of a CMV promoter (PminCMV), which lacks a CMV enhancer. Therefore, pTRE-tight is silent in the absence of binding of TetR or rTetR to the tetO sequences. When in the presence of doxycycline and the reverse tetracycline transactivator (rtTA), the pTRE is activated, resulting in transcription of the gene of interest.

Following successful cloning of the hBmi-1 fragment into the pTRE-tight vector, the 800 bp injection fragment containing the pTRE promoter, inserted hBmi-1, and the SV40 polyA was excised from the pTRE-tight-hBmi-1 construct (Figure 32C) by restriction digestion with *XhoI*. The plasmid construct structure was confirmed by restriction digestion. The pBabe-Bmi-1 vector was digested with *BamHI* and *SalI* to obtain the 981 bp hBmi-1 fragment, and digested with *XhoI*, which gave the expected ~2 kb fragment. The hBmi-1 fragment did not possess a restriction digest site for *XhoI* enzyme that would interfere with the injection fragment to be excised in the final construct.

Generation, Maintenance and Identification of pTRE-Bmi-1 Transgenic Mice:

Since the pTRE-tight system had been used successfully in vivo previously, the newly constructed pTRE-tight/Bmi-1 plasmid was sent to the transgenic core facility (NCI-Frederick) for injection of the appropriate DNA fragment in blastocysts in order to create a pTRE/Bmi-1 transgenic mouse. The injection fragment was microinjected into the male pronucleus of a one day old blastocyst, then implanted in the oviduct of a pseudopregnant female FVB mouse [215]. The resulting pups were screened by Southern blot analysis. 1 μg of pTRE-Bmi-1 injection fragment DNA and 10-20 μg of tail genomic DNA was digested with *BamHI* and separated on an agarose gel. The DNA was transferred to Hybond-N Nylon membranes (Amersham) and hybridized in QuikHyb Solution (Stratagene) with a 32P-random primed-labeled probe.

Ten founder mice were determined to carry the transgene. The founders were determined by southern blot following digestion of genomic DNA with *BamHI* and *XhoI*.

Since the injection fragment is inserted randomly into the genome during microinjection of the blastocyst, insertion in varying orientations had to be accounted for, such as head-to-head, head-to-tail, and tail-to-tail insertions. The injection fragment was ~2 kb in size when digested with *XhoI*, with a *BamHI* restriction site at 350 bp. When the genomic DNA of founders inheriting the pTRE-hBmi-1 injection fragment is digested with *BamHI*, a number of fragments can result based upon the orientation of the inserted injection fragment (Figure 33). If the fragment was inserted head-to-head, a ~700 bp fragment could result. If the fragment was inserted tail-to-tail, a ~3.2 kb fragment could be seen. Finally, if the fragment was inserted head-to-tail, a ~2 kb fragment could occur. These fragments were present in the control injection fragment (C) digested with *BamHI*, and the founders were identified by the most common insertion orientations yielding a 3.2 kb or 2 kb fragment (Figure 34). Relative copy number was estimated from signal intensity on southern blot, and ranged from one to 80 copies. Following founder identification, the highest expressing lines (A1, K9, and E4) were propagated by breeding to FVB mice and screened by PCR. The E4 line ultimately was propagated because of its willingness to breed and its large litters. For PCR, 50-200 ng of genomic tail DNA was added to a 25 μl reaction volume [10x PCR buffer, 50 mM $MgCl_2$, 2.5 mM dNTP's, 1 U Taq Polymerase, and 10 μM each of pTRE forward 5'- TGT CGA GTT TAC TCC CTA TCA GTG -3` and hBmi-1 reverse 5`-CAT TTT TGA AAA GCC CTG GA -3` primers. Cycling conditions consisted of 95 °C for 3 min, followed by 33 cycles of 94 °C for 45 sec, 56 °C for 45 sec, and 72 °C for 45 sec, then an extension at 72 °C for 10 min, resulting in a PCR product 576 bp. Mice harboring the genotype were then bred to MMTV-rtta mice to generate double positive mice, screened by using MMTV-rtta

specific primers (rtTA.497F 5`-TGC CGC CAT TAT TAC GAC AAG C-3` and rtTA.1002R 5`-ACC GTA CTC GTC AAT TCC AAG GG-3`). All methods used to breed animals were in compliance with the National Institutes of Health Animal Care and Use Committee regulations.

Induction of Transgene Expression:

Once double positive animals were successfully identified, the inducible function of the construct was tested in a set of mice. Animals harboring both transgenes (pTRE-Bmi-1 X MMTV-rtTA) possessed the inducible pTRE construct and the mammary gland specific MMTV promoter driving the rtTA gene. In the presence of doxycycline, the rtTA functionally binds to the pTRE, and drives Bmi-1 expression in the mammary gland. A dose of 2 mg/ml doxycycline [216] was administered in the drinking water for 14 days, and animals were sacrificed and mammary glands from either mammary chain were harvested for protein and RNA analysis. Glands were snap frozen in liquid nitrogen, pulverized with a mortar and pestel, and lysates were prepared in a tissue macerator with 1 ml RIPA lysis buffer containing anti-proteases. Similarly, glands collected for RNA analysis were snap frozen, pulverized, and lysed in Trizol reagent, followed by phenol-chloroform isolation and purification. Additionally, glands were collected for histopathologic examination. Glands were fixed in 4% paraformaldehyde and routinely processed into paraffin blocks from which 4 μm sections were prepared and stained with hematoxylin and eosin (H&E).

RNA samples from wildtype (WT), Bmi-1+/rtTA-, and Bmi-1+/rtTA+ mice were tested for Bmi-1 mRNA expression using RT-PCR. The RT reaction (1 μl oligoDT, 1 μl

10 mMdNTP, 10 µl H_2O) was incubated for 5 min at 65 °C, and added to 4 µl 5X buffer, 1 µl 0.1M DTT, 1 µl RNAse out, and 1 µl SSII RT enzyme per sample. The RT reaction mixture was incubated at 50 °C for 60 min, and the 70 °C mixture was incubated for 15 min, then chilled to 4 °C to obtain cDNA. The 220 bp human Bmi-1 cDNA fragment was amplified with human specific Bmi-1 primers (hBmi-1F 5` TCA TCC TTC TGC TGA TGC TG-3` and hBmi-1R 5`-GCA TCA CAG TCA TTG CTG CT/-3`). The amplified cDNA was run on a 1% agarose gel and photographed (Figure 35).

Results

Generation of pTRE-Bmi-1 X MMTV-rtTA Mice

Transgenic mice overexpressing the human Bmi-1 gene under the inducible control of the pTRE-CMV promoter were created by microinjection of the linearized pTRE-CMV promoter, hBmi-1, and the SV40 polyA tail into the male pronucleus of a blastocyst. Founder pups were screened by Southern blot analysis using tail snip DNA, and offspring were screened by PCR using specific primers recognizing the pTRE and hBmi-1. Positive offspring were bred to the MMTV-rtTA colony and animals were screened for the presence of both transgenes by PCR.

Induction of transgene expression

All heterozygous pTRE-Bmi-1 animals exhibited normal behavior and were healthy throughout the experiment. Males and females were fertile, and females were able to lactate and nurse their pups. A subset of animals possessing both the pTRE-Bmi-1 and MMTV-rtTA transgenes were given doxycycline (2 mg/ml) in their drinking water for at least 14 days. After 14 days of doxycycline administration, animals were sacrificed

in diestrus, and mammary glands were harvested for histopathology and protein and RNA analysis. Since we have shown by immunohistochemical analysis that Bmi-1 expression in the mouse mammary gland is lowest during diestrus, mice were examined at this stage of the estrus cycle. The stage of estrus was determined by using an estrus monitor to measure the electrical impedence of the vaginal epithelial cell layer. The electrical impedence of the vaginal epithelium differs based upon the thickness of the epithelium at different stages of the estrus cycle. Histopathologic examination of glands of animals with Bmi-1 overexpression for two weeks showed no significant changes in mammary gland structure or function. There was no evidence of hyperplasia, inflammation, or atypical cellular changes. PCR examination following 14 days of doxycycline administration determined that the 200 bp human Bmi-1 mRNA was overexpressed in Bmi-1+/rtTA+ animals, but not in Bmi-1+/rtTA- or wildtype (WT) animals. There was minimal expression of Bmi-1 mRNA in Bmi-1+/rtTA- animals, indicating a small amount of leakiness present in the model. Human beta-actin (500 bp) was used as a control.

Future directions and utility of the pTRE-Bmi X MMTV-rtta model

To adequately examine the role of Bmi-1 expression in mammary gland biology, three major experiments will be designed: 1) exposure to Bmi-1 overexpression chronically and throughout different stages of development, 2) breeding to other GEM models of human breast cancer, and 3) overexpression of Bmi-1 in chemically induced models of breast cancer. Chronic overexpression of Bmi-1 will determine if overexpression of Bmi-1 will impact mammary gland biology over extended periods of time. Acute, short term exposure to Bmi-1 overexpression in the mammary gland may

not be sufficient to alter or induce a phenotype, and this may require longer exposure periods. Examinations will be based on histopathologic and immunohistochemical analysis of the mammary glands following 1, 4, 6, and 12 month exposures to doxycycline.

Since Bmi-1 has been shown to be important in morphogenesis and embryonic development [217], exposure to high levels of Bmi-1 throughout the in-utero time period into the pre-weaning ages is important to address the biologic effects of Bmi-1 overexpression in the mammary gland at early stages of development. The mammary gland of the mouse develops in four stages: 1) in utero, 2) during puberty, 3) during each estrus cycle, and 4) during pregnancy [218]. In utero, rudimentary ducts are initially formed, and during puberty the ducts elongate and branch to fill the mammary fat pad. The density of ductal side branching as well as the number of alveolar buds increases with each estrus cycle, and during pregnancy large lobuloalveolar structures producing milk arise from these alveolar buds. The mammary gland is thus an incredibly proliferative organ with incredible regenerative capacity. This can also be observed during involution of the gland following estrus or pregnancy, wherein the gland loses a large majority of the epithelial cell component.

Given its role in the maintenance of stem cell populations, overexpression of Bmi-1 in utero when the rudimentary ducts are formed may cause any number of deleterious phenotypes. It has been thought that hormone exposure in utero or during the early postnatal period may influence the proliferative potential of stem cells [219-221]. If Bmi-1 overexpression has a positive influence on stem cell number within the mammary gland, this may increase the number of cells that are exposed to hormones later in life

during puberty. In addition, since some breast cancers are thought to arise from transformation of mammary stem cells [220, 222] increased numbers of stem cells within the mammary gland may translate to an increased risk for the development of mammary neoplasia.

We have previously shown that when Bmi-1 is dysregulated or overexpressed, it can act as an oncogene [118]. During puberty, when the ducts are branching to fill the fat pad, Bmi-1 overexpression may alter the branching morphology or increase the number or density of branching, leading to an abnormal phenotype. It has been shown that overexpression of genes responsible for stem cell maintenance such as Notch1 and Notch3 result in a decreased proliferation of ductal and alveolar epithelial cells during puberty, resulting in impaired ductal and lobuloalveolar development and inability to form certain milk proteins [223]. Bmi-1 overexpression during this time may have a similar effect on mammary gland morphology, or it may act to increase the proliferation of ductal and lobuloalveolar structures, making the gland more prone to tumorigenesis.

It is well known that the development of many mammary cancers is influenced by hormonal factors, particularly estrogens and their receptors [220, 224]. Exposure to estrogen over an extended period of time may increase a woman's risk of breast cancer. Increased exposure occurs in women who enter early menarche, since this increases the number of years the breast tissue is exposed to estrogen. In addition, the more years a woman menstruates, the longer the breast tissue is exposed to estrogen, and so late menopause also influences a woman's risk of breast cancer [225]. Finally, late pregnancy or never having been pregnant are risk factors because estrogen levels are low during pregnancy and breast tissue is exposed to more estrogen in women who become

pregnant for the first time after the age of 35, or in those who never become pregnant [226]. Should Bmi-1 alter or increase the density of ductal or alveolar cells during estrus, this would have a significant effect on the likelihood of mammary epithelial transformation over several estrous cycles.

Given its collaborative role with other oncogenes in the induction of leukemias and lymphomas [28, 53], and the transformation of mammary epithelial cells in vitro and in vivo [29, 118], breeding pTRE-Bmi X MMTV-rtTA transgenic mice to other GEM models of breast cancer would yield important insights on the effects of Bmi-1 overexpression in the context of other oncogenes. It has been shown that overexpression of more than one oncogene in a GEM model can significantly alter the resulting phenotype, whether it is by morphology or by increased incidence or acceleration of the disease process. Overexpression of Bmi-1 in the Eμ-myc transgenic mouse model of lymphoma resulted in a dramatic increase in incidence as well as acceleration of pre-B cell lymphomagenesis [28, 53]. We have shown that overexpression of Bmi-1 in the context of H-Ras overexpression in normal human mammary epithelial cells results in acceleration of tumor formation as well as a more poorly-differentiated, aggressive phenotype in xenograft models [118]. However, these models lack an endogenous germline mutation that is characteristic of natural breast cancer and development of neoplasias in GEM models. Therefore, the development of a bitransgenic, inducible model of oncogene collaboration between Bmi-1 and other oncogenes involved in human breast cancer would be a very versatile and powerful tool to study molecular mechanisms involved in oncogene collaboration.

The pTRE-Bmi-1 transgenic mouse would be particularly useful in determining if Bmi-1 overexpression affects the response to carcinogens. Several models of carcinogen driven mammary tumorigenesis exist, most notably the 7,12-dimethylbenz[a]anthracene (DMBA) model. The mechanism of action of DMBA is through metabolism into a diol epoxide which incorporates into DNA and causes mutations [227], as well as by blocking transport of glutathione to the liver [228]. Mice treated with DMBA generally acquire mammary tumors by 90 days following administration characterized as adenocarcinoma, squamous cell carcinoma, or myoepithelial carcinoma [229]. Through its role in suppression of the Ink4A-Arf tumor suppressor locus, Bmi-1 overexpression may result in increased incidence of mammary tumor formation, acceleration of tumorigenesis, or modification of the histologic phenotype. This would lend further support to the role of Bmi-1 as a collaborating oncogene.

IV. Future Directions

Future studies arising from this research should include 1) investigation of the stem cell phenotype of MCF10A+H-Ras+Bmi-1 spheroids, 2) characterization of the mechanisms of apoptosis inhibition and metastatic propensity by Bmi-1, and 3) exploring the collaborative relationship of Bmi-1 with other oncogenes in breast cancer.

To investigate the stem cell phenotype of MCF10A+H-Ras+Bmi-1 spheroids, it will be important to identify stem cell markers present or upregulated in these cells compared to adherent MCF10A+H-Ras+Bmi-1 cells. In vitro, this would be achieved through western blot analysis of spheroids for markers such as CD44, CD24, Oct3/4, and aldehyde dehydrogenase (ALDH). One of the important characteristics of stem cells is

their ability to escape apoptosis induced by anchorage-dependent cells detaching from the surrounding extracellular matrix (anoikis). This could be tested in vitro by culturing MCF10A+H-Ras+Bmi-1 and MCF10A+H-Ras cells in suspension culture, and assaying the cells for apoptosis and proliferation. We would hypothesize that the MCF10A+H-Ras+Bmi-1 cells would be induced to form spheres due to anchorage independence, and continue to proliferate, whereas the MCF10A+H-Ras cells would undergo anoikis. To test the stem cell properties of these spheroids in vivo, an athymic nude mouse xenograft model would be used to test the self-renewal capability of these transformed cells. The definitive test of the tumor stem cell nature of a transformed cell is the in vivo recapitulation of a tumor from a very small number of tumor cells that possess a stem cell phenotype. MCF10A+H-Ras+Bmi-1 spheroids would be disassociated by trypsinization and counted, followed by implantation of cells into the mammary fat pad in a dilution series ranging from $1X10^6$ cells to 100 cells. A similar dilution series would be performed with MCF10A+H-Ras+Bmi-1 adherent cells and MCF10A+H-Ras cells as controls. If animals with a relatively small number of cells derived from spheroids form tumors and other groups do not, this would be further evidence of the stem cell nature of these transformed cells.

The mechanism of apoptosis inhibition in MCF10A+H-Ras+Bmi-1 certainly deserves further investigation. Western blot analysis of all MCF10A derived cell lines for mediators of apoptosis such as the caspases or the BCL2 family will potentially illustrate the mechanism behind this apoptosis inhibition, and provide targets for functional analysis in vitro. In addition, the data obtained from microarray analysis can be used to identify pathways that Bmi-1 is signaling through to prevent apoptosis, and these

pathways can be targeted with specific drugs, antibodies, or shRNA to knock out these mediators to provide additional functional analysis and physiologic relevance to Bmi-1 induced apoptosis inhibition.

The mechanism leading to the striking difference in the metastatic phenotype between the MCF10A+H-Ras and MCF10A+H-Ras+Bmi-1 cells is perhaps the most interesting and obvious further pursuit. First, an analysis by western blot of the pulmonary metastases from MCF10A+H-Ras (obtained by laser microdissection) and MCF10A+H-Ras+Bmi-1 tumors for mediators involved in the metastatic phenotype such as the matrix metalloproteinases (MMPs) or angiogenic mediators (VEGF, Angl, Tie2) would be integral. Secondly, identification of such mediators in the microarray data would provide targets for functional analysis in vivo. An important functional experiment would be to knock down the expression of one or more such genes identified on the microarray or by western blot in MCF10A+H-Ras+Bmi-1 cells and test their invasive capabilities in a Matrigel invasion assay compared to cells without knock down. Ultimately, it would be important to use these cells in a mammary fat pad xenograft model to analyze for changes in spontaneous metastasis, or in a tail vein model to measure differences in embolization and establishment of pulmonary metastases.

Since H-Ras is not the only important oncogene involved in the genesis of breast cancer, collaborative studies with Bmi-1 and other oncogenes will be important. Similar experiments as those that have been performed in this dissertation research with H-Ras can be performed with other oncogenes important in breast cancer, such as c-erb-B2 (Her2neu), c-myc, TGFα, Akt, p53, BRCA1, Notch, and Wnt. Some of these mediators have been shown to be involved in the Bmi-1 pathway (e.g., p53), and it would be

important to determine the functional consequences of Bmi-1 overexpression in the presence of each mutation. Other mediators have been associated with stem cell pathways (BRCA1, Notch, Wnt), and the determination of their association with Bmi-1 in any mechanistic sense would be important to understanding the role Bmi-1 plays in influencing tumorigenesis, and establishing that the effects of Bmi-1 are not only oncogene specific, but are also global throughout the genome.

Finally, since we have shown that Bmi-1 has important effects on cell growth and transformation in vitro and tumorigenesis and metastasis in vivo, it is important to investigate the clinical relevance of the role of Bmi-1 in breast cancer through translational research. Since Bmi-1 overexpression is associated with a more aggressive phenotype, targeting Bmi-1 as a tumor marker would be potentially important in the diagnosis and treatment of aggressive breast cancer. Development of drugs to inhibit the Bmi-1 pathway would be an important potential means to treat or slow the progression of disease, including distant metastasis.

APPENDIX E

Figure 28: All enriched BioCarta pathways shared by Bmi-1 overexpressing cells. Heatmap dendrogram comparing gene expression pathways in MCF10A vs. MCF10A+Bmi-1 and MCF10A+H-Ras vs. MCF10A+H-Ras+Bmi-1, revealing a Bmi-1 specific gene expression signature; several genes associated with the ATM growth pathway, and G2/M cell cycle checkpoint, including p53 and Rb pathways, are most differentially expressed. Each column represents a comparison between two MCF10A-derived cell lines, and the red signal indicates a significant change in ATM and G2/M checkpoint signaling related to Bmi-1 expression.

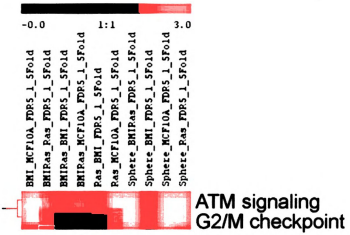

Figure 29: Genes up- and down-regulated in the ATM and G2/M cell cycle checkpoint pathways. BioCarta pathways differentially expressed in MCF10A vs. MCF10A+Bmi-1 and MCF10A+H-Ras vs. MCF10A+H-Ras+Bmi-1 reveals a unique Bmi-1 expression profile of up- and down-regulated pathways. Green represents downregulation and red represents upregulation of genes in each pathway.

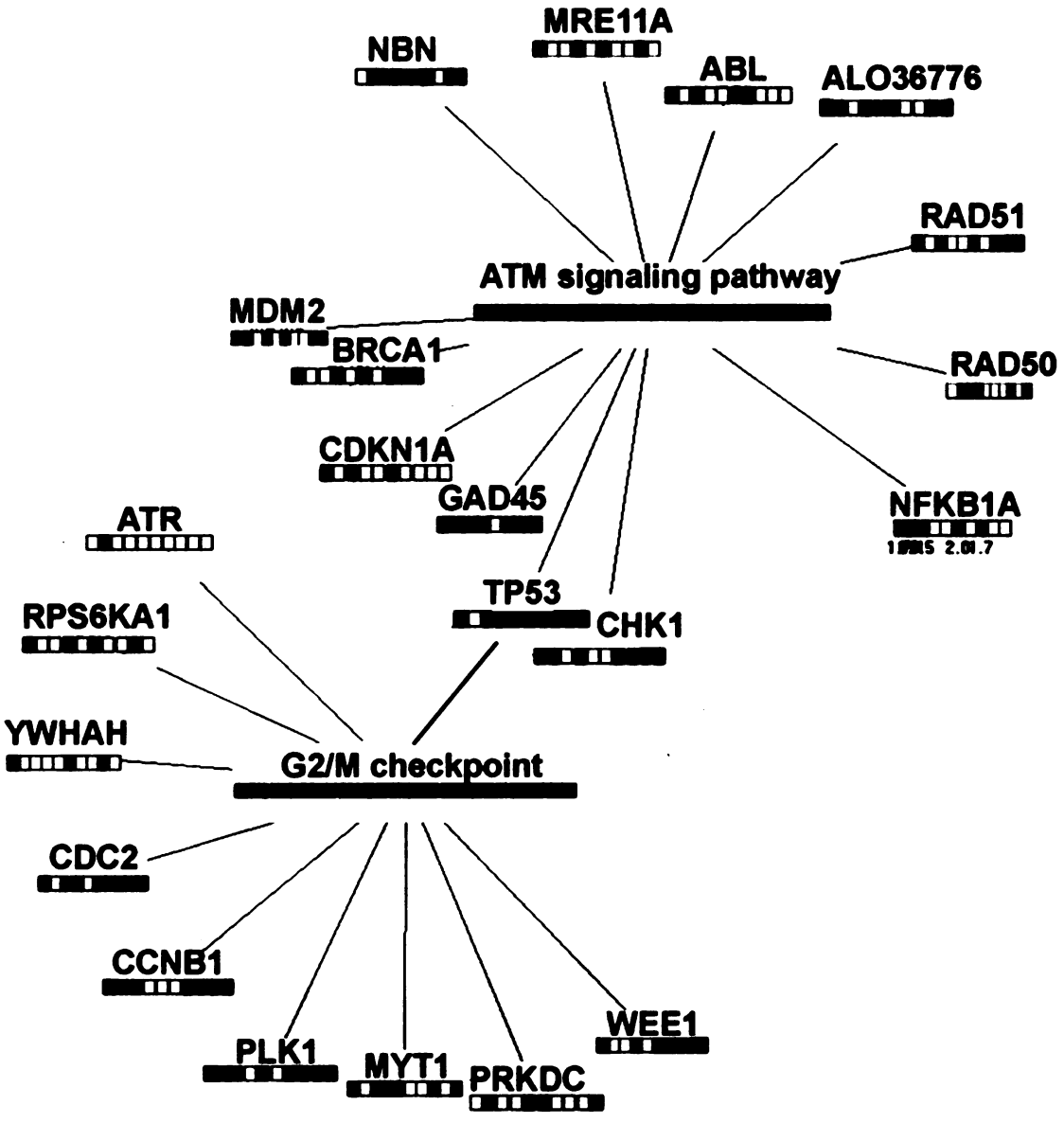

Figure 30: Gene-Ontology Biological Processes associated with Bmi-1 signature. Pathways associated with the unique Bmi-1 gene profile include cell cycle control, cell growth, and mitosis. Each column represents a comparison between two MCF10A-derived cell lines, and the red signal indicates a significant change in ATM and G2/M checkpoint signaling related to Bmi-1 expression.

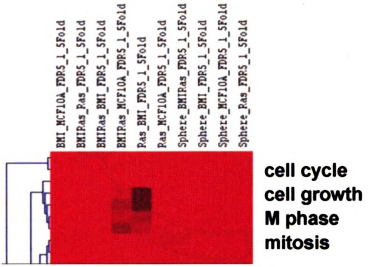

Figure 31: Vectors and expression plasmids used in development of inducible mammary-specific transgenic mouse model of Bmi-1 overexpression. (A) The ~5.2 Kb pBabepuro-hBmi-1 retroviral plasmid contains the 981 bp human Bmi-1 gene flanked by the GAG and pSV40 genes, and an ampicillin resistance gene for propagation in bacteria and a puromycin resistance gene for selection in mammalian cells. (B) The 2.6Kb pTRE-tight expression vector contains a modified Tet response element (pTRE), containing the tet operator sequence (tetO) upstream from the CMV promoter (PminCMV). (C) The final construct containing the pTRE-CMV promoter, hBmi-1 gene, SV40 polyA tail, and ampicillin resistance gene (Amp^r).

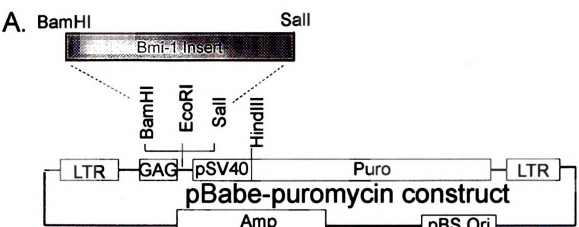

Figure 31 (continued)

B.

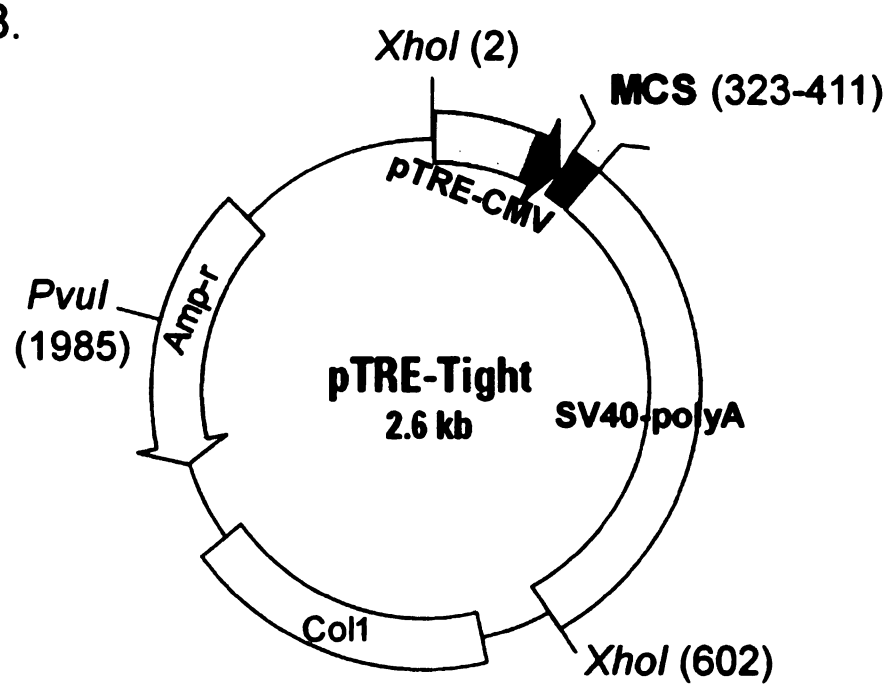

C.

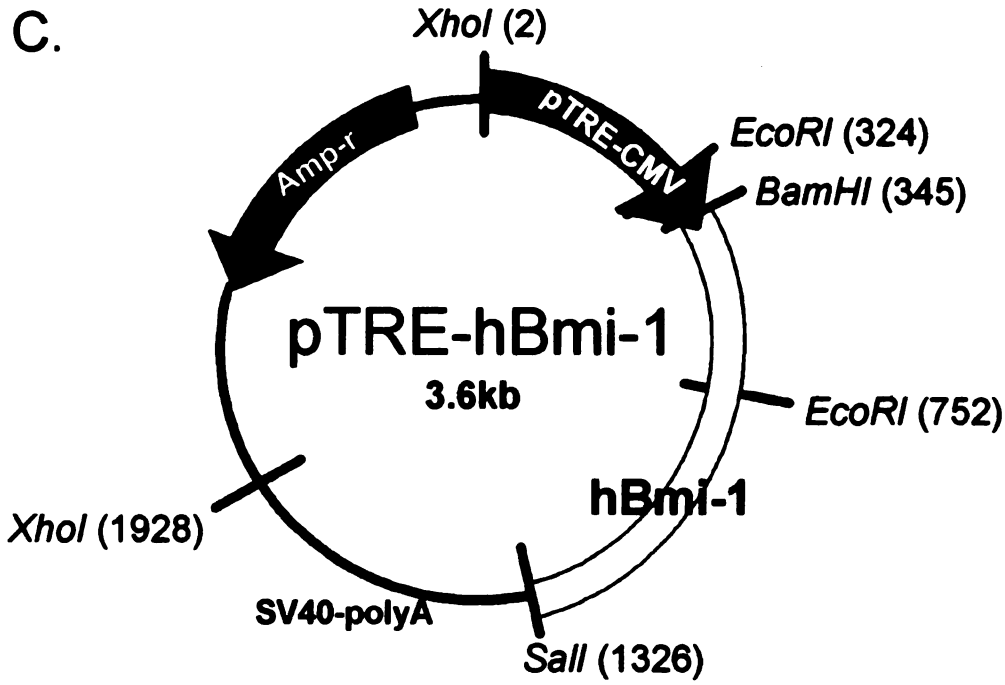

Figure 32: Possible orientation of integrations of the transgene and their respective fragment sizes following restriction enzyme digestion. Possible orientations of the transgene following random integration include head-to-head (resulting in a ~700 bp fragment), tail-to-tail (resulting in a ~3.2 kb fragment), and head to tail (resulting in a ~2 kb fragment).

Head-to-head:

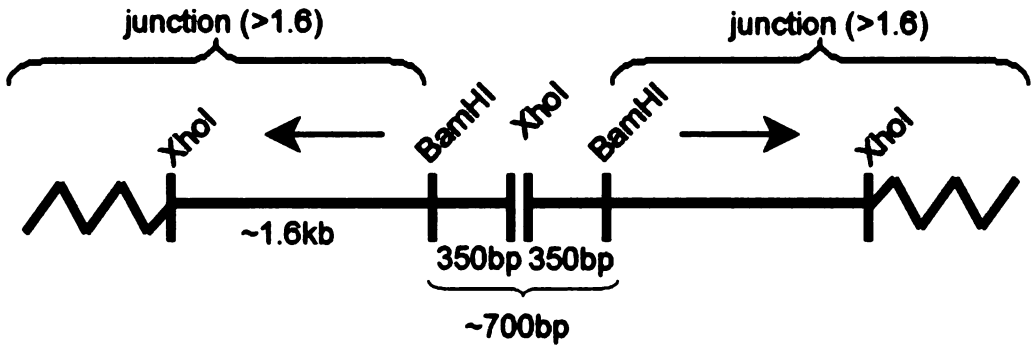

Tail-to-tail:

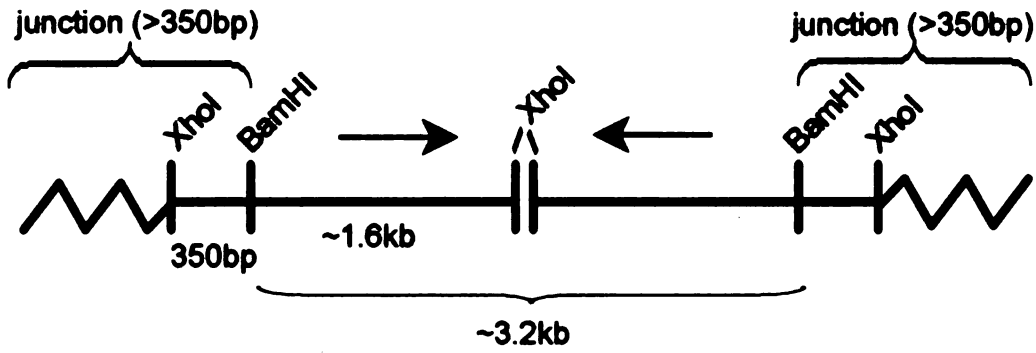

Head-to-tail:

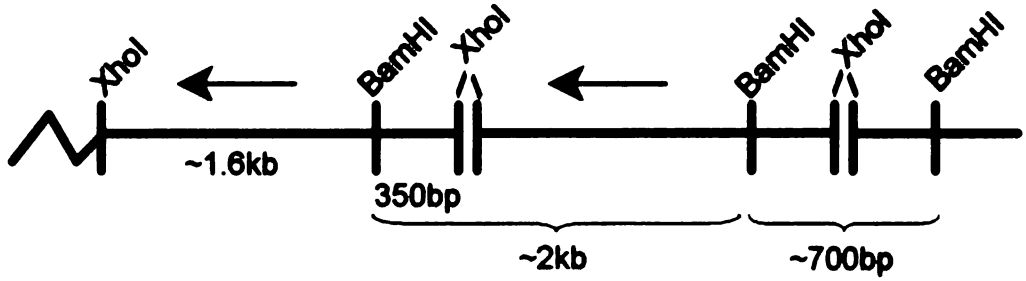

Figure 33: Southern blot analysis of 10 µg of genomic DNA from pTRE-Bmi-1 transgenic founders. Ten founder lines were identified with relative copy numbers ranging from one (H8) to eighty (A1) copies.

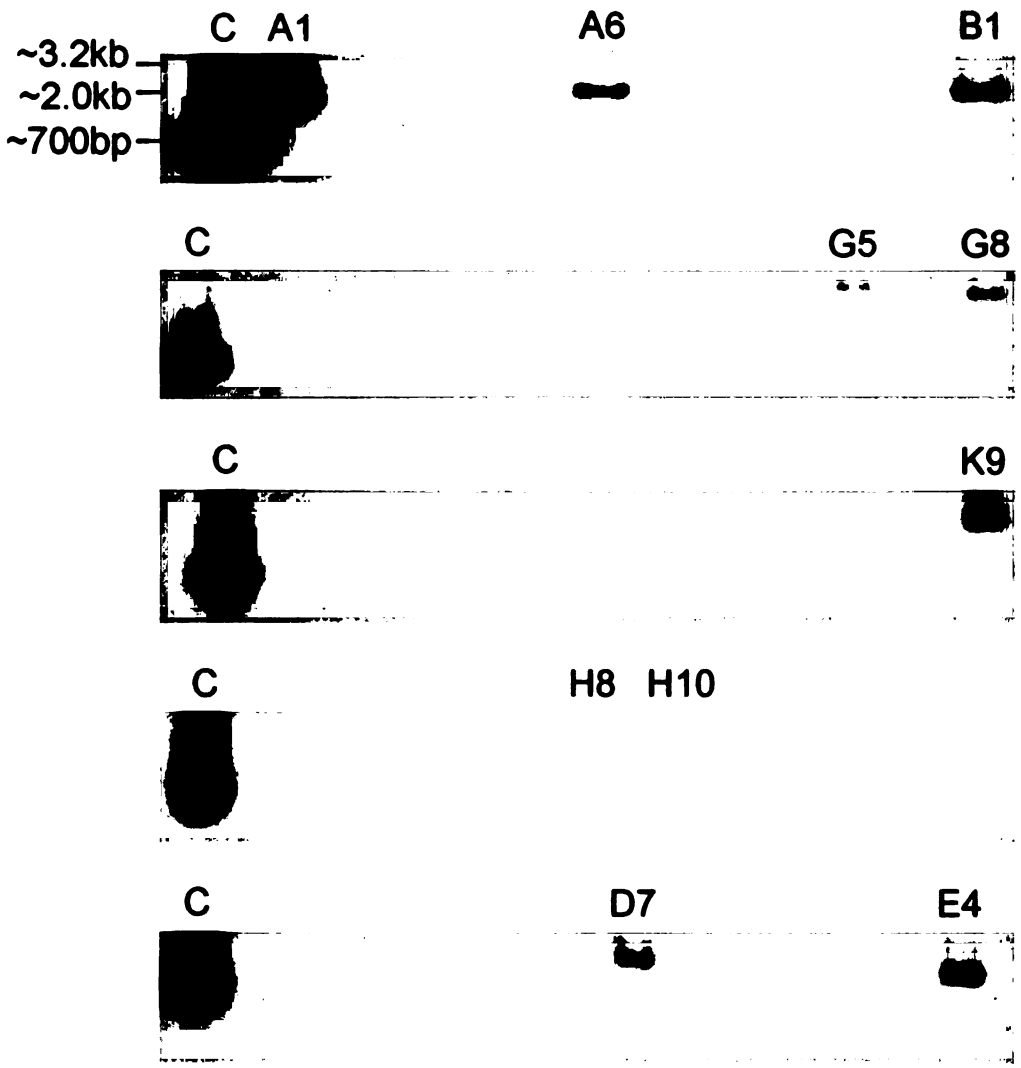

Figure 34: Tetracycline induced mammary-specific mRNA expression of Bmi-1. mRNA expression in mammary glands of single positive (pTRE-Bmi^{+}/MMTV-rtta^{-}), double positive (pTRE-Bmi^{+}/MMTV-rtta^{+}), and wildtype FVB mice following 14 days of doxycycline administration.

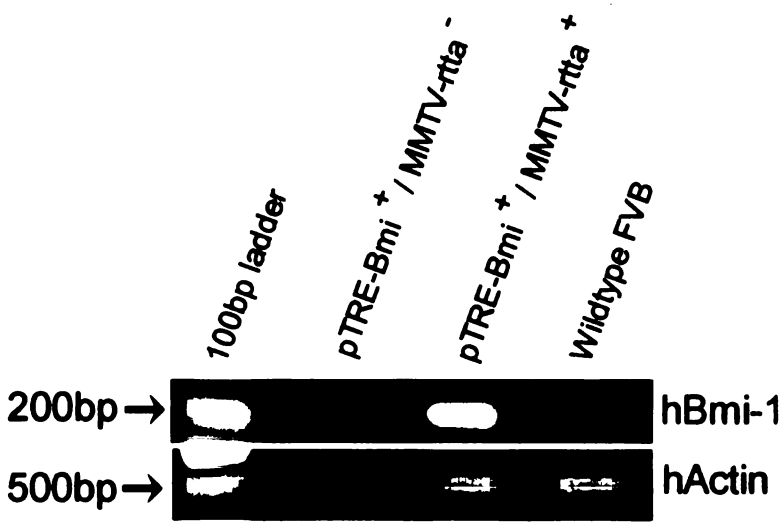

REFERENCES

1. Sparmann, A. and M. van Lohuizen, *Polycomb silencers control cell fate, development and cancer.* Nat Rev Cancer, 2006. **6**(11): p. 846-56.

2. Holliday, R., *Epigenetics: an overview.* Dev Genet, 1994. **15**(6): p. 453-7.

3. Baylin, S.B. and J.E. Ohm, *Epigenetic gene silencing in cancer - a mechanism for early oncogenic pathway addiction?* Nat Rev Cancer, 2006. **6**(2): p. 107-16.

4. Henikoff, S. and K. Ahmad, *Assembly of variant histones into chromatin.* Annu Rev Cell Dev Biol, 2005. **21**: p. 133-53.

5. Jones, P.A. and S.B. Baylin, *The fundamental role of epigenetic events in cancer.* Nat Rev Genet, 2002. **3**(6): p. 415-28.

6. Smith, C.L. and C.L. Peterson, *ATP-dependent chromatin remodeling.* Curr Top Dev Biol, 2005. **65**: p. 115-48.

7. Strahl, B.D. and C.D. Allis, *The language of covalent histone modifications.* Nature, 2000. **403**(6765): p. 41-5.

8. Barcellos-Hoff, M.H., *It takes a tissue to make a tumor: epigenetics, cancer and the microenvironment.* J Mammary Gland Biol Neoplasia, 2001. **6**(2): p. 213-21.

9. Barcellos-Hoff, M.H. and D. Medina, *New highlights on stroma-epithelial interactions in breast cancer.* Breast Cancer Res, 2005. **7**(1): p. 33-6.

10. Cavalli, G., *Chromatin and epigenetics in development: blending cellular memory with cell fate plasticity.* Development, 2006. **133**(11): p. 2089-94.

11. Mello, C.C. and D. Conte, Jr., *Revealing the world of RNA interference.* Nature, 2004. **431**(7006): p. 338-42.

12. Jones, P.L. and A.P. Wolffe, *Relationships between chromatin organization and DNA methylation in determining gene expression.* Semin Cancer Biol, 1999. **9**(5): p. 339-47.

13. Qiu, J., *Epigenetics: unfinished symphony.* Nature, 2006. **441**(7090): p. 143-5.

14. Wolffe, A.P. and M.A. Matzke, *Epigenetics: regulation through repression.* Science, 1999. **286**(5439): p. 481-6.

15. Jones, P.A. and D. Takai, *The role of DNA methylation in mammalian epigenetics.* Science, 2001. **293**(5532): p. 1068-70.

16. Luger, K., et al., *Crystal structure of the nucleosome core particle at 2.8 A resolution.* Nature, 1997. **389**(6648): p. 251-60.

17. Wolffe, A.P., *Packaging principle: how DNA methylation and histone acetylation control the transcriptional activity of chromatin.* J Exp Zool, 1998. **282**(1-2): p. 239-44.

18. Itahana, K., et al., *Control of the replicative life span of human fibroblasts by p16 and the polycomb protein Bmi-1.* Mol Cell Biol, 2003. **23**(1): p. 389-401.

19. Guney, I., S. Wu, and J.M. Sedivy, *Reduced c-Myc signaling triggers telomere-independent senescence by regulating Bmi-1 and p16(INK4a).* Proc Natl Acad Sci U S A, 2006. **103**(10): p. 3645-50.

20. Hernandez-Munoz, I., et al., *Association of BMI1 with polycomb bodies is dynamic and requires PRC2/EZH2 and the maintenance DNA methyltransferase DNMT1.* Mol Cell Biol, 2005. **25**(24): p. 11047-58.

21. Voncken, J.W., et al., *Chromatin-association of the Polycomb group protein BMI1 is cell cycle-regulated and correlates with its phosphorylation status.* J Cell Sci, 1999. **112 (Pt 24)**: p. 4627-39.

22. Bracken, A.P., et al., *The Polycomb group proteins bind throughout the INK4A-ARF locus and are disassociated in senescent cells.* Genes Dev, 2007. **21**(5): p. 525-30.

23. Levine, S.S., I.F. King, and R.E. Kingston, *Division of labor in polycomb group repression.* Trends Biochem Sci, 2004. **29**(9): p. 478-85.

24. Bracken, A.P., et al., *Genome-wide mapping of Polycomb target genes unravels their roles in cell fate transitions.* Genes Dev, 2006. **20**(9): p. 1123-36.

25. van Kemenade, F.J., et al., *Coexpression of BMI-1 and EZH2 polycomb-group proteins is associated with cycling cells and degree of malignancy in B-cell non-Hodgkin lymphoma.* Blood, 2001. **97**(12): p. 3896-901.

26. Simon, J.A. and J.W. Tamkun, *Programming off and on states in chromatin: mechanisms of Polycomb and trithorax group complexes.* Curr Opin Genet Dev, 2002. **12**(2): p. 210-8.

27. Al-Hajj, M., et al., *Therapeutic implications of cancer stem cells.* Curr Opin Genet Dev, 2004. **14**(1): p. 43-7.

28. Alkema, M.J., et al., *Characterization and chromosomal localization of the human proto-oncogene BMI-1.* Hum Mol Genet, 1993. **2**(10): p. 1597-603.

29. Dimri, G.P., et al., *The Bmi-1 oncogene induces telomerase activity and immortalizes human mammary epithelial cells.* Cancer Res, 2002. **62**(16): p. 4736-45.

30. Jacobs, J.J., et al., *Bmi-1 collaborates with c-Myc in tumorigenesis by inhibiting c-Myc-induced apoptosis via INK4a/ARF.* Genes Dev, 1999. **13**(20): p. 2678-90.

31. Lessard, J. and G. Sauvageau, *Bmi-1 determines the proliferative capacity of normal and leukaemic stem cells.* Nature, 2003. **423**(6937): p. 255-60.

32. Molofsky, A.V., et al., *Bmi-1 promotes neural stem cell self-renewal and neural development but not mouse growth and survival by repressing the p16Ink4a and p19Arf senescence pathways.* Genes Dev, 2005. **19**(12): p. 1432-7.

33. Cui, H., et al., *Bmi-1 is essential for the tumorigenicity of neuroblastoma cells.* Am J Pathol, 2007. **170**(4): p. 1370-8.

34. Cui, H., et al., *Bmi-1 regulates the differentiation and clonogenic self-renewal of I-type neuroblastoma cells in a concentration-dependent manner.* J Biol Chem, 2006. **281**(45): p. 34696-704.

35. Liu, S., et al., *Hedgehog signaling and Bmi-1 regulate self-renewal of normal and malignant human mammary stem cells.* Cancer Res, 2006. **66**(12): p. 6063-71.

36. Haga, K., et al., *Efficient immortalization of primary human cells by p16INK4a-specific short hairpin RNA or Bmi-1, combined with introduction of hTERT.* Cancer Sci, 2007. **98**(2): p. 147-54.

37. Song, L.B., et al., *Bmi-1 is a novel molecular marker of nasopharyngeal carcinoma progression and immortalizes primary human nasopharyngeal epithelial cells.* Cancer Res, 2006. **66**(12): p. 6225-32.

38. Kang, M.K., et al., *Elevated Bmi-1 expression is associated with dysplastic cell transformation during oral carcinogenesis and is required for cancer cell replication and survival.* Br J Cancer, 2007. **96**(1): p. 126-33.

39. Nowak, K., et al., *BMI1 is a target gene of E2F-1 and is strongly expressed in primary neuroblastomas.* Nucleic Acids Res, 2006. **34**(6): p. 1745-54.

40. Leung, C., et al., *Bmi1 is essential for cerebellar development and is overexpressed in human medulloblastomas.* Nature, 2004. **428**(6980): p. 337-41.

41. Vonlanthen, S., et al., *The bmi-1 oncoprotein is differentially expressed in non-small cell lung cancer and correlates with INK4A-ARF locus expression.* Br J Cancer, 2001. **84**(10): p. 1372-6.

42. Reinisch, C.M., et al., *Expression of BMI-1 in normal skin and inflammatory and neoplastic skin lesions.* J Cutan Pathol, 2007. **34**(2): p. 174-80.

43. Neo, S.Y., et al., *Identification of discriminators of hepatoma by gene expression profiling using a minimal dataset approach.* Hepatology, 2004. **39**(4): p. 944-53.

44. Kim, J.H., et al., *The Bmi-1 oncoprotein is overexpressed in human colorectal cancer and correlates with the reduced p16INK4a/p14ARF proteins.* Cancer Lett, 2004. **203**(2): p. 217-24.

45. Reinisch, C., et al., *BMI-1: a protein expressed in stem cells, specialized cells and tumors of the gastrointestinal tract.* Histol Histopathol, 2006. **21**(11): p. 1143-9.

46. Tateishi, K., et al., *Dysregulated expression of stem cell factor Bmi1 in precancerous lesions of the gastrointestinal tract.* Clin Cancer Res, 2006. **12**(23): p. 6960-6.

47. Kim, J.H., et al., *Overexpression of Bmi-1 oncoprotein correlates with axillary lymph node metastases in invasive ductal breast cancer.* Breast, 2004. **13**(5): p. 383-8.

48. Glinsky, G.V., O. Berezovska, and A.B. Glinskii, *Microarray analysis identifies a death-from-cancer signature predicting therapy failure in patients with multiple types of cancer.* J Clin Invest, 2005. **115**(6): p. 1503-21.

49. Steele, J.C., et al., *The polycomb group proteins, BMI-1 and EZH2, are tumour-associated antigens.* Br J Cancer, 2006. **95**(9): p. 1202-11.

50. Silva, J., et al., *Implication of polycomb members Bmi-1, Mel-18, and Hpc-2 in the regulation of p16INK4a, p14ARF, h-TERT, and c-Myc expression in primary breast carcinomas.* Clin Cancer Res, 2006. **12**(23): p. 6929-36.

51. Berns, A., et al., *Identification and characterization of collaborating oncogenes in compound mutant mice.* Cancer Res, 1999. **59**(7 Suppl): p. 1773s-1777s.

52. Haupt, Y., et al., *Novel zinc finger gene implicated as myc collaborator by retrovirally accelerated lymphomagenesis in E mu-myc transgenic mice.* Cell, 1991. **65**(5): p. 753-63.

53. van Lohuizen, M., et al., *Identification of cooperating oncogenes in E mu-myc transgenic mice by provirus tagging.* Cell, 1991. **65**(5): p. 737-52.

54. Krimpenfort, P., et al., *Loss of p16Ink4a confers susceptibility to metastatic melanoma in mice.* Nature, 2001. **413**(6851): p. 83-6.

55. Sharpless, N.E., et al., *Loss of p16Ink4a with retention of p19Arf predisposes mice to tumorigenesis.* Nature, 2001. **413**(6851): p. 86-91.

56. Sherr, C.J. and F. McCormick, *The RB and p53 pathways in cancer.* Cancer Cell, 2002. **2**(2): p. 103-12.

57. Kamijo, T., et al., *Tumor spectrum in ARF-deficient mice.* Cancer Res, 1999. **59**(9): p. 2217-22.

58. Hirakawa, T. and H.E. Ruley, *Rescue of cells from ras oncogene-induced growth arrest by a second, complementing, oncogene.* Proc Natl Acad Sci U S A, 1988. **85**(5): p. 1519-23.

59. Jonkers, J., et al., *Activation of a novel proto-oncogene, Fratl, contributes to progression of mouse T-cell lymphomas.* Embo J, 1997. **16**(3): p. 441-50.

60. Lloyd, A.C., et al., *Cooperating oncogenes converge to regulate cyclin/cdk complexes.* Genes Dev, 1997. **11**(5): p. 663-77.

61. Pitot, H.C., *Fundamentals of Oncology.* 1986, New York: Marcel Dekker, Inc.

62. Ragozzino, M.M., et al., *Mechanisms of oncogene cooperation: activation and inactivation of a growth antagonist.* Environ Health Perspect, 1991. **93**: p. 97-103.

63. Vogelstein, B. and K.W. Kinzler, *The multistep nature of cancer.* Trends Genet, 1993. **9**(4): p. 138-41.

64. Adams, J.M. and S. Cory, *Oncogene co-operation in leukaemogenesis.* Cancer Surv, 1992. **15**: p. 119-41.

65. Cardiff, R.D. and W.J. Muller, *Transgenic mouse models of mammary tumorigenesis.* Cancer Surv, 1993. **16**: p. 97-113.

66. Hunter, T., *Cooperation between oncogenes.* Cell, 1991. **64**(2): p. 249-70.

67. Jonkers, J. and A. Berns, *Retroviral insertional mutagenesis as a strategy to identify cancer genes.* Biochim Biophys Acta, 1996. **1287**(1): p. 29-57.

68. Land, H., L.F. Parada, and R.A. Weinberg, *Cellular oncogenes and multistep carcinogenesis.* Science, 1983. **222**(4625): p. 771-8.

69. Sinn, E., et al., *Coexpression of MMTV/v-Ha-ras and MMTV/c-myc genes in transgenic mice: synergistic action of oncogenes in vivo.* Cell, 1987. **49**(4): p. 465-75.

70. Palmieri, S., *Oncogene requirements for tumorigenicity: cooperative effects between retroviral oncogenes.* Curr Top Microbiol Immunol, 1989. **148**: p. 43-91.

71. Ruley, H.E., *Transforming collaborations between ras and nuclear oncogenes.* Cancer Cells, 1990. **2**(8-9): p. 258-68.

72. Weinberg, R.A., *Oncogenes, antioncogenes, and the molecular bases of multistep carcinogenesis.* Cancer Res, 1989. **49**(14): p. 3713-21.

73. Schutte, J., J.D. Minna, and M.J. Birrer, *Deregulated expression of human c-jun transforms primary rat embryo cells in cooperation with an activated c-Ha-ras gene and transforms rat-1a cells as a single gene.* Proc Natl Acad Sci U S A, 1989. **86**(7): p. 2257-61.

74. Jochemsen, A.G., et al., *Different activities of the adenovirus types 5 and 12 E1A regions in transformation with the EJ Ha-ras oncogene.* J Virol, 1986. **59**(3): p. 684-91.

75. Fitzgerald, K., A. Harrington, and P. Leder, *Ras pathway signals are required for notch-mediated oncogenesis.* Oncogene, 2000. **19**(37): p. 4191-8.

76. Land, H., L.F. Parada, and R.A. Weinberg, *Tumorigenic conversion of primary embryo fibroblasts requires at least two cooperating oncogenes.* Nature, 1983. **304**(5927): p. 596-602.

77. Newbold, R.F. and R.W. Overell, *Fibroblast immortality is a prerequisite for transformation by EJ c-Ha-ras oncogene.* Nature, 1983. **304**(5927): p. 648-51.

78. Ridley, A.J., et al., *Ras-mediated cell cycle arrest is altered by nuclear oncogenes to induce Schwann cell transformation.* Embo J, 1988. **7**(6): p. 1635-45.

79. Hulit, J., D. Di Vizio, and R.G. Pestell, *Inducible transgenics. New lessons on events governing the induction and commitment in mammary tumorigenesis.* Breast Cancer Res, 2001. **3**(4): p. 209-12.

80. Jacobs, J.J. and M. van Lohuizen, *Cellular memory of transcriptional states by Polycomb-group proteins.* Semin Cell Dev Biol, 1999. **10**(2): p. 227-35.

81. van Lohuizen, M., *The trithorax-group and polycomb-group chromatin modifiers: implications for disease.* Curr Opin Genet Dev, 1999. **9**(3): p. 355-61.

82. Alkema, M.J., et al., *Pertubation of B and T cell development and predisposition to lymphomagenesis in Emu Bmi1 transgenic mice require the Bmi1 RING finger.* Oncogene, 1997. **15**(8): p. 899-910.

83. Haupt, Y., et al., *bmi-1 transgene induces lymphomas and collaborates with myc in tumorigenesis.* Oncogene, 1993. **8**(11): p. 3161-4.

84. Nesbit, C.E., J.M. Tersak, and E.V. Prochownik, *MYC oncogenes and human neoplastic disease.* Oncogene, 1999. **18**(19): p. 3004-16.

85. Facchini, L.M. and L.Z. Penn, *The molecular role of Myc in growth and transformation: recent discoveries lead to new insights.* Faseb J, 1998. **12**(9): p. 633-51.

86. Henriksson, M. and B. Luscher, *Proteins of the Myc network: essential regulators of cell growth and differentiation.* Adv Cancer Res, 1996. **68**: p. 109-82.

87. Langdon, W.Y., et al., *The c-myc oncogene perturbs B lymphocyte development in E-mu-myc transgenic mice.* Cell, 1986. **47**(1): p. 11-8.

88. Rochlitz, C.F., et al., *Incidence of activating ras oncogene mutations associated with primary and metastatic human breast cancer.* Cancer Res, 1989. **49**(2): p. 357-60.

89. Sparano, J.A., et al., *Targeted inhibition of farnesyltransferase in locally advanced breast cancer: a phase I and II trial of tipifarnib plus dose-dense doxorubicin and cyclophosphamide.* J Clin Oncol, 2006. **24**(19): p. 3013-8.

90. Thor, A., et al., *ras gene alterations and enhanced levels of ras p21 expression in a spectrum of benign and malignant human mammary tissues.* Lab Invest, 1986. **55**(6): p. 603-15.

91. Bunone, G., et al., *Activation of the unliganded estrogen receptor by EGF involves the MAP kinase pathway and direct phosphorylation.* Embo J, 1996. **15**(9): p. 2174-83.

92. Kato, S., et al., *Molecular mechanism of a cross-talk between oestrogen and growth factor signalling pathways.* Genes Cells, 2000. **5**(8): p. 593-601.

93. Smith, C.A., et al., *Correlations among p53, Her-2/neu, and ras overexpression and aneuploidy by multiparameter flow cytometry in human breast cancer: evidence for a common phenotypic evolutionary pattern in infiltrating ductal carcinomas.* Clin Cancer Res, 2000. **6**(1): p. 112-26.

94. Janocko, L.E., et al., *Assessing sequential oncogene amplification in human breast cancer.* Cytometry, 1995. **21**(1): p. 18-22.

95. Theillet, C., et al., *Loss of a c-H-ras-1 allele and aggressive human primary breast carcinomas.* Cancer Res, 1986. **46**(9): p. 4776-81.

96. Kleer, C.G., et al., *Characterization of RhoC expression in benign and malignant breast disease: a potential new marker for small breast carcinomas with metastatic ability.* Am J Pathol, 2002. **160**(2): p. 579-84.

97. van Golen, K.L., et al., *Reversion of RhoC GTPase-induced inflammatory breast cancer phenotype by treatment with a farnesyl transferase inhibitor.* Mol Cancer Ther, 2002. **1**(8): p. 575-83.

98. Voncken, J.W., et al., *MAPKAP kinase 3pK phosphorylates and regulates chromatin association of the polycomb group protein Bmi1.* J Biol Chem, 2005. **280**(7): p. 5178-87.

99. Miller, F.R., et al., *Xenograft model of progressive human proliferative breast disease.* J Natl Cancer Inst, 1993. **85**(21): p. 1725-32.

100. Al-Hajj, M., et al., *Prospective identification of tumorigenic breast cancer cells.* Proc Natl Acad Sci U S A, 2003. **100**(7): p. 3983-8.

101. Dontu, G., et al., *Stem cells in normal breast development and breast cancer.* Cell Prolif, 2003. **36 Suppl 1**: p. 59-72.

102. Dontu, G. and M.S. Wicha, *Survival of mammary stem cells in suspension culture: implications for stem cell biology and neoplasia.* J Mammary Gland Biol Neoplasia, 2005. **10**(1): p. 75-86.

103. Liu, S., G. Dontu, and M.S. Wicha, *Mammary stem cells, self-renewal pathways, and carcinogenesis.* Breast Cancer Res, 2005. **7**(3): p. 86-95.

104. Pathak, S., *Organ- and tissue-specific stem cells and carcinogenesis.* Anticancer Res, 2002. **22**(3): p. 1353-6.

105. Reya, T., et al., *Stem cells, cancer, and cancer stem cells.* Nature, 2001. **414**(6859): p. 105-11.

106. Sell, S. and G.B. Pierce, *Maturation arrest of stem cell differentiation is a common pathway for the cellular origin of teratocarcinomas and epithelial cancers.* Lab Invest, 1994. **70**(1): p. 6-22.

107. Tu, S.M., S.H. Lin, and C.J. Logothetis, *Stem-cell origin of metastasis and heterogeneity in solid tumours.* Lancet Oncol, 2002. **3**(8): p. 508-13.

108. Soltysova, A., V. Altanerova, and C. Altaner, *Cancer stem cells.* Neoplasma, 2005. **52**(6): p. 435-40.

109. Singh, S.K., et al., *Identification of human brain tumour initiating cells.* Nature, 2004. **432**(7015): p. 396-401.

110. Taipale, J. and P.A. Beachy, *The Hedgehog and Wnt signalling pathways in cancer.* Nature, 2001. **411**(6835): p. 349-54.

111. Hemmati, H.D., et al., *Cancerous stem cells can arise from pediatric brain tumors.* Proc Natl Acad Sci U S A, 2003. **100**(25): p. 15178-83.

112. Smith, K.S., et al., *Bmi-1 regulation of INK4A-ARF is a downstream requirement for transformation of hematopoietic progenitors by E2a-Pbx1.* Mol Cell, 2003. **12**(2): p. 393-400.

113. Valk-Lingbeek, M.E., S.W. Bruggeman, and M. van Lohuizen, *Stem cells and cancer; the polycomb connection.* Cell, 2004. **118**(4): p. 409-18.

114. Park, I.K., et al., *Bmi-1 is required for maintenance of adult self-renewing haematopoietic stem cells.* Nature, 2003. **423**(6937): p. 302-5.

115. Iwama, A., et al., *Enhanced self-renewal of hematopoietic stem cells mediated by the polycomb gene product Bmi-1.* Immunity, 2004. **21**(6): p. 843-51.

116. Molofsky, A.V., et al., *Bmi-1 dependence distinguishes neural stem cell self-renewal from progenitor proliferation.* Nature, 2003. **425**(6961): p. 962-7.

117. Qiao, C., et al., *Human mesenchymal stem cells isolated from the umbilical cord.* Cell Biol Int, 2007.

118. Datta, S., et al., *Bmi-1 Cooperates with H-Ras to Transform Human Mammary Epithelial Cells via Dysregulation of Multiple Growth-Regulatory Pathways.* Cancer Research, 2007. **67**(21): p. 10286-10295.

119. Dahmane, N. and A. Ruiz i Altaba, *Sonic hedgehog regulates the growth and patterning of the cerebellum.* Development, 1999. **126**(14): p. 3089-100.

120. Wechsler-Reya, R.J. and M.P. Scott, *Control of neuronal precursor proliferation in the cerebellum by Sonic Hedgehog.* Neuron, 1999. **22**(1): p. 103-14.

121. Wang, V.Y. and H.Y. Zoghbi, *Genetic regulation of cerebellar development.* Nat Rev Neurosci, 2001. **2**(7): p. 484-91.

122. Sawa, M., et al., *BMI-1 is highly expressed in M0-subtype acute myeloid leukemia.* Int J Hematol, 2005. **82**(1): p. 42-7.

123. Kennedy, C., et al., *Cell proliferation in the normal mouse mammary gland and inhibition by phenylbutyrate.* Mol Cancer Ther, 2002. **1**(12): p. 1025-33.

124. Longacre, T.A. and S.A. Bartow, *A correlative morphologic study of human breast and endometrium in the menstrual cycle.* Am J Surg Pathol, 1986. **10**(6): p. 382-93.

125. Green, J.E., et al., *The C3(1)/SV40 T-antigen transgenic mouse model of mammary cancer: ductal epithelial cell targeting with multistage progression to carcinoma.* Oncogene, 2000. **19**(8): p. 1020-7.

126. Kavanaugh, C. and J.E. Green, *The use of genetically altered mice for breast cancer prevention studies.* J Nutr, 2003. **133**(7 Suppl): p. 2404S-2409S.

127. Shibata, M.A., et al., *The C3(1)/SV40 T antigen transgenic mouse model of prostate and mammary cancer.* Toxicol Pathol, 1998. **26**(1): p. 177-82.

128. Maroulakou, I.G., et al., *Prostate and mammary adenocarcinoma in transgenic mice carrying a rat C3(1) simian virus 40 large tumor antigen fusion gene.* Proc Natl Acad Sci U S A, 1994. **91**(23): p. 11236-40.

129. Maroulakou, I.G., et al., *Reduced p53 dosage associated with mammary tumor metastases in C3(1)/TAG transgenic mice.* Mol Carcinog, 1997. **20**(2): p. 168-74.

130. Abd El-Rehim, D.M., et al., *Expression of luminal and basal cytokeratins in human breast carcinoma.* J Pathol, 2004. **203**(2): p. 661-71.

131. Nielsen, T.O., et al., *Immunohistochemical and clinical characterization of the basal-like subtype of invasive breast carcinoma.* Clin Cancer Res, 2004. **10**(16): p. 5367-74.

132. Honrado, E., J. Benitez, and J. Palacios, *Histopathology of BRCA1- and BRCA2-associated breast cancer.* Crit Rev Oncol Hematol, 2006. **59**(1): p. 27-39.

133. Ford, D., et al., *Genetic heterogeneity and penetrance analysis of the BRCA1 and BRCA2 genes in breast cancer families. The Breast Cancer Linkage Consortium.* Am J Hum Genet, 1998. **62**(3): p. 676-89.

134. Lakhani, S.R., *The pathology of hereditary breast cancer.* Dis Markers, 1999. **15**(1-3): p. 113-4.

135. Honrado, E., et al., *Pathology and gene expression of hereditary breast tumors associated with BRCA1, BRCA2 and CHEK2 gene mutations.* Oncogene, 2006. **25**(43): p. 5837-45.

136. Lakhani, S.R., *The pathology of familial breast cancer: Morphological aspects.* Breast Cancer Res, 1999. **1**(1): p. 31-5.

137. Bertucci, F., et al., *Gene expression profiling shows medullary breast cancer is a subgroup of basal breast cancers.* Cancer Res, 2006. **66**(9): p. 4636-44.

138. Qiu, T.H., et al., *Global expression profiling identifies signatures of tumor virulence in MMTV-PyMT-transgenic mice: correlation to human disease.* Cancer Res, 2004. **64**(17): p. 5973-81.

139. Guy, C.T., R.D. Cardiff, and W.J. Muller, *Induction of mammary tumors by expression of polyomavirus middle T oncogene: a transgenic mouse model for metastatic disease.* Mol Cell Biol, 1992. **12**(3): p. 954-61.

140. Lin, E.Y., et al., *Progression to malignancy in the polyoma middle T oncoprotein mouse breast cancer model provides a reliable model for human diseases.* Am J Pathol, 2003. **163**(5): p. 2113-26.

141. van de Vijver, M.J., *The pathology of familial breast cancer: The pre-BRCA1/BRCA2 era: historical perspectives.* Breast Cancer Res, 1999. **1**(1): p. 27-30.

142. Ferrini, F.S., et al., *Schirrous invasive ductal carcinoma of the breast overexpress p53 oncoprotein.* Sao Paulo Med J, 2001. **119**(1): p. 4-6.

143. Aouni, N.E., et al., *Medullary breast carcinoma: a case report with cytological features and histological confirmation.* Diagn Cytopathol, 2006. **34**(10): p. 701-3.

144. Ridolfi, R.L., et al., *Medullary carcinoma of the breast: a clinicopathologic study with 10 year follow-up.* Cancer, 1977. **40**(4): p. 1365-85.

145. Liu, S., et al., *BRCA1 regulates human mammary stem/progenitor cell fate.* Proc Natl Acad Sci U S A, 2008. **105**(5): p. 1680-5.

146. Wright, M.H., et al., *Brca1 breast tumors contain distinct CD44+/CD24- and CD133+ cells with cancer stem cell characteristics.* Breast Cancer Res, 2008. **10**(1): p. R10.

147. Ringrose, L. and R. Paro, *Epigenetic regulation of cellular memory by the Polycomb and Trithorax group proteins.* Annu Rev Genet, 2004. **38**: p. 413-43.

148. Raaphorst, F.M., *Deregulated expression of Polycomb-group oncogenes in human malignant lymphomas and epithelial tumors.* Hum Mol Genet, 2005. **14 Spec No 1**: p. R93-R100.

149. Bea, S., et al., *BMI-1 gene amplification and overexpression in hematological malignancies occur mainly in mantle cell lymphomas.* Cancer Res, 2001. **61**(6): p. 2409-12.

150. Jacobs, J.J., et al., *The oncogene and Polycomb-group gene bmi-1 regulates cell proliferation and senescence through the ink4a locus.* Nature, 1999. **397**(6715): p. 164-8.

151. Dimri, G.P., *What has senescence got to do with cancer?* Cancer Cell, 2005. **7**(6): p. 505-12.

152. Kim, R.H., et al., *Bmi-1 cooperates with human papillomavirus type 16 E6 to immortalize normal human oral keratinocytes.* Exp Cell Res, 2007. **313**(3): p. 462-72.

153. Guo, W.J., et al., *Mel-18 acts as a tumor suppressor by repressing Bmi-1 expression and down-regulating Akt activity in breast cancer cells.* Cancer Res, 2007. **67**(11): p. 5083-9.

154. Berman, H., et al., *Genetic and epigenetic changes in mammary epithelial cells identify a subpopulation of cells involved in early carcinogenesis.* Cold Spring Harb Symp Quant Biol, 2005. **70**: p. 317-27.

155. Cowell, J.K., et al., *Molecular characterization of the t(3;9) associated with immortalization in the MCF10A cell line.* Cancer Genet Cytogenet, 2005. **163**(1): p. 23-9.

156. Band, V., et al., *Human papilloma virus DNAs immortalize normal human mammary epithelial cells and reduce their growth factor requirements.* Proc Natl Acad Sci U S A, 1990. **87**(1): p. 463-7.

157. Elenbaas, B., et al., *Human breast cancer cells generated by oncogenic transformation of primary mammary epithelial cells.* Genes Dev, 2001. **15**(1): p. 50-65.

158. Seeburg, P.H., et al., *Biological properties of human c-Ha-ras1 genes mutated at codon 12.* Nature, 1984. **312**(5989): p. 71-5.

159. Debnath, J., et al., *The role of apoptosis in creating and maintaining luminal space within normal and oncogene-expressing mammary acini.* Cell, 2002. **111**(1): p. 29-40.

160. Landis, M.W., et al., *Cyclin D1-dependent kinase activity in murine development and mammary tumorigenesis.* Cancer Cell, 2006. **9**(1): p. 13-22.

161. Yu, Q., et al., *Requirement for CDK4 kinase function in breast cancer.* Cancer Cell, 2006. **9**(1): p. 23-32.

162. Dawson, P.J., et al., *MCF10AT: a model for the evolution of cancer from proliferative breast disease.* Am J Pathol, 1996. **148**(1): p. 313-9.

163. Giunciuglio, D., et al., *Invasive phenotype of MCF10A cells overexpressing c-Ha-ras and c-erbB-2 oncogenes.* Int J Cancer, 1995. **63**(6): p. 815-22.

164. Moon, A., et al., *H-ras, but not N-ras, induces an invasive phenotype in human breast epithelial cells: a role for MMP-2 in the H-ras-induced invasive phenotype.* Int J Cancer, 2000. **85**(2): p. 176-81.

165. Santner, S.J., et al., *Malignant MCF10CA1 cell lines derived from premalignant human breast epithelial MCF10AT cells.* Breast Cancer Res Treat, 2001. **65**(2): p. 101-10.

166. Shin, I., et al., *H-Ras-specific activation of Rac-MKK3/6-p38 pathway: its critical role in invasion and migration of breast epithelial cells.* J Biol Chem, 2005. **280**(15): p. 14675-83.

167. Serrano, M., et al., *Oncogenic ras provokes premature cell senescence associated with accumulation of p53 and p16INK4a.* Cell, 1997. **88**(5): p. 593-602.

168. Sun, P., et al., *PRAK is essential for ras-induced senescence and tumor suppression.* Cell, 2007. **128**(2): p. 295-308.

169. Wang, W., et al., *Sequential activation of the MEK-extracellular signal-regulated kinase and MKK3/6-p38 mitogen-activated protein kinase pathways mediates oncogenic ras-induced premature senescence.* Mol Cell Biol, 2002. **22**(10): p. 3389-403.

170. Chen, G., et al., *The p38 pathway provides negative feedback for Ras proliferative signaling.* J Biol Chem, 2000. **275**(50): p. 38973-80.

171. el-Deiry, W.S., *Regulation of p53 downstream genes.* Semin Cancer Biol, 1998. **8**(5): p. 345-57.

172. Nakano, K. and K.H. Vousden, *PUMA, a novel proapoptotic gene, is induced by p53.* Mol Cell, 2001. **7**(3): p. 683-94.

173. Flatt, P.M., et al., *p53-dependent expression of PIG3 during proliferation, genotoxic stress, and reversible growth arrest.* Cancer Lett, 2000. **156**(1): p. 63-72.

174. Boehm, J.S. and W.C. Hahn, *Understanding transformation: progress and gaps.* Curr Opin Genet Dev, 2005. **15**(1): p. 13-7.

175. Clark, G.J. and C.J. Der, *Aberrant function of the Ras signal transduction pathway in human breast cancer.* Breast Cancer Res Treat, 1995. **35**(1): p. 133-44.

176. von Lintig, F.C., et al., *Ras activation in human breast cancer.* Breast Cancer Res Treat, 2000. **62**(1): p. 51-62.

177. Sarkisian, C.J., et al., *Dose-dependent oncogene-induced senescence in vivo and its evasion during mammary tumorigenesis.* Nat Cell Biol, 2007. **9**(5): p. 493-505.

178. Dahl, C., et al., *Human mast cells express receptors for IL-3, IL-5 and GM-CSF; a partial map of receptors on human mast cells cultured in vitro.* Allergy, 2004. **59**(10): p. 1087-96.

179. Tang, B., et al., *TGF-beta switches from tumor suppressor to prometastatic factor in a model of breast cancer progression.* J Clin Invest, 2003. **112**(7): p. 1116-24.

180. Kim, L.S., et al., *Vascular endothelial growth factor expression promotes the growth of breast cancer brain metastases in nude mice.* Clin Exp Metastasis, 2004. **21**(2): p. 107-18.

181. Huang, K.H., et al., *[Association of Bmi-1 mRNA expression with differentiation, metastasis and prognosis of gastric carcinoma].* Nan Fang Yi Ke Da Xue Xue Bao, 2007. **27**(7): p. 973-5.

182. Feng, Y., et al., *[Expression and significance of Bmi-1 in breast cancer].* Ai Zheng, 2007. **26**(2): p. 154-7.

183. Mihic-Probst, D., et al., *Consistent expression of the stem cell renewal factor BMI-1 in primary and metastatic melanoma.* Int J Cancer, 2007. **121**(8): p. 1764-70.

184. Glinsky, G.V., *Death-from-cancer signatures and stem cell contribution to metastatic cancer.* Cell Cycle, 2005. **4**(9): p. 1171-5.

185. Fantozzi, A. and G. Christofori, *Mouse models of breast cancer metastasis.* Breast Cancer Res, 2006. **8**(4): p. 212.

186. Clayton, A.J., et al., *Incidence of cerebral metastases in patients treated with trastuzumab for metastatic breast cancer.* Br J Cancer, 2004. **91**(4): p. 639-43.

187. Bendell, J.C., et al., *Central nervous system metastases in women who receive trastuzumab-based therapy for metastatic breast carcinoma.* Cancer, 2003. **97**(12): p. 2972-7.

188. Tsukada, Y., et al., *Central nervous system metastasis from breast carcinoma. Autopsy study.* Cancer, 1983. **52**(12): p. 2349-54.

189. Strickland, L.B., et al., *Progression of premalignant MCF10AT generates heterogeneous malignant variants with characteristic histologic types and immunohistochemical markers.* Breast Cancer Res Treat, 2000. **64**(3): p. 235-40.

190. Jessani, N., et al., *Breast cancer cell lines grown in vivo: what goes in isn't always the same as what comes out.* Cell Cycle, 2005. **4**(2): p. 253-5.

191. Vernon, A.E., S.J. Bakewell, and L.A. Chodosh, *Deciphering the molecular basis of breast cancer metastasis with mouse models.* Rev Endocr Metab Disord, 2007. **8**(3): p. 199-213.

192. Clarke M., et al., *Effects of chemotherapy and hormonal therapy for early breast cancer on recurrence and 15-year survival: an overview of the randomised trials.* Lancet, 2005. **365**(9472): p. 1687-717.

193. Brackstone, M., J.L. Townson, and A.F. Chambers, *Tumour dormancy in breast cancer: an update.* Breast Cancer Res, 2007. **9**(3): p. 208.

194. Fisher, B., et al., *Findings from recent National Surgical Adjuvant Breast and Bowel Project adjuvant studies in stage I breast cancer.* J Natl Cancer Inst Monogr, 2001(30): p. 62-6.

195. Wallgren, A., et al., *Risk factors for locoregional recurrence among breast cancer patients: results from International Breast Cancer Study Group Trials I through VII.* J Clin Oncol, 2003. **21**(7): p. 1205-13.

196. Glinsky, G.V., *Genomic models of metastatic cancer: functional analysis of death-from-cancer signature genes reveals aneuploid, anoikis-resistant, metastasis-enabling phenotype with altered cell cycle control and activated Polycomb Group (PcG) protein chromatin silencing pathway.* Cell Cycle, 2006. **5**(11): p. 1208-16.

197. Avruch, J., et al., *Ras activation of the Raf kinase: tyrosine kinase recruitment of the MAP kinase cascade.* Recent Prog Horm Res, 2001. **56**: p. 127-55.

198. Ries, S., et al., *Opposing effects of Ras on p53: transcriptional activation of mdm2 and induction of p19ARF.* Cell, 2000. **103**(2): p. 321-30.

199. Valentijn, A.J., N. Zouq, and A.P. Gilmore, *Anoikis.* Biochem Soc Trans, 2004. **32**(Pt3): p. 421-5.

200. Parsons, J.T., *Focal adhesion kinase: the first ten years.* J Cell Sci, 2003. **116**(Pt 8): p. 1409-16.

201. Downward, J., *Ras signalling and apoptosis.* Curr Opin Genet Dev, 1998. **8**(1): p. 49-54.

202. Frame, S. and A. Balmain, *Integration of positive and negative growth signals during ras pathway activation in vivo.* Curr Opin Genet Dev, 2000. **10**(1): p. 106-13.

203. Joneson, T. and D. Bar-Sagi, *Ras effectors and their role in mitogenesis and oncogenesis.* J Mol Med, 1997. **75**(8): p. 587-93.

204. Mayo, M.W., et al., *Requirement of NF-kappaB activation to suppress p53-independent apoptosis induced by oncogenic Ras.* Science, 1997. **278**(5344): p. 1812-5.

205. Sotiriou, C., et al., *Breast cancer classification and prognosis based on gene expression profiles from a population-based study.* Proc Natl Acad Sci U S A, 2003. **100**(18): p. 10393-8.

206. Brennan, D.J., et al., *Application of DNA microarray technology in determining breast cancer prognosis and therapeutic response.* Expert Opin Biol Ther, 2005. **5**(8): p. 1069-83.

207. Kaklamani, V.G. and W.J. Gradishar, *Gene expression in breast cancer.* Curr Treat Options Oncol, 2006. **7**(2): p. 123-8.

208. Mullan, P.B. and R.C. Millikan, *Molecular subtyping of breast cancer: opportunities for new therapeutic approaches.* Cell Mol Life Sci, 2007. **64**(24): p. 3219-32.

209. Perou, C.M., et al., *Molecular portraits of human breast tumours.* Nature, 2000. **406**(6797): p. 747-52.

210. Gebauer, G., et al., *Identification of genes associated with tumor progression using microarrays.* Anticancer Res, 2005. **25**(3A): p. 1477-82.

211. Yi, M., et al., *WholePathwayScope: a comprehensive pathway-based analysis tool for high-throughput data.* BMC Bioinformatics, 2006. **7**: p. 30.

212. Xiong, Y., et al., *p21 is a universal inhibitor of cyclin kinases.* Nature, 1993. **366**(6456): p. 701-4.

213. Pellegrini, L., et al., *Insights into DNA recombination from the structure of a RAD51-BRCA2 complex.* Nature, 2002. **420**(6913): p. 287-93.

214. Cong, F. and S.P. Goff, *c-Abl-induced apoptosis, but not cell cycle arrest, requires mitogen-activated protein kinase kinase 6 activation.* Proc Natl Acad Sci U S A, 1999. **96**(24): p. 13819-24.

215. Hogan, B., F. Costantini, and E. Lacy, *Manipulating the Mouse Embryo. A Laboratory Manual.* 1986, Cold Spring Harbor: Cold Spring Harbor Laboratory. 332.

216. Gunther, E.J., et al., *A novel doxycycline-inducible system for the transgenic analysis of mammary gland biology.* Faseb J, 2002. **16**(3): p. 283-92.

217. van der Lugt, N.M., et al., *Posterior transformation, neurological abnormalities, and severe hematopoietic defects in mice with a targeted deletion of the bmi-1 proto-oncogene.* Genes Dev, 1994. **8**(7): p. 757-69.

218. Ormandy, C.J., et al., *Investigation of the transcriptional changes underlying functional defects in the mammary glands of prolactin receptor knockout mice.* Recent Prog Horm Res, 2003. **58**: p. 297-323.

219. Baik, I., et al., *Association of fetal hormone levels with stem cell potential: evidence for early life roots of human cancer.* Cancer Res, 2005. **65**(1): p. 358-63.

220. Thomsen, A.R., et al., *Estrogenic effect of soy isoflavones on mammary gland morphogenesis and gene expression profile.* Toxicol Sci, 2006. **93**(2): p. 357-68.

221. Trichopoulos, D., *Hypothesis: does breast cancer originate in utero?* Lancet, 1990. **335**(8695): p. 939-40.

222. Petersen, O.W., et al., *Epithelial progenitor cell lines as models of normal breast morphogenesis and neoplasia.* Cell Prolif, 2003. **36 Suppl 1**: p. 33-44.

223. Hu, C., et al., *Overexpression of activated murine Notch1 and Notch3 in transgenic mice blocks mammary gland development and induces mammary tumors.* Am J Pathol, 2006. **168**(3): p. 973-90.

224. Mori, T., H. Nagasawa, and H.A. Bern, *Long-term effects of perinatal exposure to hormones on normal and neoplastic mammary growth in rodents: a review.* J Environ Pathol Toxicol, 1979. **3**(1-2): p. 191-205.

225. Chlebowski, R.T., et al., *Influence of estrogen plus progestin on breast cancer and mammography in healthy postmenopausal women: the Women's Health Initiative Randomized Trial.* Jama, 2003. **289**(24): p. 3243-53.

226. Bilimoria, M.M. and M. Morrow, *The woman at increased risk for breast cancer: evaluation and management strategies.* CA Cancer J Clin, 1995. **45**(5): p. 263-78.

227. Singletary, K.W. and J.A. Milner, *DNA binding and adduct formation of 7,12-dimethylbenz[a]-anthracene by rat mammary epithelial cell aggregates in vitro.* Carcinogenesis, 1986. **7**(1): p. 95-8.

228. Cao, Y., et al., *Effect of 7,12-dimethylbenz[a]anthracene (DMBA) on gut glutathione metabolism.* J Surg Res, 2001. **100**(1): p. 135-40.

229. Yin, Y., et al., *Characterization of medroxyprogesterone and DMBA-induced multilineage mammary tumors by gene expression profiling.* Mol Carcinog, 2005. **44**(1): p. 42-50.